

Editorial corner – a personal view

Molecular functionality and self-assembled polymer compositions

R. A. Shanks*

School of Applied Sciences, RMIT University, GPO Box 2476V, Melbourne, 3001, Australia

Most organic molecules exhibit shapes with low inter-conversion energy, called conformations. As polymer molecules are larger, conformation becomes much more significant than molecular structure because larger molecules have many possible conformations in addition to an increase in the associated inter-conversion energy. Conformational control enables self-assembly into supramolecular structures. Common supramolecular structures are crystals, polymer dispersed fillers, solvated additives, interactions between blended polymers and surface adsorptions.

Polymer science has advanced to where each of the components of a composition can be designed to migrate to the specific locations so that controlled properties can be introduced. Polymer scientists are able to design polymer conformation through symmetry, specific interactions, and molecular orientation. While this can be used in nano-composites and molecular imprinted patterns, it is beneficial in all polymer compositions.

Migration of fillers and additives to the required positions are useful tools to assemble the required structure. In addition to uniformly dispersed fillers, more can be done with fillers that link to form agglomerates or that are preformed into aggregates such as chains or branched clusters that impart new properties such as electrical conductivity, rheological and mechanical innovations. While shear and orientation from processing are useful, it is the molecular interactions and symmetry that provide the thermodynamic impetus for self-assembly and subsequent supramolecular chemistry. Shear can-

not impart what thermodynamics does not allow, though shear can accelerate the kinetics.

When the interactions and symmetry are designed into a system, then supramolecular structure can automatically form. This is demonstrated by proteins where the primary structure of the amino acid chain controlled the secondary conformation, tertiary folding and the quaternary clustering of protein sub-units into the biologically active form. Adapting this analogy synthetic polymers can be designed with components that spontaneously form supramolecular constructions. The need for nano-components is less important than the need for the system to possess suitable interactive chemistry.

Polymer science has emerged as the field where elaborate structures are designed with macromolecules, resembling the approach to building and machine design in the macroscopic world. When the components of polymer compositions contain complementary chemical and symmetrical form they can self-assemble into supramolecular structures with specific properties.



Prof. Dr. Robert A. Shanks
Member of International Advisory Board

*Corresponding author, e-mail: robert.shanks@rmit.edu.au
© BME-PT and GTE

Facile synthesis of two-photon absorbing polymers through radical copolymerization

X. Bi^{1*}, Z. Wu¹, Z. Xu²

¹Department of Chemistry, University of Missouri-Kansas City, Kansas City, Missouri 64110, USA

²Department of Chemistry and Biochemistry, University of Missouri-St. Louis, St. Louis, Missouri 63121, USA

Received 9 April 2007; accepted in revised form 6 June 2007

Abstract. A two-photon absorbing polymer has been prepared through radical copolymerization of methyl acrylate and a synthesized monomer containing a two-photon absorbing chromophore (*E,E,E*)-1,3,5-tristyrylbenzene (**1**), under conventional radical polymerization conditions. The synthesized polymer was characterized by nuclear magnetic resonance (NMR), infra-red spectroscopy (IR) and gel permeation chromatography (GPC). The linear and nonlinear optical properties were studied by measurement of UV-Vis absorption, fluorescent emission and two-photon cross-section. This synthetic strategy provided a facile approach for synthesis of photonic materials with adjustable chromophore concentration and high molecular weights.

Keywords: polymer synthesis, molecular engineering, two-photon absorbing polymer, radical copolymerization

1. Introduction

For the last decade, synthesis of highly active organic two-photon absorbing materials has attracted much interest because of their importance in science and their potential applications in many fast-growing technological areas such as optical power limiting [1, 2], three-dimensional (3-D) storage media [3, 4], two-photon fluorescence microscopy [5, 6], up-conversion lasing [7, 8], and two-photon photodynamic therapy [9, 10]. The fulfillment of above technological applications relies greatly on the development of organic materials with superior two-photon absorption (TPA) activities. Since 1990s, intensive studies have been conducted and great progress has been made on the discovery of structure-activity relationship in TPA molecules [11–19]. Earlier studies have focused on linear quadrupolar molecular structures, and found that the conjugation length, π -electron center, and chemical functional groups at the end of electron

conjugation are three important factors for the enhancement of TPA activities [11, 15, 16]. Recent studies have demonstrated superior TPA properties of octupolar multi-branched structures in comparison to linear structures [12, 13, 20]. Despite the advances in molecular structure development, most TPA molecules need to be incorporated into polymers to form thin films for many practical applications [21]. In most cases, the TPA molecules are doped in a host polymer matrix [21–23]. The disadvantage of this approach is that TPA molecules may aggregate and undergo phase separation under intense laser irradiation, which leads to the decreasing performance of the material. Moreover, the solubility of chromophores in the polymer is limited, and maximization of chromophore density is difficult. Some TPA conjugated polymers have been reported [24, 25], but synthetic strategies for high molecular-weight TPA materials are still lacking. In this research, we explore the strategy to covalently attach the TPA molecules to the polymethyl

*Corresponding author, e-mail: xiangdongb@yahoo.com
© BME-PT and GTE

acrylate backbone through radical copolymerization of methyl acrylate and a TPA molecule-containing monomer. This approach has practical values in many respects as the TPA molecules in the synthesized materials are stable and phase separation is avoided, and therefore, a consistent behavior of the materials is maintained. Secondly, desired chromophore density can be achieved, high molecular weight polymers can be synthesized, and conventional polymerization procedures can be used. Further more, with the tolerance of radical polymerization to various functionalities, various TPA polymers bearing functional groups can be synthesized and further modified for different applications.

The model of branched two-photon absorbing chromophore employed in this research is (*E,E,E*)-1,3,5-tristyrylbenzene (**1**) which has previously been synthesized and was found to exhibit excellent nonlinear optical properties [26–28]. To covalently attach the molecular structure of **1** to polymer backbone, a synthetic strategy is developed as depicted in Figure 1. A monomer containing chromophore **6** is first synthesized and is copolymerized with methyl acrylate under radical polymerization conditions. The resulting polymer product is extensively characterized and its linear and non-linear optical properties are studied using multiple analytical methods.

2. Experimental

2.1. Materials and instruments

All chemicals were purchased from Aldrich Chemical Company or Acros Chemical Company and used without further purification. Solvents such as dimethylformamide (DMF) or dimethyl sulfoxide (DMSO) were treated with dry molecular sieves and distilled under vacuum. Tetrahydrofuran (THF) was treated with either Na-benzophenone or calcium hydride, and distilled under nitrogen before use. All reactions were conducted under nitrogen. Heck reactions were performed in a Schlenk Tube equipped with a Teflon valve. ¹H NMR spectra were measured by a Bruker AM 250 (250 MHz) spectrometer. ¹³C NMR spectra were recorded at 62.9 MHz on a Bruker AM 250 (250 MHz) spectrometer. All samples were referenced to the deuterated solvents. IR spectra were recorded on a Spectrum 2000 (Perkin Elmer) FT-IR spectrometer. TPA cross-sections ($\pm 15\%$ uncertainty) of synthesized molecules were determined by nonlinear optical transmission measurement [29] using a Quanta-Ray MOPO-730 laser. Molecular weights were determined using gel permeation chromatography (GPC) equipped with a Waters 410-differential refractometer. A flow rate of 1.0 ml/min was used and samples were prepared in THF. Polystyrene standards were used for calibration.

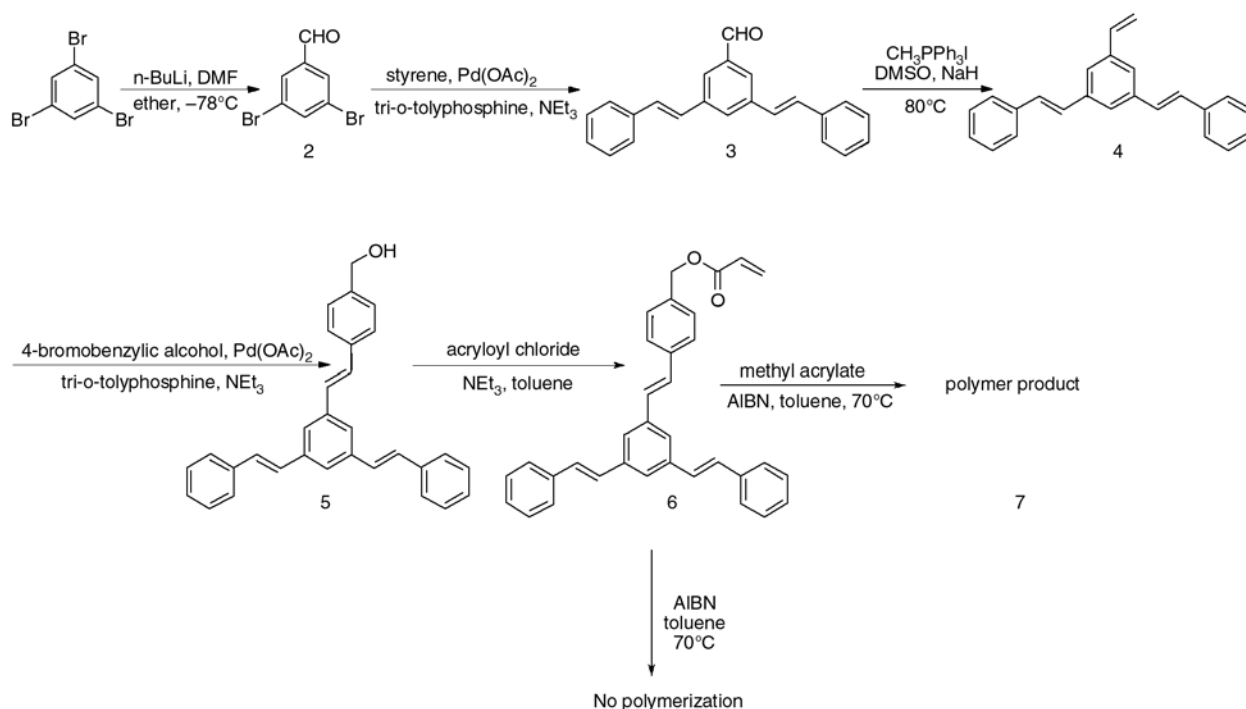


Figure 1. Synthesis of two-photon absorbing polymer through radical copolymerization

2.2. Synthesis

Preparation of (*E,E,E*)-1,3,5-tristyrylbenzene (**1**)

1,3,5-tristyrylbenzene was prepared by Heck reaction of 1,3,5-tribromobenzene and styrene following a reported procedure [28] in 51% yield. ^1H NMR (CDCl_3 , 250 MHz) δ 7.20–7.59 (24 H, m, ArH and Ar–CH=CH–Ar). ^{13}C NMR (CDCl_3 , 62.9 MHz) δ 138.27, 137.44, 129.52, 128.99, 128.59, 128.03, 126.82, and 124.18.

Preparation of **2**

To a 500 ml round-bottom flask was charged with 1,3,5-tribromobenzene (10 g, 31.1 mmol) and ether (250 ml) under nitrogen. The solution was cooled to -78°C . Butyl lithium solution (2.5 M, 12.4 ml, 31.1 mmol) was injected via a syringe. The reaction mixture was kept at this temperature for 45 minutes. DMF (2.65 ml, 34.2 mmol) was added dropwise through a syringe. The solution was allowed to warm to room temperature and stirred for 6 hours. The reaction was quenched with dilute hydrochloric acid and extracted with ether. The organic layer was separated and dried over magnesium sulfate. Solvent was evaporated and crystallization of the residue in ethanol gave product (3.36 g, yield 41%). ^1H NMR (CDCl_3): δ 9.90 (1 H, s, CHO), 7.93 (2 H, s, ArH) and 7.91 (1 H, s, ArH). ^{13}C NMR (CDCl_3): δ 189.4, 139.8, 132.1, 131.4 and 124.2.

Preparation of **3**

To a Schlenk tube equipped with a Teflon valve was weighed **2** (0.545 g, 2.06 mmol), styrene (0.614 ml, 5.37 mmol), $\text{Pd}(\text{OAc})_2$ (46.3 mg, 0.206 mmol), tri-*o*-tolylphosphine (125.6 mg, 0.41 mmol), triethylamine (5 ml, 14.8 mmol) and DMF (5 ml). Bubble nitrogen to the solution, seal the tube and put in oil bath at 95°C for 3 days. The reaction mixture was poured into water, extracted with ethyl acetate. The organic layer was dried over magnesium sulfate. Purification of the crude product by column chromatography (silica gel, hexanes/ethyl acetate 10:1) gave pure product (0.409 g, 64%). ^1H NMR (CDCl_3): δ 10.09 (1 H, s, CHO) and 7.92–7.14 (17 H, m, ArH and Ar–CH=CH–Ar). ^{13}C NMR (CDCl_3): δ 192.5, 138.9, 137.4, 136.9, 130.9, 130.5, 129.0, 128.4, 127.2, 127.0 and 126.5.

Preparation of **4**

To a 25 ml round-bottom flask was added NaH (27.8 mg, 1.1 mmol) and dry DMSO (2 ml). The solution was warmed up to $75\text{--}80^\circ\text{C}$ for 45 minutes then cooled to 0°C . A solution of $\text{CH}_3\text{PPh}_3\text{I}$ (444 mg, 1.1 mmol) in DMSO was injected dropwise. The suspension was stirred at room temperature for 10 minutes. A solution of **3** (310 mg, 1 mmol) in DMSO was added by a syringe. The reaction was kept at 70°C overnight. The mixture was poured into water, extracted with ethyl acetate, dried over magnesium sulfate, and further purified by column chromatography on silica gel to yield the desired product (1.05 g, 95%). ^1H NMR (CDCl_3): δ 7.61–7.12 (17 H, ArH and Ar–CH=CH–Ar), 6.83 (1 H, m, Ar–CH=CH₂), 5.91 (1 H, d, Ar–CH=CH₂) and 5.38 (1 H, d, Ar–CH=CH₂). ^{13}C NMR (CDCl_3): δ 138.5, 138.1, 137.4, 136.8, 129.4, 128.9, 128.5, 128.0, 126.8, 124.3, 123.9 and 114.7.

Preparation of **5**

Compound **5** was synthesized by Heck reaction of **4** with 4-bromobenzyl alcohol following a similar procedure as for the preparation of **3** (yield 37%). ^1H NMR (CDCl_3): δ 7.58–7.19 (23 H, m, ArH and Ar–CH=CH–Ar), 4.73 (2 H, s, benzylic) and 2.06 (1 H, s, *br*, OH). ^{13}C NMR (CDCl_3): δ 140.6, 138.3, 138.2, 137.4, 136.9, 129.5, 129.0, 128.6, 128.5, 128.0, 127.7, 127.1, 127.0, 126.8, 124.2 and 65.4.

Preparation of **6**

To a 25 ml round-bottom flask was charged with toluene (2 ml), acryl chloride (64.7 mg, 0.72 mmol) and triethylamine (71 μl , 0.72 mmol). The solution was stirred at room temperature for 10 minutes. A solution of **5** (98.7 mg, 0.24 mmol) in toluene (1 ml) was added. The mixture was purified by column chromatography on silica gel to give product **6** (65.1 mg, 58%). ^1H NMR (CDCl_3): δ 7.59–7.20 (23 H, m, ArH and Ar–CH=CH–Ar), 6.50 (1 H, d, –OC(O)CH=CH₂), 6.20 (1 H, m, –OC(O)CH=CH₂), 5.89 (1 H, d, –OC(O)CH=CH₂) and 5.23 (2 H, s, benzylic). ^{13}C NMR (CDCl_3): δ 184.1, 138.3, 138.1, 137.6, 137.4, 135.5, 131.5, 129.6, 129.3, 129.0, 128.5, 128.0, 127.1, 127.0, 126.8, 126.7, 124.2 and 66.3.

Polymer synthesis

To a Schlenk tube was added **6** (51 mg, 0.109 mmol), methyl acrylate (49 μ l, 0.54 mmol), 2,2'-azobisisobutyronitrile (AIBN, 5.4 mg, 0.033 mmol) and toluene (0.3 ml). The tube was degassed, sealed, and heated to 70°C overnight. Polymer **7** was precipitated in methanol (60 mg, 61%) and purified by dissolve-precipitate methods to removed small molecules and dried under vacuum. $^1\text{H NMR}$ (CDCl_3): δ 7.73–7.35 (m, *br*, ArH and Ar-CH=CH-Ar), 5.32 (*br*, benzylic), 3.65 (*br*, -COOMe), 2.38 (*br*, -CH-COOMe), 1.94–1.50 (m, *br*, -CH₂-CH(COOMe)); FT-IR (KBr) $\nu_{\text{max}}/\text{cm}^{-1}$ 3030 (C-H), 2954 (C-H), 1739 (C=O), 1601 (C=C), 1452 (-CH₂-), 1384, 1265, 1170 (C-O), 967 (C-H, aromatic), 831, 754 (-CH₂-) and 697 (C-H, aromatic).

3. Results and discussion

The synthesis of TPA chromophore-containing monomer (**6**) started with tribromobenzene (Figure 1), which reacted with DMF to give 3,5-dibromobenzaldehyde (**2**), according to a reported procedure [30]. A Heck reaction of **2** with 2 equivalents of styrene resulted in compound **3**, followed by a Wittig reaction with $\text{CH}_3\text{PPh}_3\text{I}$ to afford the olefin **4**, with a procedure described by Greenwald [31]. Further reaction of **4** with 4-bromobenzylalcohol under Heck reaction conditions yielded the chromophore **5**, in which the TPA chromophore molecule (**1**) was constructed with an active hydroxyl group at the end for further organic transformations. Esterification of **5** with acryloyl chloride gave the chromophore-containing monomer **6** for further polymerization. Attempt of the self-

polymerization of **6** was not successful, which might be due to steric hindrance of the bulky chromophore structure. However, copolymerization of **6** with methyl acrylate yielded a copolymer with the TPA molecules randomly attached to the polymer backbone. The copolymerization was conducted in the presence of AIBN with a loading ratio of methyl acrylate to **6** as 5:1. The molar concentration of the chromophore in the synthesized copolymer is calculated to be 21.7% based on proton NMR integration.

The polymer product (**7**) was further characterized by FT-IR (Figure 2b). For comparison, the FT-IR spectrum of compound **1** was also displayed (Figure 2a). In Figure 2b, a strong C=O stretch at 1739 cm^{-1} is observed from the carboxylate branches connected to polymethyl acrylate backbone. Other characteristic peaks such as 1170 (C-O stretch), 2954 (C-H stretch), and 1452 cm^{-1} (-CH₂- bending) also match the reported absorptions of polymethyl acrylate [32]. By comparison to Figure 2a, the IR absorptions at 3030 (C-H stretch), 1601 and 1496 (C=C stretch), 967 and 696 (aromatic C-H), and 754 cm^{-1} (-CH₂- bending) can be identified as peaks from the two-photon chromophore that covalently attached to the polymer backbone. The synthesized polymer is readily soluble in THF, methylene chloride, and chloroform. The UV-Vis absorption and fluorescent emission of the synthesized polymer resemble those of molecule **1** (Figure 3) as they both exhibit similar maximum absorption, emission, and profiles. Similar to molecule **1**, the UV-Vis absorption peak of the polymer occurs at 313 nm and there is no linear absorption observed above 400 nm. Under inten-

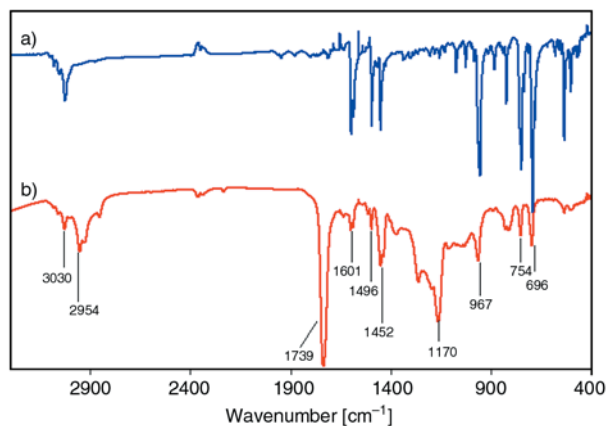


Figure 2. FT-IR of (*E,E,E*)-1,3,5-tristyrylbenzene (a) and synthesized two-photon absorbing polymer (b)

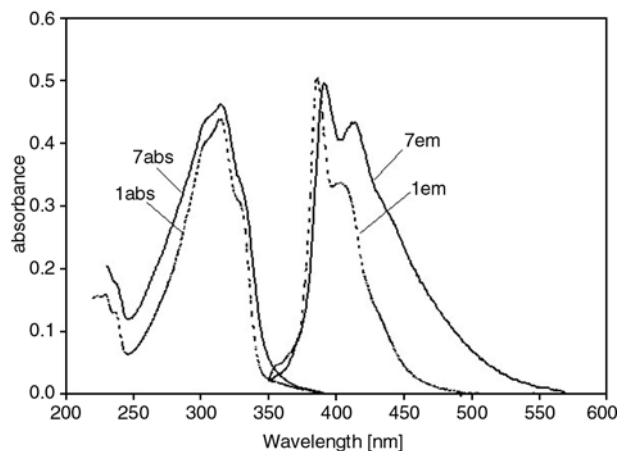


Figure 3. UV-Vis and fluorescence emission spectra of (*E,E,E*)-1,3,5-tristyrylbenzene (**1**) and the synthesized two-photon absorbing polymer (**7**)

sive laser excitation at 532 nm, however, a strong absorption is observed and an up-converted fluorescent emission occurs at 390 nm, which is featured for two two-photon absorption. The TPA cross-sections of molecule **1** and the polymer at 532 nm were determined using transmission two-photon absorption measurement [29]. The TPA cross-section of the synthesized polymer is about $44\ 670 \cdot 10^{-50}$ s cm⁴ in nanosecond time domain, while that of molecule **1** is about $17\ 700 \cdot 10^{-50}$ s cm⁴. The higher apparent TPA cross-section of the polymer could be the result of higher local density of TPA chromophores within a polymer chain, since the total two-photon absorption is proportional to the square of number density. Further GPC analysis indicates that the polymer exhibits a fairly high molecular weight (M_w 7 750, M_n 25 300) with the polydispersity index (PDI) of 3.2. A solution of the synthesized polymer in THF is stored for a week and no significant difference is observed on its optical properties, indicating that the polymer product is optically stable. Further stability experiments under laser irradiation and heat are under investigation.

4. Conclusions

This research has demonstrated a facile synthesis of a two-photon absorbing polymer through conventional radical polymerization of methyl acrylate and a synthesized monomer containing a two-photon absorbing chromophore. The synthesized polymer shows similar optical properties comparable to the chromophore molecule alone and is optically stable. This method offers a convenient procedure to synthesize high molecular weight two-photon absorbing materials. The concentration of chromophore can be adjusted by varying the ratio of bulk monomer to chromophore-containing monomer, and the physical properties of bulk materials can be tuned for specific application by using different commercial monomers. The advantage of radical polymerization procedure also provides the possibility to synthesize functional two-photon absorbing materials for a verity of applications.

References

[1] Bhawalkar J. D., He G. S., Prasad P. N.: Nonlinear multiphoton processes in organic and polymeric materials. *Reports on Progress in Physics*, **59**, 1041–1070 (1996).

[2] Ehrlich J. E., Wu X. L., Lee I. Y. S., Hu Z. Y., Röckel H., Marder S. R., Perry J. W.: Two-photon absorption and broadband optical limiting with bis-donor stilbenes. *Optics Letters*, **22**, 1843–1845 (1997).

[3] Cumpston B. H., Ananthavel S. P., Barlow S., Dyer D. L., Ehrlich J. E., Erskine L. L., Heikal A. A., Kuebler S. M., Lee I. Y. S., McCord-Maughon D., Qin J., Röckel H., Rumi M., Wu X. L., Marder S. R., Perry J. W.: Two-photon polymerization initiators for three-dimensional optical data storage and microfabrication. *Nature*, **398**, 51–54 (1999).

[4] Parthenopoulos D. A., Rentzepis P. M.: Three-dimensional optical storage memory. *Science*, **245**, 843–845 (1989).

[5] Denk W., Svoboda K.: Photon upmanship: why multiphoton imaging is more than a gimmick. *Neuron*, **18**, 351–357 (1997).

[6] Denk W., Strickler J. H., Webb W. W.: Two-photon laser scanning fluorescence microscopy. *Science*, **248**, 73–76 (1990).

[7] Mukherjee A.: Two-photon pumped upconverted lasing in dye doped polymer waveguides. *Applied Physics Letters*, **62**, 3423–3425 (1993).

[8] Zhao C. F., He G. S., Bhawalkar J. D., Park C. K., Prasad P. N.: Newly synthesized dyes and their polymer/glass composites for one- and two-photon pumped solid-state cavity lasing. *Chemistry of Materials*, **7**, 1979–1983 (1995).

[9] Bhawalkar J. D., Kumar N. D., Zhao C. F., Prasad P. N.: Two-photon photodynamic therapy. *Journal of Clinical Laser Medicine and Surgery*, **15**, 201–204 (1997).

[10] Prasad P. N., Bhawalkar J. D., Kumar N. D., Lal M.: Multifunctional polymers as multi-role materials for photonics. *Macromolecular Symposia*, **118**, 467–472 (1997).

[11] Albota M., Beljonne D., Bredas J. L., Ehrlich J. E., Fu J. Y., Heikal A. A., Hess S. E., Kogej T., Levin M. D., Marder S. R., McCord-Maughon D., Perry J. W., Rockel H., Rumi M., Subramaniam C., Webb W. W., Wu I. L., Xu C.: Design of organic molecules with large two-photon absorption cross sections. *Science*, **281**, 1653–1656 (1998).

[12] Chung S.-J., Kim K.-S., Lin T.-C., He G. S., Swiatkiewicz J., Prasad P. N.: Cooperative enhancement of two-photon absorption in multi-branched structures. *The Journal of Physical Chemistry: B*, **103**, 10741–10745 (1999).

[13] Kannan R., He G. S., Lin T. C., Prasad P. N., Vaia R. A., Tan L. S.: Toward highly active two-photon absorbing liquids. synthesis and characterization of 1,3,5-triazine-based octupolar molecules. *Chemistry of Materials*, **16**, 185–194 (2004).

[14] Kannan R., He G. S., Yuan L. X., Xu F. M., Prasad P. N., Dombroskie A. G., Reinhardt B. A., Baur J. W., Vaia R. A., Tan L. S.: Diphenylaminofluorene-based two-photon-absorbing chromophores with various -electron acceptors. *Chemistry of Materials*, **13**, 1896–1904 (2001).

- [15] Kim O. K., Lee K. S., Woo H. Y., Kim K. S., He G. S., Swiatkiewicz J., Prasad P. N.: New class of two-photon-absorbing chromophores based on dithienothiophene. *Chemistry of Materials*, **12**, 284–286 (2000).
- [16] Reinhardt B. A., Brott L. L., Clarson S. J., Dillard A. G., Bhatt J. C., Kannan R., Yuan L. X., He G. S., Prasad P. N.: Highly active two-photon dyes: design, synthesis, and characterization toward application. *Chemistry of Materials*, **10**, 1863–1874 (1998).
- [17] Rumi M., Ehrlich J. E., Heikal A. A., Perry J. W., Barlow S., Hu Z. Y., McCord-Maughon D., Parker T. C., Röckel H., Thayumanavan S., Marder S. R., Beljonne D., Bredas J. L.: Structure-property relationships for two-photon absorbing chromophores: bis-donor diphenylpolyene and bis(styryl)benzene derivatives. *Journal of American Chemical Society*, **122**, 9500–9510 (2000).
- [18] Varnavski O., Samuel I. D. W., Palsson L. O., Beavington R., Burn P. L., Goodson T.: Investigations of excitation energy transfer and intramolecular interactions in a nitrogen corded distyrylbenzene dendrimer system. *The Journal of Chemical Physics*, **116**, 8893–8903 (2002).
- [19] Yan Y-X., Tao X-T., Sun Y-H., Wang C-K., Xu G-B., Yang J-X., Ren Y., Zhao X., Wu Y-Z., Yu X-Q., Jiang M-H.: Synthesis and nonlinear optical properties of novel multi-branched two-photon polymerization initiators. *Journal of Materials Chemistry*, **14**, 2995–3000 (2004).
- [20] Wei P., Bi X. D., Wu Z., Xu Z.: Synthesis of Triphenylamine-Cored Dendritic Two-Photon Absorbing Chromophores. *Organic Letters*, **7**, 3199–3202 (2005).
- [21] Hua J. L., Li B., Meng F. S., Ding F., Qian S. X., Tian H.: Two-photon absorption properties of hyper-branched conjugated polymers with triphenylamine as the core. *Polymer*, **45**, 7143–7149 (2004).
- [22] Guo F. Q., Guo R., Jiang Z. W., Zhang Q. J., Huang W. H., Guo B.: Optical properties of a novel nonlinear chromophore doped polymer and application for two-photon microfabrication. *Physica Status Solidi (a)*, **202**, 2515–2520 (2005).
- [23] Wang D., Zhou G. Y., Ren Y., Yu X. Q., Cheng X. F., Yang S. J., Xu X. G., Shao Z. S., Jiang M. H.: Linear and nonlinear optical properties of two-photon absorption dye doped linear copolymer. *Solid State Communications*, **121**, 339–344 (2002).
- [24] Chung S. J., Maciel G. S., Pudavar H. E., Lin T. C., He G. S., Swiatkiewicz J., Prasad P. N.: Two-photon properties and excitation dynamics of poly(p-phenylenevinylene) derivatives carrying phenylanthracene and branched alkoxy pendants. *The Journal of Physical Chemistry. A*, **106**, 7512–7520 (2002).
- [25] Hohenau A., Cagran C., Kranzelbinder G., Scherf U., Leising G.: Efficient continuous-wave two-photon absorption in para-phenylene-type polymers. *Advanced Materials*, **13**, 1303–1307 (2001).
- [26] Benschafut R., Rabinovitz M., Dee-Noor-Barzilay Z., Meijere A.: Metal reduction of di- and trisubstituted styrylbenzenes: formation of the highly charged tetra- and hexaanions. *Journal of Physical Organic Chemistry*, **12**, 333–339 (1999).
- [27] Malkes L. Y., Kovalenko N. P.: Synthesis of triaryl-substituted 1,3,5-trivinylbenzenes. *Zhurual Obshchei Khimii*, **2**, 297–298 (1966).
- [28] Meier H., Hanold N., Kalbitz H.: Synthesis of hexastyrylbenzenes. *Synthesis*, **3**, 276–278 (1997).
- [29] He G. S., Yuan L. X., Cheng N., Bhawalkar J. D., Prasad P. N., Brott L. L., Clarson S. J., Reinhardt B. A.: Nonlinear optical properties of a new chromophore. *Journal of the Optical Society of America B: Optical Physics*, **14**, 1079–1087 (1997).
- [30] Miller T. M., Neenan T. X., Zayas R., Bair H. E.: Synthesis and characterization of a series of monodisperse, 1,3,5-phenylene-based hydrocarbon dendrimers including C₂₇₆H₁₈₆ and their fluorinated analogues. *Journal of American Chemical Society*, **114**, 1018–1025 (1992).
- [31] Greenwald R., Chaykovsky M., Corey E. J.: The Wittig reaction using methylsulfinyl carbanion-dimethyl sulfide. *Journal of Organic Chemistry*, **28**, 1128–1129 (1963).
- [32] Alipour M., Massoumi B., Safa K. D., Entezami A. A.: Living radical polymerization of methyl methacrylate, methyl acrylate and their block copolymers with acrylonitrile by atom-transfer radical polymerization. *Iranian Polymer Journal*, **10**, 99–106 (2001).

Optimization of synthetic conditions CMC-g-poly (acrylic acid)/Celite composite superabsorbent by Taguchi method and determination of its absorbency under load

A. Pourjavadi*, M. S Amini-Fazl, M. Ayyari

Polymer Research Laboratory, Department of Chemistry, Sharif University of Technology, Azadi Ave.,
P.O.Box 11365-9516, Tehran, Iran

Received 21 April 2007; accepted in revised form 17 June 2007

Abstract. A novel biopolymer-based composite hydrogel was synthesized through chemical crosslinking by graft copolymerization of partially neutralized acrylic acid onto the carboxymethyl cellulose (CMC). The Taguchi method, a robust experimental design, was employed for the optimization of the synthesis based on the swelling capacity of the hydrogels. This method was applied for the experiments and standard L16 orthogonal array with five factors and four levels. In the synthesis of the composite superabsorbent, N,N'-methylene bisacrylamide (MBA) as crosslinker, ammonium persulfate (APS) as initiator, acrylic acid (AA) as monomer, CMC/Celite weight ratio and neutralization percent (NU) were used as important factors. From the analysis of variance of the test results, the most effective factor controlling equilibrium swelling capacity was obtained and maximum water absorbency of the optimized final product was found to be 310 g/g. The surface morphology of the gel was examined using scanning electron microscopy. Furthermore in this research, swelling capacity of composite SAPs was determined under realistic condition (saline solution absorbency under load).

Keywords: *polymer gels, Taguchi method, absorbency under load*

1. Introduction

Superabsorbent polymer (SAP) hydrogels are special polymeric materials that can absorb large amounts of water, saline solutions or physiological fluids as high as 10–1000 times their own weight due to a considerable amount of hydrophilic groups in their structure. The super-swelling characteristics of SAPs make them ideal for use in water absorbing applications such as disposable diapers, feminine napkins, and agriculture, cosmetic and absorbent pads [1–3]. Because of their exceptional properties, i. e. biocompatibility, biodegradability, renewability, and non-toxicity, polysaccharides and proteins are the main part of the natural-based superabsorbent hydrogels. The higher production cost and low gel strength of these superabsorbents,

however, restrict their wide application. To improve these limitations, inorganic compounds with low cost can be used. The introduction of inorganic fillers to a polymer matrix increases its strength and stiffness properties. Recently, much attention has been paid to inorganic materials for the preparation of superabsorbent composites, such as montmorillonite [4, 5], attapulgite [6, 7], kaolin [8, 9], mica [10, 11], bentonite and sercite [12, 13]. Mineral powders of Celite are hydrated layered aluminosilicates with reactive –OH groups on the surface. Celite powder can be dispersed to some extent in water and cross-linked with acrylic acid and CMC. The interaction of mineral powders, reactive site of natural polymers and monomers result in a superabsorbent composite.

*Corresponding author, e-mail: purjavad@sharif.edu
© BME-PT and GTE

To optimize the affecting variables on swelling capacity of SAPs, Taguchi method can be used [14]. The Taguchi method [15] is a powerful design of experiments tool developed by G. Taguchi. It provides a simple, efficient, and systematic approach to optimize designs for performance, quality, and cost. The parameter design is the key step in the Taguchi method to achieve high quality without increase in cost and the same is adopted in this article. The evaluation of results has been standardized by this method, which can easily be applied by researchers. Among other advantages of the Taguchi method, one can name the possibility of performing experiments in a parallel form [16–19].

There are few studies on the swollen gel strength consideration. When the superabsorbents are under load, the swelling capacity is decreased, so another parameter, i. e. absorbency under load (AUL) is often defined and reported especially in technical data. Although the values of load-free absorbency (free swelling) are usually given in the basic scientific literature, the more realistic values, i. e. AUL are often reported in the technical data sheets and patent articles [20]. Since AUL values are logically changed in proportion to mechanical strength of the swollen gel, AUL can be considered as a measure of the gel strength of SAPs. So, many efforts have been made to achieve superabsorbents having higher AUL or higher strength of the swollen gel [20–22].

Achieving the composite hydrogels with high absorption capabilities has been attempted by researchers. Therefore, optimization of the operational conditions for synthesis in order to prepare samples with high water absorbency is of high importance. Therefore, in this work, optimization of synthesis conditions of a superabsorbent composites based on CMC in the presence of Celite particles to achieve maximum water absorbency was performed by Taguchi method. Also swelling capacity of composite SAPs was determined under realistic conditions (saline solution absorbency under load).

2. Experimental

2.1. Materials

The polysaccharide carboxymethyl cellulose (CMC) with a degree of substitution (D.S) 0.52 was purchased from Merck and Celite (from Khorassan

Co., Iran.) N,N'-methylene bisacrylamide (MBA, from Fluka), ammonium persulfate (APS, from Fluka), acrylic acid (AA, from Merck) were of analytical grade and used without further purification. All other chemicals were also analytical grade. Double distilled water was used for the hydrogel preparation and swelling measurements.

2.2. Instrumental analysis

Samples were characterized as KBr pellets using a Mattson-1000 FTIR spectrophotometer. Morphology of the dried gel structures was studied by scanning electron microscopy (SEM). Dried superabsorbent powders were coated with thin layer gold and imaged in a SEM instrument (Leo, 1455 VP).

2.3. Experimental design

2.3.1. Selection of factors and their levels

According to the basic knowledge of composite hydrogels, the concentration of crosslinking agent (MBA), initiator (APS) and monomer (AA), and neutralization percent (NU), CMC/Celite weight ratio are the key synthesis factors affecting the final swelling properties of the hydrogels. These parameters were varied at four levels as shown in Table 1. The applied ranges of the variables were chosen based on the literature and our preliminary experiments.

Table 1. Experimental control factors and their levels

Control factors	Level-1	Level-2	Level-3	Level-4
MBA [mol/l]	0.004	0.009	0.016	0.048
APS [mol/l]	0.005	0.010	0.016	0.021
CMC/Celite	1/0.25	0.75/0.5	0.5/0.75	0.25/1
AA [mol/l]	0.60	0.92	1.23	1.54
NU %	20	50	70	100

2.3.2. Selection of orthogonal array and assignment of factors

Standard tables known as orthogonal arrays (OA) are used to design the experiments in the Taguchi method. An OA with a four level and five factors are shown in Table 2. This OA is particularly designed with the symbol of L16. Each row in the array represents a trial condition with the factor levels, which are indicated by the numbers in the row. The columns correspond to the factors specified in this study, and each column contains four level 1, four level 2, four level 3, and four level 4 condi-

Table 2. Experimental layout of an L16 orthogonal array according to Taguchi’s suggestion

Trial number	Factors and their levels				
	F1	F2	F3	F4	F5
1	1	1	1	1	1
2	1	2	2	2	2
3	1	3	3	3	3
4	1	4	4	4	4
5	2	1	2	3	4
6	2	2	1	4	3
7	2	3	4	1	2
8	2	4	3	2	1
9	3	1	3	4	2
10	3	2	4	3	1
11	3	3	1	2	4
12	3	4	2	1	3
13	4	1	4	2	3
14	4	2	3	1	4
15	4	3	2	4	1
16	4	4	1	3	2

tions (a total of 16 conditions) for the factors assigned to the column. Therefore, the evaluation of results has been standardized by this method, which can easily be applied by researchers. In this article, the results were analyzed statistically by the analysis of variance (ANOVA) method using Qualitek-4 software.

2.4. Graft copolymerization

Various amounts of CMC (0.25–1 g) were dissolved in 25 ml distilled water and were added to a three-necked reactor equipped with a mechanical stirrer (Heidolph RZR 2021, three blade propeller type, 200 rpm). The reactor was immersed in a thermostatted water bath preset at 80°C. After complete dissolution of CMC, various amounts of Celite powder (0.25–1 g in 5 ml water) were added to the solution and allowed to stir for 10 min. Then, certain amounts of AA (2–5 ml) and MBA (0.03–0.4 g in 5 ml water) were added to the reaction mixture and allowed to stir for 5 min. Then the initiator solution (0.05–0.2 g APS in 5 ml water) was added to the mixture. After stirring for 5 min, the completion of the reaction, to neutralize (20–100%) acrylic groups, appropriate amount of NaOH (0.22–2.75 gr in 5 ml water) was added. The obtained gel was poured to excess nonsolvent ethanol (200 ml) and remained for 3 h to dewater. Then ethanol was decanted, and the product was cut into small pieces (diameter 5 mm). Again, 200 ml fresh ethanol was added, and the hydrogel

was stored for a week. The dried gel particles were filtered and placed in an oven at 55°C for a week. After grinding, the powdered composite superabsorbent hydrogel was stored away from moisture, heat, and light.

2.5. Swelling measurements

An accurately weighed sample (0.1± 0.01 g) of the powdered composite with average particle sizes between 40 and 60 mesh (250–400 μm) was immersed in 200 ml distilled water for 3 h. The equilibrium swelling (ES) capacity was measured at room temperature by ‘tea bag’ method and using the Equation (1):

$$ES [g/g] = \frac{\text{weight of swollen gel} - \text{weight of dried gel}}{\text{weight of dried gel}} \tag{1}$$

2.6. Measurement of AUL

A macro-porous sintered glass filter plate (porosity # 0, *d* = 80 mm, *h* = 7 mm) was placed in a Petri dish (*d* = 118 mm, *h* = 12 mm), and a weighed, dried SAP sample (0.1±0.01 g) was uniformly placed on the surface of a polyester gauze located on the sintered glass. A cylindrical solid weight (Teflon, *d* = 60 mm, variable height) which could slip freely in a glass cylinder (*d* = 60 mm, *h* = 50 mm) was used to apply the desired load (applied pressure 6205 Pa) to the dry SAP particles Figure 1. Then, 0.9% saline solution was added so that the liquid level was equal to the height of the sintered glass filter. The dish and its contents were covered to prevent surface evaporation and probable change in the saline concentration. After

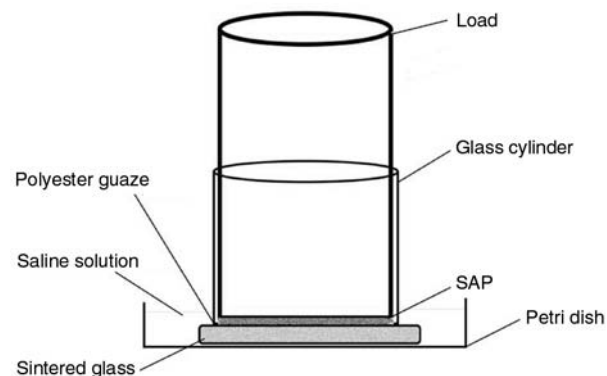


Figure 1. Scheme of the absorbcency under load (AUL) tester

150 min, the swollen particles were weighed again and AUL was calculated using the Equation (2):

$$\text{AUL } [\text{g/g}] = \frac{W_2 - W_1}{W_1} \quad (2)$$

where W_1 and W_2 denote the weight of dry superabsorbent and swollen hydrogel, respectively.

3. Results and discussion

3.1. Synthesis and characterization

Graft copolymerization of acrylic acid onto carboxymethyl cellulose was carried out in the presence of a crosslinking agent (MBA), powdery Celite and ammonium persulfate as an initiator. The persulfate decomposes on heating and produces sulfate anion-radicals that abstract hydrogen atoms from the hydroxyl groups of CMC backbones. This redox system results in active centers capable of radically initiating the polymerization of acrylic acid, leading to a graft copolymer. Since a crosslinking agent (MBA) is present in the system, the copolymer comprises a crosslinked structure. Celite powder cross-links with the acrylic acid and the CMC. The carboxylate groups of the grafted poly (acrylic acid) can react with the –OH groups on the Celite surface. The substitution of –OH groups in the surface of Celite by carboxylate groups results in the ester formation. The clay in the polymerization reaction can be considered as acting in one or both of two ways: a) The Celite particles act as a crosslinking agent. This means that the carboxylate groups of the sodium poly (acrylate) chains react with Celite. b) Celite particles prevent the polymer chains from growing by a chain transfer mechanism [10].

3.1.1. Infrared spectroscopic analysis

FT-IR spectroscopy was used for identify the product. The FT-IR spectra of the initial substrates and CMC-g-poly (sodium acrylate)/Celite composite are depicted in Figure 2. Figure 2a represents the spectrum of Celite. The bands at 1080 cm^{-1} could be attributed to the stretching of the siloxane (–Si–O–Si–) group, and this was confirmed by the –Si–O–Si– bending vibration at 481 cm^{-1} . The band at 790 cm^{-1} was attributed to SiO–H vibration [23, 24].

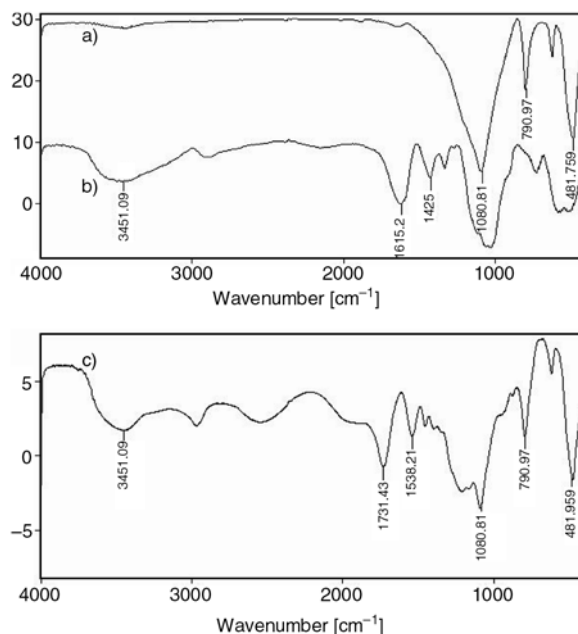


Figure 2. FT-IR spectra of (a) Celite, (b) CMC, (c) CMC-g-poly (sodium acrylate)/Celite composite

In the spectrum of CMC Figure 2b two strong peaks were observed at 1615 and 1425 cm^{-1} due to the asymmetrical and symmetrical stretching of COO^- groups. Characteristic absorption peak of CMC appeared at 3451 cm^{-1} for the hydroxyl group.

Figure 2c shows the FT-IR spectrum of CMC-g-poly (sodium acrylate)/Celite composite. Two new absorption peaks appeared at 1731 and 1538 cm^{-1} may be attributed to the reaction between carboxylate groups of CMC and acrylic acid with hydroxyl groups on Celite.

3.2. Optimization of the grafting conditions

The relationship between the swelling ratio and network structure parameters given by Flory [25] is usually used as the Equation (3):

$$q_m^{5/3} = \frac{\left(\frac{i}{2\nu_u S^{*1/2}} \right)^2 + \frac{1 - \chi_1}{\nu_1}}{\frac{\nu_e}{V_0}} \quad (3)$$

where q_m is swelling ratio; i/ν_u is the concentration of the fixed charge of the unswollen networks; S^* is the ionic strength of the swollen solution; ν_e/V_0 is the crosslinking density which refers to the number of effectively crosslinked chains in unit volume.

The term $(1/2 - \chi_1)/v_1$ stands for the network-medium affinity.

According to Equation (3), there are many variables affecting the ultimate swelling capacity. Some of these variables have been selected in this research. These parameters and the related levels are presented in Table 1. After selecting the mentioned variables, an OA table was formed by Qualitek-4 software (Table 2). The experimental layout after assigning the values of the parameters is shown in Table 3. According to Table 3, 16 experiments were carried out and the ES capacities were measured. The test results are shown in Table 4. Having used the Qualitek-4 software, the optimized circumstances and the contribution of each factor are obtained by ANOVA analysis. It should be emphasized that the interaction between the variables were neglected. The optimized values of the ES capacity, MBA, APS, AA concentration, CMC/ Celite and NU % are 310 g/g, 0.004 mol/l, 0.016 mol/l, 1.54 mol/l, 0.25/1 gr, 50% respectively.

After conducting the synthesis of hydrogel with above optimized reaction composition for three times and measuring the ES capacities, following data were obtained: 315, 310, 308 (g water/g dried gel). Observed slight errors can be attributed to applied materials and apparatus for the synthesis.

Table 3. Experimental layout after assigning the values of the parameters

Trial	MBA	APS	CMC/Celite	AAc	Nu
1	0.004	0.005	1/0.25	0.60	20
2	0.004	0.010	0.75/0.5	0.92	50
3	0.004	0.016	0.5/0.75	1.23	70
4	0.004	0.021	0.25/1	1.54	100
5	0.009	0.005	0.75/0.5	1.23	100
6	0.009	0.010	1/0.25	1.54	70
7	0.009	0.016	0.25/1	0.60	50
8	0.009	0.021	0.5/0.75	0.92	20
9	0.016	0.005	0.5/0.75	1.54	50
10	0.016	0.010	0.25/1	1.23	20
11	0.016	0.016	1/0.25	0.92	100
12	0.016	0.021	0.75/0.5	0.60	70
13	0.048	0.005	0.25/1	0.92	70
14	0.048	0.010	0.5/0.75	0.60	100
15	0.048	0.016	0.75/0.5	1.54	20
16	0.048	0.021	1/0.25	1.23	50

Table 4. Experimental results for equilibrium swelling (ES) capacity

Trial number	1	2	3	4	5	6	7	8	9	10	11	12	13	14	15	16
ES [g/g]	96	171	205	289	95	94	239	101	115	43	65	85	39	59	31	30

The contribution of factors according to ANOVA table derived for this study is as shown in Table 5. It can be seen from the ANOVA results that the most effective factor is MBA concentration.

To determine the swelling capacity of composite SAPs under realistic condition, gels of different water absorbance capacity were used, selected samples exhibited heighten absorbency (optimized final product), medium absorbency (sample 6), and the lowest absorbency (sample 16) that had already absorbed saline solution under 6205 Pa load.

As shown in Figure 3. The minimum time needed for the highest AUL in the case of each load was determined to be 150 min. After this time, the AUL values remained unchanged. In addition, AUL decreases with the increase in loading, as expected (data are not shown). The most important factor among these forces is the ionic interaction due to the presence of mobile ions such as Na⁺ and K⁺ in the superabsorbent network structure. These mobile ions cannot leave the network due to the charge equilibrium in the gel phase. The presence

Table 5. The results of analysis of variance

Factor	Degree of freedom	Sum. of square	Contribution of factor [%]
MBA [mol/l]	1	51881.25	57.09
APS [mol/l]	3	7108.25	7.93
CMC/Celite [g/g]	4	14394.75	16.06
AA [mol/l]	4	4551.25	5.07
NU %	2	11666.25	13.02

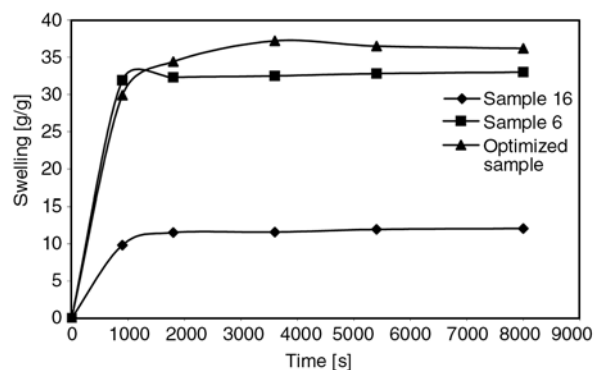


Figure 3. Time dependence of the AUL values for the different water absorbance. capacities (highest absorbency (optimized final product), medium absorbency (sample 6), and the lowest absorbency (sample 16) swollen in saline solution (Under pressure 6205 Pa)

of charges in the SAP structure causes an osmotic pressure difference between the gel and the solvent phase. This pressure difference produces a strong driving force to diffuse solvent to the gel phase. The diffusion process continues until the osmotic pressure difference becomes zero. The osmotic pressure difference is reduced in salt solutions, which leads to less swelling in comparison with distilled water. Solvent acts like a plasticizer for the polymer. It is well known that the higher the plasticizer content, the lower the elastic modulus will be.

3.3. Scanning electron microscopy

Hydrogels water absorbency and its retention rate depend on hydrogel porosity and mean pore size. Hence, one of the most important properties, which should be considered, is hydrogel microstructure morphologies. This porous micro structure brings about an increased surface area and capillary effect [26]. Figure 4 shows the SEM photographs of CMC and optimized final product. These pictures verify

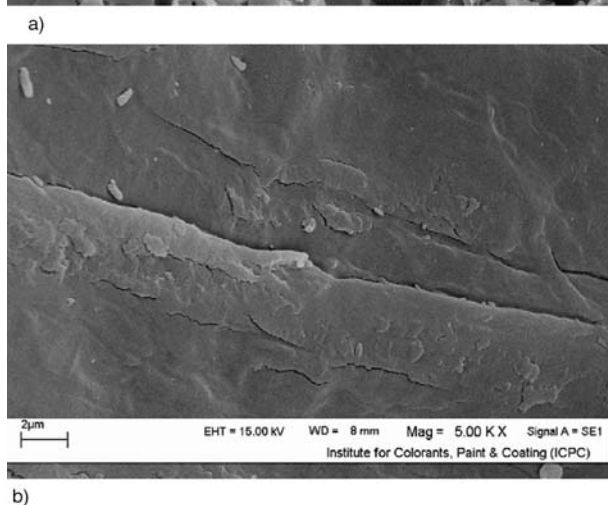
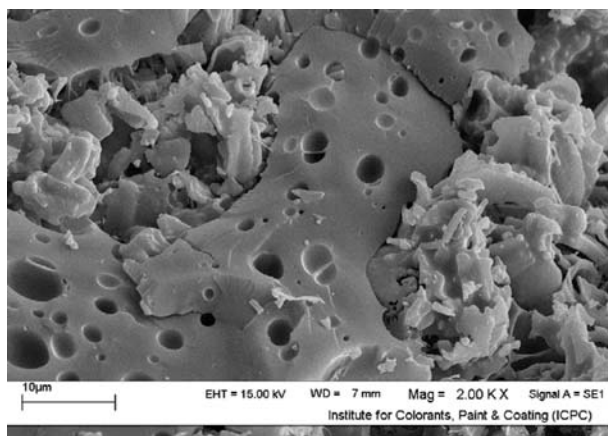


Figure 4. SEM photographs of optimized final product (a) and CMC (b)

that graft copolymers have a porous structure. It is supposed that these pores are the regions of water permeation and interaction sites of external stimuli with the hydrophilic groups of the graft copolymers.

4. Conclusions

In this work, a novel composite hydrogel, CMC-g-poly (acrylic acid)/Celite composite was prepared by graft copolymerization of AA onto CMC backbones in the presence of a crosslinking agent and powdery Celite. The synthesis conditions of superabsorbent hydrogel were optimized by Taguchi method. The maximum water absorbency (310 g/g) was achieved among the different variables; the MBA concentration had the greatest effect on the results. The Taguchi method was found to be promising tool to obtain the optimum conditions for such studies. The absorbency under load (AUL) data is usually given in the patent literature and technical data sheets offered by industrial SAP manufacturers. Swelling capacity of composite SAPs (absorbed saline solution under pressure of 6205 Pa) was measured at 25°C.

References

- [1] Buchholz F., Graham T.: Modern superabsorbent polymer technology. Wiley, New York (1998).
- [2] Kudelia V.: Encyclopedia of polymer science and engineering. Wiley, New York (1985).
- [3] Pó R.: Water-absorbent polymers: A patent survey. *Journal of Macromolecular Science-Polymer Review*, **34**, 607–662 (1994).
- [4] Lee W-F., Yang L-G.: Superabsorbent polymeric materials. XII. Effect of montmorillonite on water absorbency for poly (sodium acrylate) and montmorillonite nanocomposite superabsorbents. *Journal of Applied Polymer Science*, **92**, 3422–3429 (2004).
- [5] Kabiri K., Zohuriaan-Mehr M.: Porous superabsorbent hydrogel composites: synthesis, morphology and swelling rate. *Macromolecular Materials and Engineering*, **289**, 653–661 (2004).
- [6] Li A., Wang A.: Synthesis and properties of clay-based superabsorbent composite. *European Polymer Journal*, **41**, 1630–1637 (2005).
- [7] Zhang J., Chen H., Wang A.: Study on superabsorbent composite. III. Swelling behaviors of polyacrylamide/attapulgite composite based on acidified attapulgite and organo-attapulgite. *European Polymer Journal*, **41**, 2434–2435 (2005).

- [8] Pourjavadi A., Amini-Fazl M. S., Ayyari M.: Taguchi optimized synthesis of collagen-g-poly (acrylic acid)/kaolin composite superabsorbent hydrogel. *European Polymer Journal*, submitted (2007).
- [9] Wu J., Wei Y., Lin J., Lin S. B.: Study on starch-graft-acrylamide/mineral powder superabsorbent composite. *Polymer*, **44**, 6513–6520 (2003).
- [10] Lin J., Wu J., Yang Z., Pu M.: Synthesis and properties of poly (acrylic acid)/mica superabsorbent nanocomposite. *Macromolecular Rapid Communications*, **22**, 422–424 (2001).
- [11] Lee W-F., Chen Y-C.: Effect of intercalated reactive mica on water absorbency for poly (sodium acrylate) composite superabsorbents. *European Polymer Journal*, **41**, 1605–1612 (2005).
- [12] Santiago F., Mucientes A., Osorio M., Rivera C.: Preparation of composites and nanocomposites based on bentonite and poly(sodium acrylate). Effect of amount of bentonite on the swelling behaviour. *European Polymer Journal*, **43**, 1–9 (2007).
- [13] Wu J., Lin J., Zhou M., Wei C.: Synthesis and properties of starch-graft-polyacrylamide/clay superabsorbent composite. *Macromolecular Rapid Communications*, **21**, 1032–1034 (2000).
- [14] Roy R. K.: *Design of experiments using the Taguchi approach*. Wiley, New York (2001).
- [15] Garcia-Diaz A., Philips D.: *Principles of experimental design and analysis*. Chapman and Hall, London (1995).
- [16] Montgomery D. C.: *Design and analysis of experiments*. Wiley, New York (2001).
- [17] Johnson R.: *Miller and Freund's probability and statistics for engineers*. Prentice-Hall of India, New Delhi (2001).
- [18] Ross P.: *Taguchi techniques for quality engineering*. McGraw-Hill, New York (1989).
- [19] Qin J.: Process for the preparation of modified polysaccharides having improved absorbent properties. US Patent 5470964, USA (1995).
- [20] Ramazani-Harandi M., Zohuriaan-Mehr M., Yousefi A., Ershad-Langroudi A., Kabiri K.: Rheological determination of the swollen gel strength of superabsorbent polymer hydrogels. *Polymer Testing*, **25**, 470–474 (2006).
- [21] Kabiri K., Zohuriaan-Mehr M.: Superabsorbent hydrogel composites. *Polymers for Advanced Technologies*, **14**, 438–444 (2003).
- [22] Ma S., Liu M., Chen Z.: Preparation and properties of a salt-resistant superabsorbent polymer. *Journal of Applied Polymer Science*, **93**, 2532–2541 (2004).
- [23] Qi X., Liu M., Chen Z., Liang R.: Preparation and properties of diatomite composite superabsorbent. *Polymers for Advanced Technologies*, **18**, 184–193 (2007).
- [24] Khraisheh M. A. M., Allenb S. J., Al-Ghouti M. A., Ahmadb M. N.: Effect of OH and silanol groups in the removal of dyes from aqueous solution using diatomite. *Water Research*, **39**, 922–932 (2005).
- [25] Flory P. J.: *Principles of polymer chemistry*. Cornell University Press, New York (1953).
- [26] Lim D-W., Yoon K-J, Ko S-W.: Synthesis of AA-based superabsorbent interpenetrated with sodium PVA sulfate. *Journal of Applied Polymer Science*, **78**, 2525–2532 (2000).

Preparation of vinyl chloride – vinyl ether copolymers via partial etherification from PVC

H. Mekki*, M. Belbachir

Laboratoire de Chimie des Polymères, Département de Chimie, Faculté des Sciences, Université d'Oran Es-Senia, BP N° 1524, El M' Naouer, Oran 31000, Algérie

Received 2 April 2007; accepted in revised form 21 June 2007

Abstract. The chemical modifications of poly (vinyl chloride) with aliphatic and aromatic alcohols compounds have been investigated at room temperature and atmospheric pressure, catalysed by a new green basic catalyst, the Maghnite-K⁺. The presence of ether groups in the products is proven by infra red spectroscopy (IR) as well as by nuclear magnetic resonance spectroscopy (¹H NMR), and characterized by intrinsic viscosity as well as by gel permeation chromatography (GPC).

Keywords: polymer membranes, Maghnite-K, PVC, grafting copolymers, Algerian clay, basic catalyst

1. Introduction

The purpose of this work was to highlight the chemical interaction of poly (vinyl chloride) with diverse alcohols and trying to introduce them onto polymer chain.

PVC is one of the most important commercial polymers due to its low production costs and its excellent stability to acids and bases [1]. However, there is some shortcoming such as limited thermal and mechanical stability or sensitivity to ultraviolet radiation [2].

By chemical modifications reactions of PVC with appropriate compounds, new polymers with improved physical properties can be obtained [3, 4].

The nucleophilic substitution of chlorine atoms with thiophenolate [1], amine [5] and thiol [6] has been intensively studied in recent years.

On the other hand, it has recently been shown [6, 7] that PVC can also be used as an interesting starting membrane material for gas separation when the polymer is chemically modified.

In the present communication, we show that reaction of PVC with alcohols catalysed by Maghnite-K⁺ in THF solution gives a new white copolymer (VC-Ether) product which is soluble in DMF, DMSO, partially soluble in toluene and chloroform and insoluble in pentane and water.

2. Experimental part

2.1. Materials

1. Commercial bulk polymerized PVC was obtained from ENIP (Skikda Algeria, type 4000M Kwert = 65–66), its average molecular weights determined by Gel Permeation Chromatography were $M_w = 149\,000$ g/mole and $M_n = 71\,700$ g/mole. It was used as the base polymer.
2. Tetrahydrofuran, ethanol and pentane were supplied from Prolabo (Paris, France) and used as good solvent and nonsolvents respectively.
3. Ethanol (Prolabo, France), ethylene glycol (Merck) and phenol (Fluka) were used as reagents.

*Corresponding author, e-mail: Hafida_mekki@yahoo.com
© BME-PT and GTE

4. The preparation of Maghnite-K was carried out with the method described by Belbachir and coworkers [8–11], using 100 g of the raw Algerian clay (Maghnia; West Algeria) and 20 g of potassium hydroxide (KOH, Fisher Scientific). It was crushed for 20 min with a Prolabo ceramic balls grinder, then dried through baking at 105°C for 2 h and cooled to room temperature.

2.2. Modifications of PVC

PVC (3 g; 48 mmole) was dissolved in 30 ml of THF (solution 1).

48 mmole from each alcohol (ethanol 2.2 g, ethylene glycol 3 g and phenol 4.5 g) was mixed each one with 3 g of Maghnite-K and agitated for 15 minutes at room temperature and added to the solution 1.

After 4 hours the reactions were stopped, filtered and precipitated in cold ethanol. The modified polymers were purified using THF/Pentane (for sample with ethanol: copolymer 1) and THF/Ethanol (for sample with ethylene glycol: copolymer 2, and phenol: copolymer 3).

The yield of the grafted PVC was optimized after 4 hours, and it was been between 50 and 83%.

2.3. Test methods

¹H NMR spectra were recorded at room temperature, on a 300 MHz Bruker Avance spectrometer, using deuterated DMSO or chloroform. as solvents. FT-IR measurements were performed on thin cast films of polymers using ATI MATTSON FT-IR spectrometer.

GPC measurements of the grafted PVC samples were carried out using a WISP 712, Waters Associates chromatograph, THF was used as solvent and the instrument was calibrated to a first approximation with polystyrene of known molecular weights. The flow rate of tetrahydrofuran was 10 ml/min.

Intrinsic viscosity measurements were performed on SEMATECH Viscologic TI 1 apparatus at 25°C using THF as solvent.

3. Results and discussion

Reaction of PVC with various alcohols in a THF solution gives primarily the corresponding copolymers in high transformation yield (Figure 1). The

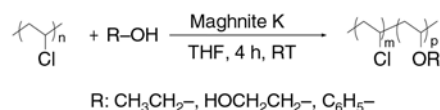


Figure 1. Grafting of PVC with various alcohols using Maghnite-K

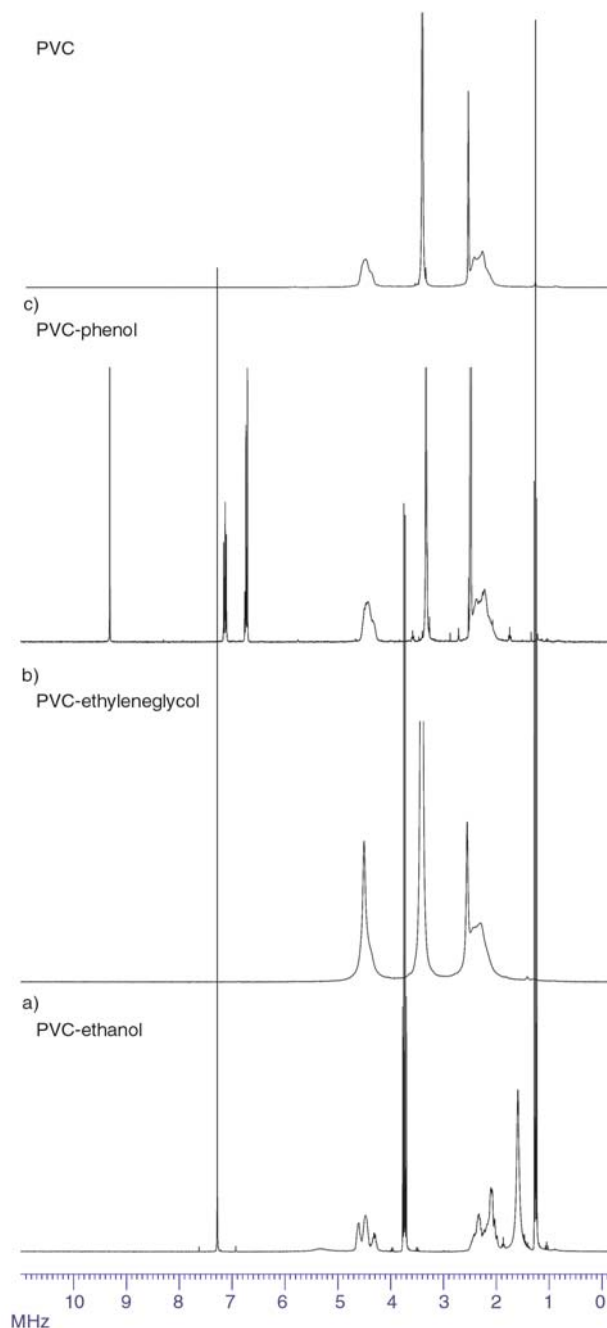


Figure 2. ¹H NMR spectra of alcohols grafting on PVC. a) PVC-g-ethanol (CDCl₃), b) PVC-g-ethylene glycol (CDCl₃) and c) PVC-g-phenol (DMSO-d₆)

resulting products are soluble in many organic solvents such as ethyl acetate, DMF, DMSO and THF. PVC itself is not soluble in ethyl acetate.

3.1. Characterizations of modified PVC

The modification reactions were performed as indicated in experimental part section.

Samples were withdrawn, purified and analysed by ¹H NMR spectroscopy.

In Figure 2 the corresponding spectra of the modified PVCs are shown. With the appearance of alcohols proton peaks [7, 12].

1. In copolymer 1 (Figure 2a) two signals at 1.24 ppm and 3.73 ppm corresponding to CH₃ and CH₂ of ethanol respectively arise.
2. In copolymer 2 (Figure 2b) a signal at 3.74 ppm appear corresponding to CH₂ of ethylene glycol.
3. In copolymer 3 (Figure 2c) aromatic's signal (6.7–7.2 ppm) are appeared.

The variation of the chemical structure through the grafting of various alcohols onto the PVC was confirmed by FT-IR as shown in Figure 3.

The most significant change in each spectra of the grafted PVC was the appearance of the red-shifted (1042–1047 cm⁻¹) absorption band due to the C–O stretching vibration of ethers.

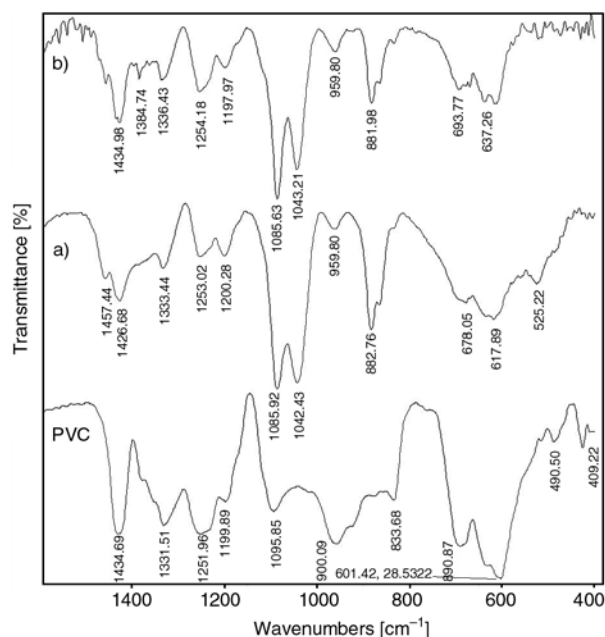


Figure 3. FT-IR spectra of alcohols grafting on PVC. a) PVC-g-ethanol and b) PVC-g-ethylene glycol

Table 1. *M_n*, *M_w*, *I*, intrinsic viscosity and color of copolymer 1, 2 and 3

Samples	<i>M_n</i> ^a	<i>M_w</i> ^a	<i>I</i> ^b	Intrinsic viscosity ^c [ml/g]	Color
PVC	71 700	149 100	2.00	8.12	white
Copolymer 1	76 400	159 600	2.09	8.65	white
Copolymer 2	89 500	172 300	1.90	14.74	white
Copolymer 3	25 800	43 200	1.57	nd	yellow

nd: not determined

^adetermined by GPC with polystyrene standard; ^b*I* – polydispersity index (*M_w*/*M_n*); ^cin THF at 25°C

Also, the major characteristic peaks for PVC appeared at 720, 760, 800 cm⁻¹ representing C–Cl stretching bands.

It is important to note that, GPC analysis of the PVC and various copolymers shows a sharp decrease in the molecular weight in relation to that of the starting PVC in sample with phenol, and outstanding increase in sample with ethanol, a light increase in sample with ethylene glycol, as shown in Table 1.

Also comparison of the intrinsic viscosities (Table 1) of PVC and copolymers 1, 2 and 3 shows a same variations during modification with ethanol, ethylene glycol and phenol. At the moment it is not possible to suggest a mechanism for this process which appears to take place under very mild conditions. Further work is necessary to shed light on this.

4. Conclusions

This study reveals that:

PVC can be chemically modified by various alcohols using Maghnite-K⁺ as catalyst without appreciable dehydrochlorination.

The PVC modified with alcohols is not explosive under ambient conditions.

The conversion rate of PVC to copolymer (VC-Ether) product is high (~63%).

It has been shown that ethanol; ethylene glycol and phenol are appropriate agents to introduce ether groups onto the PVC.

The presence of the ether groups in PVC changes markedly the chemical and physical properties of the systems.

Acknowledgements

We are grateful to Professor Samuel Lesko (Veeco Metrology Group, Dourdan, France) for the AFM analysis, Professor Alain Rameau (institut Charles Sadron, Strasbourg, France) for the GPC analysis and Malika Akeb, (LCP, universit  d'Oran, Alg rie) for the NMR analysis of copolymers.

References

- [1] Reinecke H., Mijangos C.: Synthesis and characterization of poly(vinyl chloride)-containing amino groups. *Polymer*, **38**, 2291–2294 (1997).
- [2] Kim D S., Kang J S., Kim Y. K., Lee Y. M.: Surface modification of a poly (vinyl chloride) membrane by UV irradiation for reduction in sludge adsorption. *Desalination*, **146**, 301–305 (2002).
- [3] Anzai. J. I., Liu. C. C.: Potentiometric response of PVC/crown ether membrane electrodes to nonionic organic compounds. *Sensors and Actuators B: Chemical*, **5**, 171–172 (1991).
- [4] Bromberg L., Levin G., Kedem O.: Transport of metals through gelled supported liquid membranes containing carrier. *Journal of Membrane Science*, **71**, 41–50 (1992).
- [5] Bicak N., Sherrington N. C., Bulbul H.: Vinylamine polymer via chemical modification of PVC. *European Polymer Journal*, **37**, 801–805 (2001).
- [6] Herrero M., Tiemblo P., Reyes-Labarta J., Mijangos C., Reinecke H.: PVC modification with new functional groups. Influence of hydrogen bonds on reactivity, stiffness and specific volume. *Polymer*, **43**, 2631–2636 (2002).
- [7] Tiemblo P., Guzman J., Riande E., Mijangos C., Reinecke H.: Effect of physical aging on the gas transport properties of PVC and PVC modified with pyridine groups. *Polymer*, **42**, 4817–4824 (2002).
- [8] Belbachir M., Bensaoula A.: Composition and method for catalysis using bentonites. U S Patent 7094823, USA (2006).
- [9] Harrane A., Meghabar R., Belbachir M.: Polymerization of ϵ -caprolactone using a montmorillonite clay as catalyst. *Designed Monomers and Polymers*, **8**, 11–24 (2005).
- [10] Yahiaoui A., Belbachir M., Soutif J. C., Fontaine L.: Synthesis and structural analyses of poly (1, 2-cyclohexene oxide) over solid acid catalyst. *Materials Letters*, **59**, 759–767 (2005).
- [11] Reguieg F., Sahli N., Belbachir M., Lutz P. J.: One-step synthesis of bis-macromonomers of poly(1,3-dioxolane) catalysed by maghnite-H⁺. *Journal of Applied Polymer Science*, **99**, 3147–3152 (2006).
- [12] Kennedy J. P., Zhengjie P.: Addition of unsaturated hydrocarbons to poly(vinyl chloride) and functionalization thereof. U S Patent 6831133, USA (2004).

Synthesis, characterization and rheological property of biphenyl-based polyarylene ether nitrile copolymers

X. B. Liu*, R. H. Du, L. L. Hao, S. Wang, G. P. Cao, H. Jiang

Institute of Microelectronic & Solid State Electronic, State Key Laboratory of Electronic Thin Films & Integrated Devices, University of Electronic Science & Technology of China, Chengdu 610054, P.R. China

Received 19 April 2007; accepted in revised form 21 June 2007

Abstract. The high molecular weight biphenyl-based polyarylene ether nitrile copolymers were synthesized by nucleophilic substitution reaction of 2,6-dichlorobenzonitrile (DCBN) with varying molar ratios of 4,4'-dihydroxybiphenyl (BP) and hydroquinone (HQ). The BP content of the copolymers has influence on glass transition temperature (T_g), initial decomposition temperature (T_{id}), mechanical properties and the crystallinity. All the copolymers could be dissolved in NMP, DMF and DMAc on heating, and were stable up to 450°C with a high char yield above 50% at 800°C in nitrogen atmosphere. The glass transition temperature, the melting temperature and tensile strength of copolymers were found to increase with increase in concentration of the BP units in the polymer. The dynamical viscosity and the storage modulus have been influenced by the BP concentration, frequency, temperature and time. This rheological results show that these copolymers have best thermoplastic processability and stability at 300–400°C.

Keywords: polymer synthesis, molecular engineering, thermal properties, rheology, mechanical properties, polyarylene ether nitrile copolymer

1. Introduction

In recent decades, polyarylene ether nitrile (PEN) as special engineering plastics has gained wide applications for its excellent properties in aerospace, electric and automotive industry. Various bisphenols have been studied for synthesis of PEN via nucleophilic aromatic substitution polymerization, these PEN materials exhibit excellent thermal stabilities over a wide-range of temperature [1–6]. The cyano group serves as a potential site for cross-linking reaction and can make polymer transform from thermoplastic to thermosetting [7–11]. Matsuo *et al.* [3] systematically studied the synthesis of 2,6-dihalobenzonitrile with different kinds of bisphenol including the 4,4'-dihydroxybiphenyl and found that mechanical properties of biphenyl-based PEN were better than that of the correspon-

ding ketone or sulfone containing polymers. However the above-mentioned PEN is a homopolymer and insolubility has limited their applications in many areas. Many attempts have been made to improve the solubility of the PEN by copolymerization or incorporation of pendant group [4, 5, 10, 11, 12]. Mechanical property such as elongation is low for PEN homopolymer have limited its applications [3, 6, 12]. In this paper, we report the synthesis of polyarylene ether nitrile copolymers derived from 2,6-dichlorobenzonitrile (DCBN) with hydroquinone (HQ) and 4,4'-dihydroxybiphenyl (BP), and the characterizations of copolymers by thermal properties, mechanical properties and rheological properties.

*Corresponding author, e-mail: Liuxb@ustc.edu.cn
© BME-PT and GTE

2. Experimental

2.1. Materials

2,6-dichlorobenzonitrile, hydroquinone and 4,4'-dihydroxybiphenyl were available commercially and purified by sublimation before use. Anhydrous K_2CO_3 was dried under vacuum at $100^\circ C$ before use. N-methyl pyrrolidone (NMP) was distilled under reduced pressure over calcium hydride and stored over 4 Å molecular sieves.

2.2. Polymer synthesis

The procedure of the synthesis of the PEN copolymer has been described in earlier reports [6], and the structure of the polymer synthesized is shown in Figure 1.

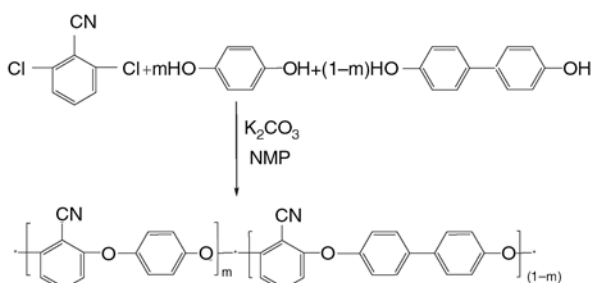


Figure 1. Polymerization of PEN (BP/HQ) copolymer

2.3. Preparation of polymer films

The polymer was dissolved in DMF again to get a solution with 7–10% polymer content. After vigorous stirring, the solution was cast onto a clean glass plate to obtain the film. The film then was heated at elevated temperature to $160^\circ C$ to remove the solvent completely. The films with a thickness of 20–30 μm were obtained.

3. Characterization

Inherent viscosities of the samples were determined at $20^\circ C$ for 0.5% polymer solution in DMF using Ubbelohde viscometer. The FT-IR spectra of the films were recorded using Nicolet 20 SXB-IR spec-

trophotometer. The 1H -NMR and ^{13}C -NMR spectroscopy were recorded using BRUKER AV400 NMR instrument using DMF- d_7 as the solvent. Glass transition temperature (T_g) and melting point (T_m) were measured on TA Instrument Q-100 DSC, at a heating rate of $10^\circ C/min$ under nitrogen atmosphere. The thermogravimetric analysis of the copolymers was carried out under nitrogen atmosphere using TA Instrument Q-50 series thermogravimetric analyzer at a heating rate of $10^\circ C/min$. The wide angle X-ray scattering (WAXD) data were performed at room temperature using a Rigaku DMAX1400 diffractometer (DMAX1400, Rigaku, Japan; $\lambda = 0.15406$ nm) operated at 40 kV and 100 mA with $CuK\alpha$ radiation. The specimens were fixed on the equipment and data were collected with a step interval of $0.02^\circ C$ at a rate of $4^\circ C/min$.

Tensile strength and elongation at break of the films were measured on a SANS mechanical testing instrument (Shenzhen New SANS material testing machine factory, Shenzhen, China), and gained as average value for every five samples. The rheological behaviors of copolymers were carried out using TA instrument AR-G2 oscillatory rheometer with a heating rate of $10^\circ C/min$ under air condition.

4. Results and discussion

Polyarylene ether nitriles copolymers were synthesized by nucleophilic substitution reaction of 2,6-dichlorobenzonitrile with 4,4'-dihydroxybiphenyl and hydroquinone. The molar ratio, yields and inherent viscosity values of the reactions are shown in Table 1.

4.1. Solubility

All samples are insoluble in common organic solvents including dipolar aprotic solvents like DMSO, DMF, DMAc and NMP at room temperature, but three copolymers can dissolve in NMP, DMF and DMAc solvent on heating.

Table 1. Conditions for the synthesis of PEN (BP/HQ)

Sample	Molar ratio (BP:HQ)	Inherent viscosity [g/dl]	Dehydration time [h] at 140 – $160^\circ C$	Polycondensation time [h] at 180 – $200^\circ C$	Yield ratio [%]
PEN-2	25:75	0.86	2.5	4	98.3
PEN-3	50:50	0.91	2.5	4	98.8
PEN-4	75:25	1.21	2.5	4	99.0
PEN-5	100:0	insoluble	2.5	4	98.5

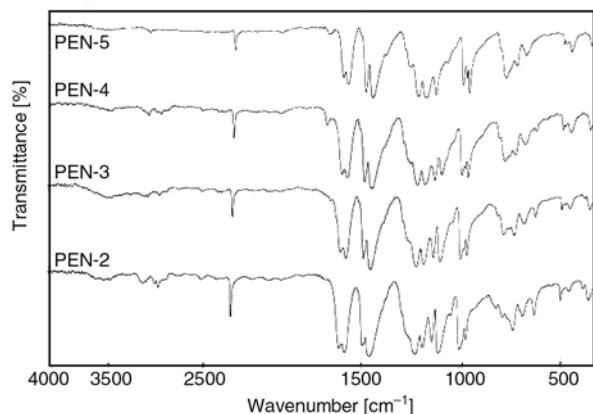


Figure 2. FT-IR spectra of PEN (BP/HQ) polymer

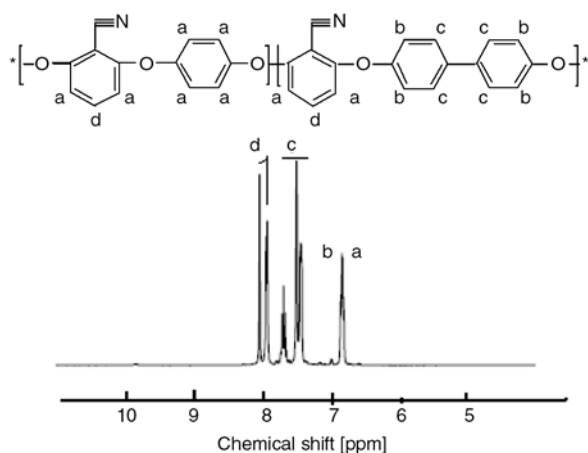


Figure 3. ¹H-NMR spectrum of copolymer PEN-3

4.2. FT-IR and NMR characterization

The structure of the copolymers was characterized with a FT-IR spectroscopy as shown in Figure 2. From top to bottom the five samples have a structure of BP: HQ = 100:0, 75:25, 50:50, and 25:75, respectively. For all polymers, the characteristic stretching vibration absorption of –OH of BP and HQ at 3290 and 3260 cm^{-1} disappeared. The absorption at 2231 cm^{-1} is characteristic symmetrical stretching of CN group. The absorptions at 1247 and 1280 cm^{-1} are assigned to –C–O–C– of BP, and absorption at 1190 cm^{-1} is the characteristic peak of –C–O–C– of HQ, both of them are ortho to CN, respectively. The absorption of CN groups at 2231 decreased with the increase of BP concentration, because of the CN concentration decreased with the increase of BP concentration. Figure 3 and Figure 4 are ¹H-NMR and ¹³C-NMR spectra of copolymer PEN-3 as a typical copolymer sample. The characteristic assignment of ¹H-NMR and ¹³C-NMR peaks are displayed in Figure 3 and Figure 4. The chemical shift (δ , ppm) of ¹H-NMR: 6.8, 7.0 (Ar–O, o), 7.4 (Ar–Ar–O, m), 7.6, 8.0 (Ar–CN, p). The chemical shift (δ , ppm) of ¹³C-NMR: 95 (Ar–CN), 110 (Ar–CN, m), 113 (–CN), 120 (–O–Ar–O, o), 122 (–O–Ar–Ar–O–, m), 128 (–Ar–), 136 (Ar–CN, p), 152 (O–Ar), 155

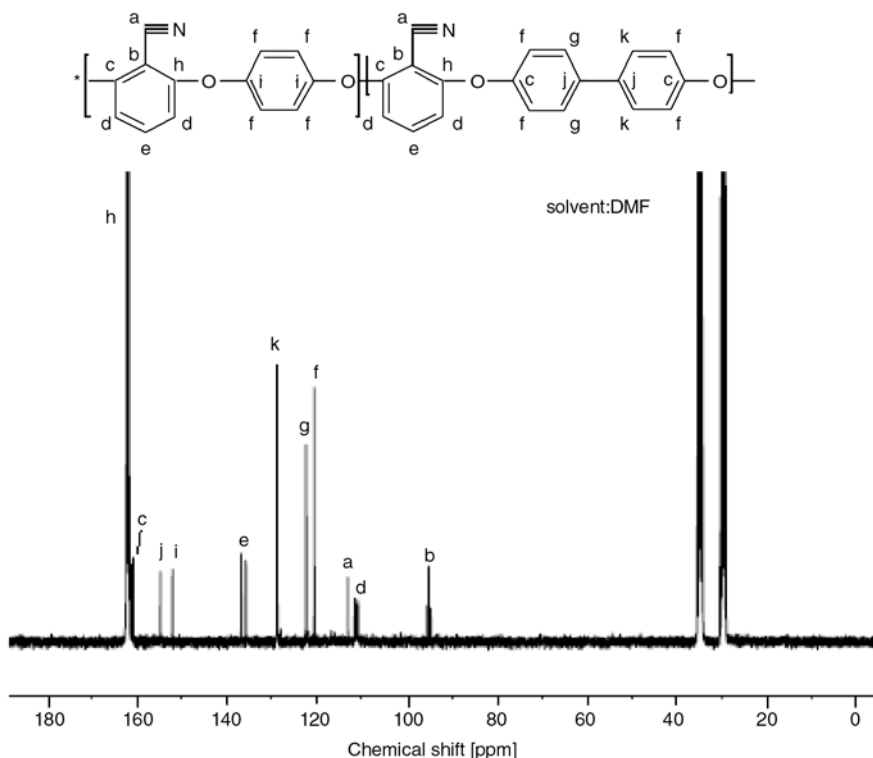


Figure 4. ¹³C-NMR spectrum of copolymer PEN-3

(–O–Ar–Ar–O–, p), 160 (Ar–CN, o), 161 (–O–Ar). From the chemical shift information, the Ar–CN, –Ar– and –Ar–Ar– segments were existed in main chain of PEN. All these information confirmed that BP, DCBN and HQ have reacted as showed in Figure 1.

4.3. Mechanical measurement and analysis

The mechanical measurement such as tensile strength and elongation at break are listed in Table 2. The values of tensile strength increase with the increasing content of BP, which may be attributed to the rigidity brought about by the BP component. The mechanical measurements of the samples also show that tensile strength of PEN (BP/HQ) is higher than that of PEN (RS/HQ) copolymer [6]. The elongation at break of PEN-3 was the highest in all copolymers, which may be attributed to the irregularity in main chain according to the low crystalline behaviors.

4.4. Thermal properties

The glass transition temperatures of the copolymers were calculated from the curves of DSC shown in Figure 5 and Table 2. It can be seen that T_g increases with the increasing BP content in the copolymers, and the T_g of PEN (BP/HQ) copolymers is higher than that of PEN (RS/HQ) [6]. From the Figure 5, PEN-2 and PEN-5 have apparent melting transition, which is 255 and 348°C, respec-

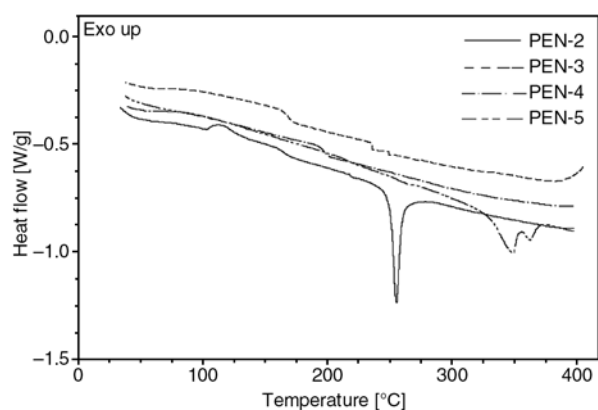


Figure 5. The DSC spectra of PEN(BP/HQ) copolymers

Table 2. Thermal and mechanical property of PEN (BP/HQ) copolymer

Polymer	T_g [°C]	ΔH_g [J/g]	T_m [°C]	ΔH_m [J/g]	T_{id} [°C]	Tensile strength [MPa]	Elongation at break [%]
PEN-2	189	0.19	255	26.1	471	113	7
PEN-3	167	0.32	–	–	511	118	9
PEN-4	201	0.28	325	27.2	495	123	6
PEN-5	216	0.07	348, 352	28.5	520	–	–

tively. But the melting point of PEN-4 is not observed. PEN-5 has double melting transition peaks, which may be contributed to regular macromolecular structure and thermotropic nematic transition. Figure 6 shows the TGA curves of polymers. From Figure 6a, the initial decomposition temperature (T_{id}) of three copolymers is higher than 450°C. The thermal properties of three samples are listed in the Table 2. The T_{id} of BP homopolymer is higher than 500°C, the introduction of HQ decreases T_{id} of the copolymers, but with the HQ content increase, the T_{id} of the copolymer increase again, which could be attributed to the decrease of distance between CN groups on the main chain, and the increase of the regularity of the macromolecular structure. Figure 6b is TGA derivative curves of copolymers, the decomposition stages were observed. The PEN-2 is one stage decomposition

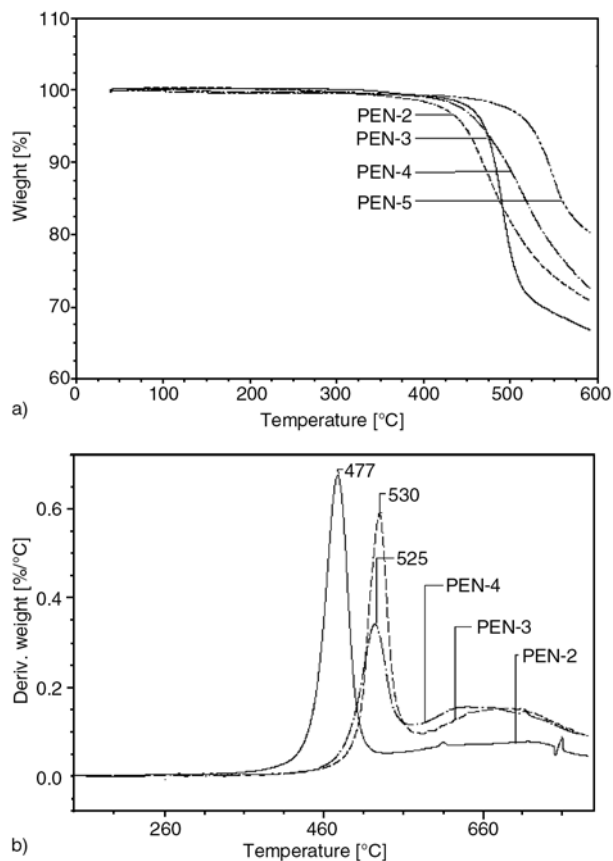


Figure 6. TGA curves of PEN (BP/HQ) copolymers, a) weight loss percent, b) derivative curves

model; the main decomposition temperature is 477°C. But PEN-3 and PEN-4 exhibit two stages decomposition mechanism, the main decomposition temperature is 525–530°C, the decomposition

temperature at the second stage is about 600°C, which may be led by high BP concentration into macromolecular main chains.

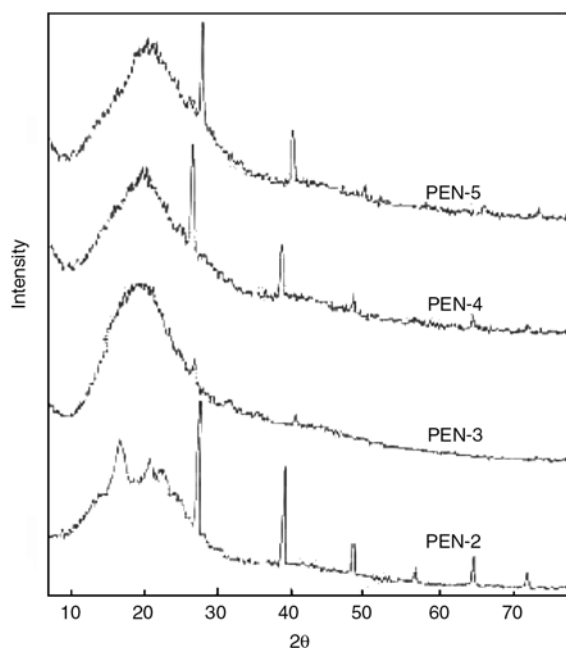


Figure 7. The XRD spectra of PEN(BP/HQ) copolymers

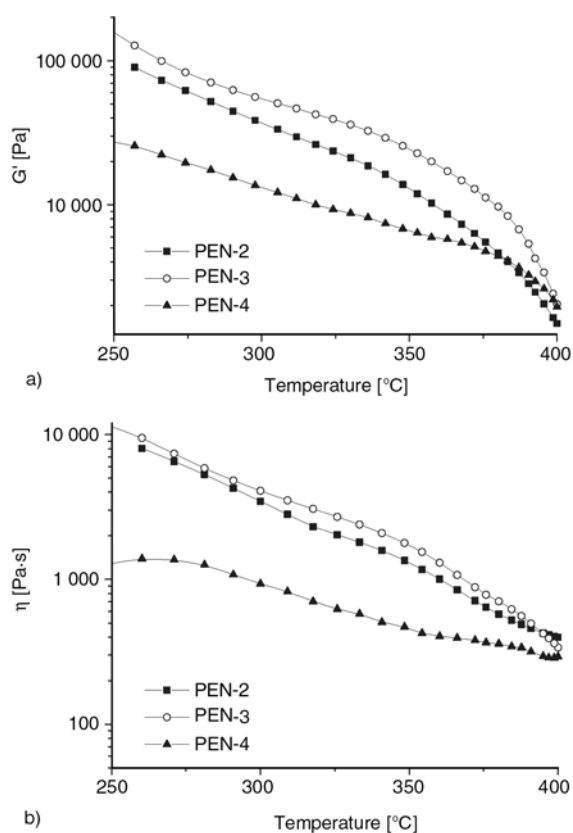


Figure 8. The storage modulus and dynamic viscosity of copolymers with temperature at 10 Hz
a) storage modulus; b) dynamic viscosity

4.5. WXR analysis of PEN

Figure 7 is the WXR spectra of copolymers. The regular structure could increase the crystallinity of polymer. Copolymer PEN-2, PEN-4 and PEN-5 have apparent semi-crystalline polymer nature, but the copolymer PEN-3 which further confirms the tendency towards the amorphous nature, has fewer tendency to crystallize the BP-based PEN and HQ-based PEN, and has a lower melting transition temperature. The results are very well corresponding with DSC results and the mechanical measurements.

4.6. The rheological behaviors of copolymers

Figure 8 shows the relationships between the storage modulus (G') (Figure 8a) or the dynamic viscosity (η) (Figure 8b) and the temperature at frequency 10 Hz. The storage modulus and viscosity of all copolymers decreased with the increase of temperature. The viscosity of copolymer decreased gradually with the increase of temperature from 250 to 400°C, and the viscosity of copolymer increase with the increase of BP concentration. But the storage modulus decreased quickly from 350 to 400°C. So, these copolymer have good thermoplastic processing properties at 300–400°C, which improved the processing temperature window of PEN homopolymer.

Figure 9a shows the storage modulus (G') of the copolymers with frequency. The increase of the storage modulus shows more significant in the high frequency range (>1 Hz), also, it is observed that the storage modulus of the copolymer with high concentration of BP increase more significantly at the high frequency. The storage modulus of copolymers reached to plateau at the low frequency (<1 Hz), which were led by tangling with macromolecular chains. The dynamic viscosity (η) decreased with the increase of frequency, and the dynamic viscosity (η) increase with the BP concentration at same frequency.

Figure 10 shows that the effects of storage modulus and dynamic viscosity on time at 320°C. From the results, all copolymers are basically stable at 320°C for 60 min. It means that the copolymer could be

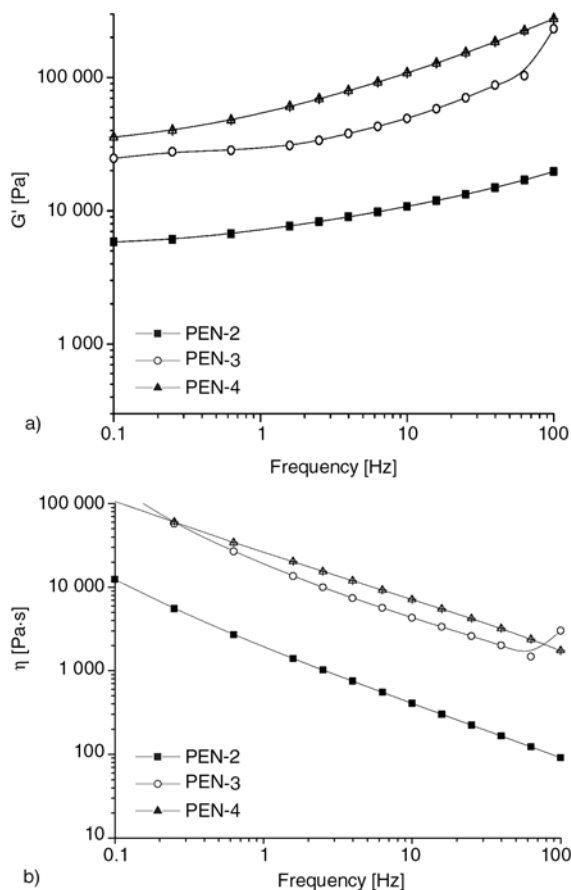


Figure 9. The storage modulus and dynamic viscosity of copolymers with frequency at 320°C
a) storage modulus; b) dynamic viscosity

processed at 320°C by thermoplastic processing methods. But the storage modulus and viscosity of the PEN-3 increase significantly after 30 min, which may be contributed to the curing reaction of CN group, this is confirmed by FTIR spectroscopy (Figure 11), and the triazine character could be observed at 1520 cm^{-1} . The storage modulus (G') and the dynamic viscosity (η) increase with the BP concentration at same time, which may be attributed to the rigidity brought about by the BP component.

5. Conclusions

High molecular weight PEN (BP/HQ) copolymers can be synthesized by nucleophilic substitution reaction of DCBN with BP and HQ in NMP medium using K_2CO_3 as catalyst, and exhibit excellent thermal and mechanical properties, the introduction of BP enhances the T_g and T_{id} of the copolymers. All copolymers have good rheological behaviors, the dynamic viscosity decreased stably

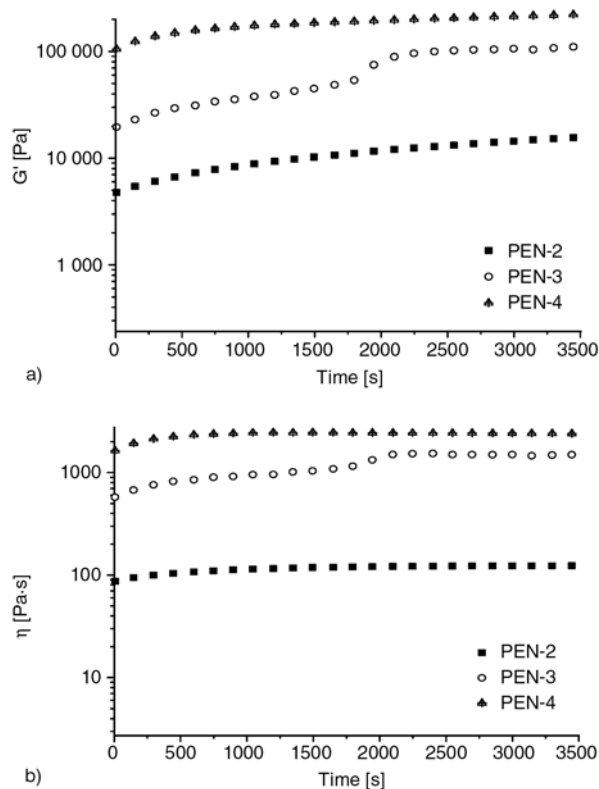


Figure 10. The storage modulus and dynamic viscosity of copolymers with time at 320°C
a) storage modulus; b) dynamic viscosity

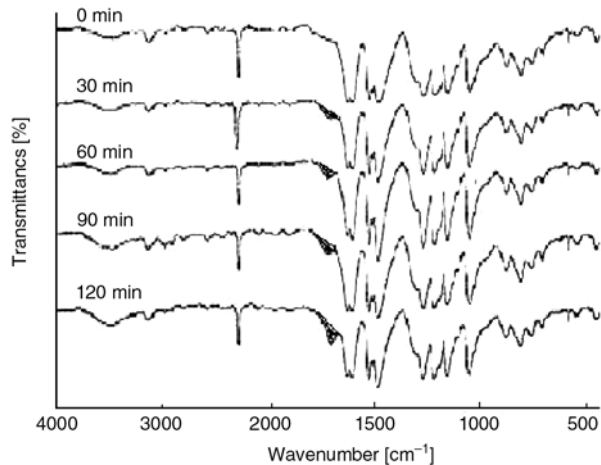


Figure 11. The FTIR spectra of PEN-3 cured at different time for at 320°C (the shadow Indicate the characteristic absorption of triazine)

with the increase of the temperature; the dynamic viscosity decreased quickly with the increase of the frequency, and was constant basically with the increase of time at 320°C, which are basement of the future processes and application in special engineering plastics.

Acknowledgements

The research was financially supported by National Natural Science Foundation (NO.59783003) and 'Excellent Talents Program' of University of Electronic Science and Technology of China.

References

- [1] Mohanty D. K., Hedrick J. L., Gobetz K., Johnson B. C., Yilgor I., Yilgor E., Yang R., McGrath J. E.: Poly(arylene ether sulfones) and related materials via a potassium carbonate, N-methyl pyrrolidone process. *Polymer Preprints*, **23**, 284–285 (1982).
- [2] Takahashi T., Kato H., Ma S. P., Sasaki T., Sakurai K.: Morphology of a wholly aromatic thermoplastic, poly(ether nitrile). *Polymer*, **36**, 3803–3808 (1995).
- [3] Matsuo S., Murakami T., Takasawa R. J.: Synthesis and properties of new crystalline poly(arylene ether nitriles). *Journal of Polymer Science, Part A: Polymer Chemistry*, **31**, 3439–3446 (1993).
- [4] Saxena A., Sadhana R., Rao V. L., Kanakavel M., Ninan K. N.: Synthesis and properties of polyarylene ether nitrile copolymers. *Polymer Bulletin*, **50**, 219–226 (2003).
- [5] Saxena A., Rao V. L., Ninan K. N.: Synthesis and properties of polyether nitrile copolymers with pendant methyl groups. *European Polymer Journal*, **39**, 57–61 (2003).
- [6] Zhang J. H., Liu X. B.: Synthesis and properties of polyarylene ether nitrile copolymers. *Chinese Journal of Synthetic Chemistry*, **7**, 42–45 (1999).
- [7] Sivaramakrishnan K. V., Marvel C. S.: Aromatic polyethers, polysulfones, and polyketones as laminating resins. II. *Journal of Polymer Science: Polymer Chemistry*, **12**, 651–662 (1974).
- [8] Keller T. M.: Phthalonitrile-based high temperature resin. *Journal of Polymer Science, Part A: Polymer Chemistry*, **26**, 3199–3212 (1988).
- [9] Keller T. M.: Imide-containing phthalonitrile resin. *Polymer*, **34**, 952–955 (1993).
- [10] Hill A. R., Meng Y., Hay A. S., Abu-Yousef I. A.: Poly(arylene ether)s from new biphenols containing imidoarylene and dicyanoarylene moieties. *Journal of Polymer Science, Part A: Polymer Chemistry*, **38**, 1318–1322 (2000).
- [11] Saxena A., Rao V. L., Prabhakaran P. V., Ninan K. N.: Synthesis and characterization of polyamides and poly(amide-imide)s derived from 2,2-bis(4-aminophenoxy) benzonitrile. *European Polymer Journal*, **39**, 401–405 (2003).
- [12] Li C., Gu Y., Liu X.: Synthesis and properties of phenolphthalein-based polyarylene ether nitrile copolymers. *Materials Letters*, **60**, 137–141 (2005).

Action of water in the degradation of low-density polyethylene studied by X-ray photoelectron spectroscopy

S. Massey¹, A. Adnot¹, A. Rjeb², D. Roy^{1*}

¹Laboratoire de Physique Atomique et Moléculaire, Département de physique, de génie physique et d'optique, et Centre de Recherche sur les Propriétés des Interfaces et la Catalyse, Faculté des Sciences et de Génie, Université Laval, Cité Universitaire, Québec, G1K 7P4, Canada

²Laboratoire de physique théorique et appliquée, Faculté des sciences Dhar El Mahraz, Université Sidi Med Ben Abdallah BP 1796 Fès Atlas, Maroc

Received 15 May 2007; accepted in revised form 21 June 2007

Abstract. Industrial low-density polyethylene (LDPE) was aged in stagnant distilled water during one year. Two types of this material were studied. The first one was without additives and the second type was doped with 4% of hindered-amine light stabilizers (HALS). Using X-ray photoelectron spectroscopy (XPS), the evidence that an oxidation occurs was demonstrated for the two types of LDPE (with and without HALS). One objective was to observe the chemical groups resulting of the ageing and to propose a mechanism of hydrolytic degradation for LDPE. The analysis of C1s spectra shows that the main oxidation products are C–O and C=O groups. Unlike the hydrolytic degradation of polypropylene, there is no presence of O=C–O groups, which suggests that there is no oxidative chain scission during hydrolytic ageing of the LDPE. The other objective of the study was to observe if the HALS can have an influence in the hydrolytic ageing of the LDPE. The values of the atomic concentration of the oxygen for the two types of samples show that the HALS could slightly slow down the oxidation of the LDPE.

Keywords: damage mechanism, low-density polyethylene, hydrolytic degradation, X-ray photoelectron spectroscopy, oxidation

1. Introduction

Polyethylene is one of the most used polymers in modern society. Unfortunately, the polymers, like polyethylene, undergo ageing and this phenomenon can induce non reversible chemical transformations in the structure of the macromolecules that can modify the recycling capability of some thermoplastics. Many agents can start the chemical degradation and an oxidation can occur in the polymer if the material is in contact with oxygen. Many studies proposed different chemical mechanisms to explain the processes of degradation of polyethylene, like degradation by light [1, 2], heat [1, 3] or weathering conditions [4, 5].

The action of water on polymers is another source of degradation of polymers. Many studies were done on the subject, but only concentrations of oxidation or macroscopic characteristics were measured, like lifetime for mechanical failure [6], tensile strain [7] or crystallinity percentage [8]. These experiments were mainly done at high temperatures [6–8]. In the authors' knowledge, the influence of water during ageing from a chemical point of view is not reported at room temperature. The aim of this work is then to determine if water is an important factor in the ageing of additive-free low-density polyethylene (LDPE) and HALS-stabilized LDPE at the chemical level by studying the chemical

*Corresponding author, e-mail: droy@phy.ulaval.ca
© BME-PT and GTE

bonds after ageing in distilled water during one year, and to propose a mechanism of degradation of the polymer.

2. Experimental section

The industrial LDPE samples were made by ENIP (*Entreprise Nationale des Industries Pétrochimiques*), Algeria (trademark: PEBD B21 ENIP, Skikda). The samples were received in the form of film made by extrusion blow moulding. The density and the melt flow index of the received material are 0.923 g/cm^3 and 0.019 g/min , respectively. Four samples, of about 2 cm by 2 cm, were used; two of them are unstabilized LDPE and the two others are LDPE stabilized with 4% of HALS from Ampacet™. All the samples were immersed in distilled water during one year at room temperature. Also, two unaged samples (one unstabilized and one 4% HALS stabilized) were analyzed by XPS as reference. The two kinds of LDPE samples used in this experiment came from the same source to make sure that the properties of the polymer were similar; the use of two identical samples is to ensure the validity of the results. After the ageing period, the samples were dried with compressed air.

XPS measurements were carried in a Kratos Axis-Ultra system in a UHV chamber with an electrostatic-magnetic hybrid lens and a 300 W monochromatic $\text{AlK}\alpha$ X-ray source (20 mA, 15 kV). The analysed surface was approximately $400 \mu\text{m}$ by $800 \mu\text{m}$. The angle of the X-ray beam is 60° with respect to the sample normal ($60^\circ/n$) and the take-off angle was $0^\circ/n$ for all the measurements. The data analysis was done with the software CasaXPS provided with the XPS setup. XPS surveys and C1s spectra were analyzed in this work. Because of the surface charging of non-conducting samples [9, 10], the peaks appeared shifted on the energy scale; the energy calibration was done by setting the C1s peak at 285.2 eV for the Csp^3 peak. During the peak synthesis, a Shirley background subtraction [11] was used and the Gaussian/Lorentzian shape ratio was 40 for all the spectra.

3. Results and discussion

The XPS surveys of all the unstabilized LDPE samples and of all the 4% HALS stabilized LDPE samples studied are presented in Figures 1 and 2, respectively. The zeros of the higher spectra were

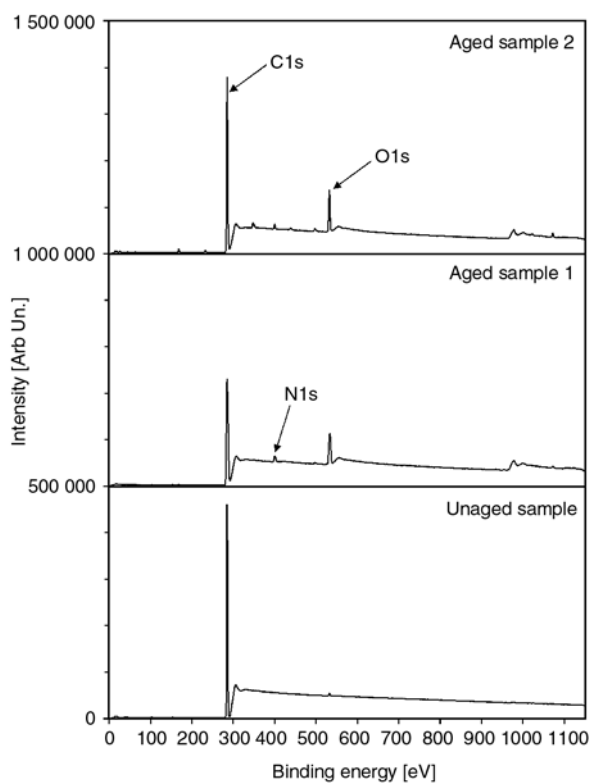


Figure 1. XPS survey spectra of the unstabilized LDPE samples

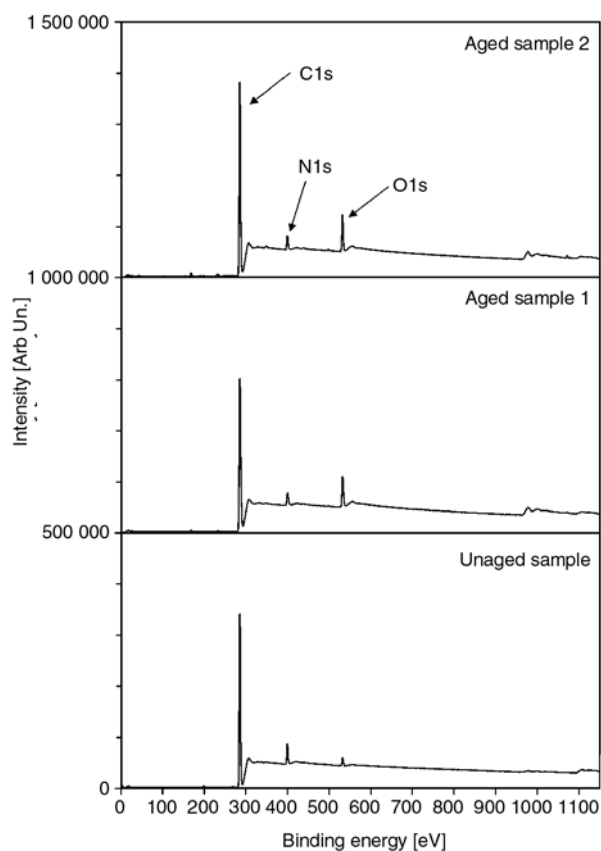


Figure 2. XPS survey spectra of the 4% HALS stabilized LDPE samples

Table 1. Atomic concentration^a [%] of the elements in the samples of LDPE

Sample	C1s	O1s	N1s	Contaminants (<1%)
Unstabilized LDPE (unaged sample)	99.1	0.7	0.1	–
Unstabilized LDPE (aged sample 1)	87.4	9.3	2.7	Ca, Cl, Cu, Na, S, Si
Unstabilized LDPE (aged sample 2)	87.9	8.6	1.6	Ca, Cl, Cu, Mg, Na, S, Si
LDPE w/4% HALS (unaged sample)	90.8	1.8	6.7	Al, Cl, Na, S, Zn
LDPE w/4% HALS (aged sample 1)	87.5	7.0	4.8	Al, Ca, Cl, Na, S, Si
LDPE w/4% HALS (aged sample 2)	87.2	6.7	4.7	Al, Ca, Cl, Na, S, Si, Zn

^aThe error of the concentrations is estimated at $\pm 0.1\%$

shifted for a better presentation for both Figures. Three major peaks are observed on the survey spectra. These peaks are C1s at 285 eV, which is associated to the polymer, O1s at 532 eV which seems to indicate an oxidation of the polymer, and N1s at 400 eV, which is attributed to HALS that contain amines. The hypotheses for the origin of the presence of the two last peaks are that oxygen is mainly observed in degraded samples and that nitrogen is observed mainly in 4% HALS stabilized samples. An interesting fact for nitrogen is a decrease of N1s for the 4% HALS stabilized aged samples that is probably due to the loss of the additive with the time [8, 12, 13], as shown in Table 1. An increase of N1s is observed for the aged unstabilized LDPE samples comparing to the unaged sample. This phenomenon was also observed in the study of hydrolytic degradation of polypropylene [14]. An

assumption of this increase is the presence of gaseous nitrogen coming from dissolved air in water. As time goes by, nitrogen could contaminate the surface of the samples. Other minor peaks are also present and their relative atomic concentrations are given in Table 1. The various origins of these impurities are more difficult to determine because their sources can be multiple; the samples come from industry and their history is unknown. The atomic concentrations are based on the surface of the peaks in the XPS surveys.

To be sure that the presence of oxygen in the survey spectra is due to oxidation of the polymer samples and not simply the insertion of water molecules in the polymer matrix, C1s spectra were analysed by peak synthesis. Results of the analysis of the unstabilized and 4% HALS stabilized samples are shown in Figures 3 and 4, respectively. All the peak syn-

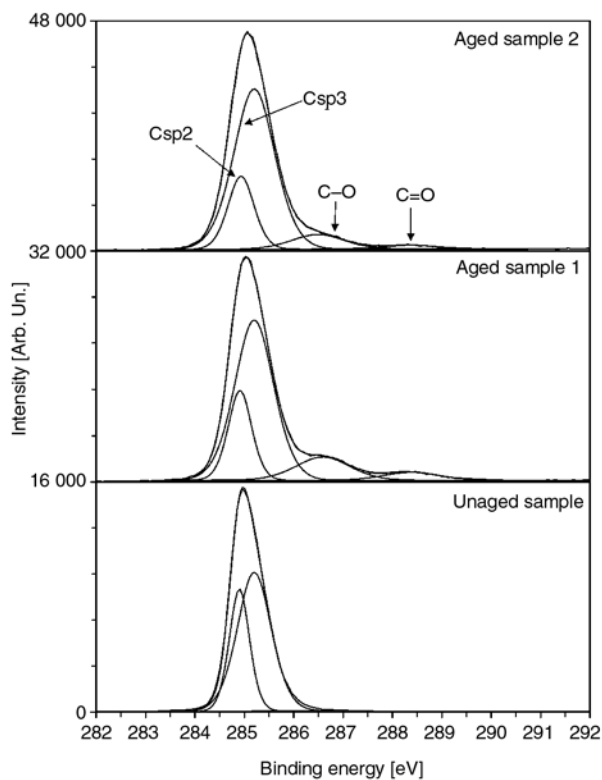


Figure 3. Results of the synthesis of the C1s spectra of the unstabilized LDPE samples

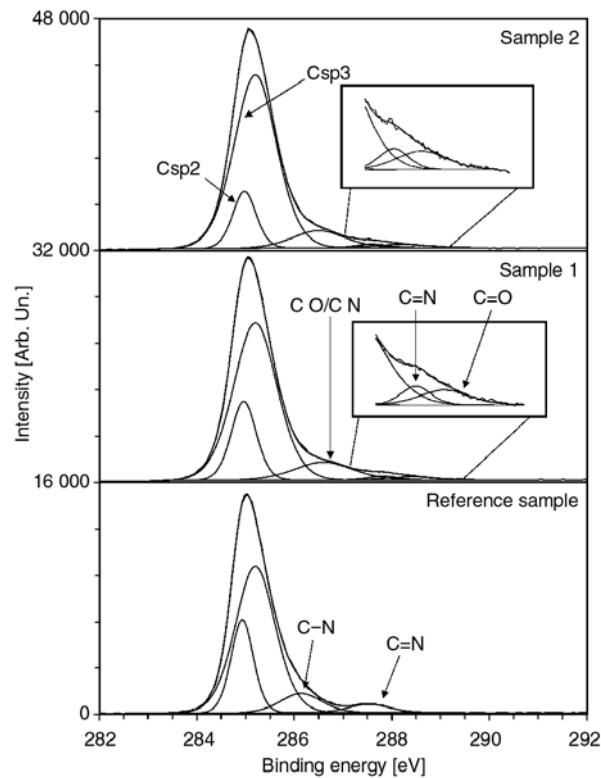


Figure 4. Results of the synthesis of the C1s spectra of the 4% HALS stabilized LDPE samples

theses were done with a maximal residual standard deviation of 1.38157 or less (data given by the software CasaXPS), and all the spectra were shifted to higher energies to consider the inhomogeneous charge effect in non-conducting insulators [9, 10] by setting the C_{sp3} peak at 285.2 eV. The peak synthesis of the $C1s$ spectrum of the unstabilized unaged sample gives two resulting peaks that are associated to C_{sp3} (285.2 eV) and C_{sp2} (284.9 eV) hybridizations [15, 16]. The origin of the two peaks is probably due to the industrial processes of polymerization that can induce some imperfections in the structure of the material. For the case of the 4% HALS stabilized unaged sample, the $C1s$ peak is clearly asymmetric, as seen in Figure 4. The atomic concentrations shown in Table 1 suggest that nitrogen is the only element present that can be bonded with carbon to a significant degree to cause this shape of the $C1s$ peak. The peak synthesis of the spectrum gives four peaks at 284.9 eV (C_{sp2}), 285.2 eV (C_{sp3}), 286.1 eV (C–N) and 287.5 eV (C=N) [15–17]. The last two peaks are probably associated with the HALS incorporated in the polymer matrix.

The asymmetric shape of the $C1s$ peaks of the degraded samples reveals the existence of bonds other than those of pure not modified LDPE. As shown in Table 1, oxygen is the main element present to a significant degree that can cause asymmetry of the $C1s$ peak for the aged unstabilized samples by binding with carbon atoms. Considering that contaminants listed in Table 1 cannot make bonds observable by XPS with carbon due to their low atomic concentration, the atomic functions found by decomposition of $C1s$ spectra of unstabilized LDPE samples (Figure 3) are C_{sp2} (~284.9 eV), C_{sp3} (285.2 eV), C–O (~286.5 eV) and C=O (~288.4 eV) [14–16, 18, 19]. Under the same assumptions and considering that bonds between nitrogen and carbon can be detected by

XPS due to the significant intensity of the N1s peak (Figure 2 and Table 1), the results of the decomposition of the $C1s$ spectra of the 4% HALS stabilized LDPE samples are C_{sp2} (~284.9 eV), C_{sp3} (285.2 eV), C–O/C–N (~286.5 eV) and C=N (~287.7 eV) and C=O (~288.3 eV) [14–19]. Due to the proximity of the C–O and C–N peaks, there is no possibility to separate these two peaks. The approximated values listed above are an average of the results of the $C1s$ spectra decomposition.

An assumption of the mechanisms of the degradation of LDPE by water is presented in Figure 5. The first step of the degradation, based on the literature [1, 3], is a loss of a proton (H^+) due to the polarity of the water molecules or the ionic potential of the negative ions present in the water (e.g. OH^-) by charge transfer complexes (CTCs) [20]. The rupture of the C–H bond occurs by electrostatic attraction of the proton [14, 21]. An oxidation of the polymer can follow the loss of a proton as showed in Figure 5, resulting in the formation of alcohol (C–OH) groups by association of the macroradical and an OH^- group produced in water, or the oxidation of the macroradical by O^{2-} originated in water. The last case is not stable in time and can stabilize by two ways. The first way is the formation of an alcohol group by the association with a proton. The second one is the formation of ketone (C=O) by the loss of the second proton bonded to the carbon atom that is bonded to oxygen (Figure 5). One should note that C–O groups in Figures 3 and 4 could not be associated to hydroperoxides (C–OOH) because of the weak enthalpy of dissociation of the O–O bond (35–40 kcal/mol) [22–24]. The hydroperoxide groups are often cited in the LDPE oxidation [1, 3].

Chemical conversions can occur between the various chemical groups because the stability of the chemical species is inversely proportional to their enthalpy of dissociation (potential energy of disso-

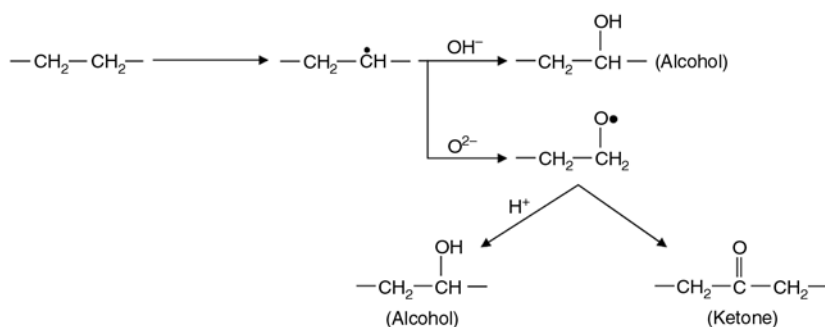


Figure 5. Proposed mechanisms for the hydrolytic degradation of the LDPE

ciation) [25]. By comparing the enthalpy of dissociation of chemical groups C–OH (383 kJ/mol) and C=O (178 kJ/mol) at a temperature of 25°C, a tendency of stabilization toward alcohols is present augmenting the probability of the presence of alcohols [14]. Another interesting point is the possibility that LDPE does not undergo chain scission during hydrolytic degradation. After the ageing time, the degraded samples do not show any cracking or loss of flexibility in comparison with unaged samples. This observation and also the absence of the O=C–O groups in Figures 3 and 4, suggest that the hydrolytic degradation of LDPE does not break macromolecular chains, unlike the hydrolytic ageing of polypropylene [14].

As shown in Table 1, the atomic concentration of oxygen is higher for the unstabilized LDPE degraded samples than for the 4% HALS stabilized LDPE samples. The presence of HALS can decrease the oxidation of LDPE by scavenging oxygen present at the surface of the polymer [26]. It is evident that HALS contribute to a certain degree to the retardation of oxidative degradation of LDPE in water, but the efficiency of the HALS for hydrolytic ageing is less than the ageing in air [6].

4. Conclusions

Unstabilized and 4% HALS stabilized industrial LDPE samples were aged in stagnant distilled water during one year to observe how the degradation of the polymer occurs. Using XPS technique, the evidence that an oxidation occurs was demonstrated for all LDPE samples by formation of C–O and C=O groups. These groups were determined by analysis of the C1s spectra. It was then possible to propose mechanisms of degradation that suggest that there is no chain scission during hydrolytic degradation of the material. This assumption is based on the fact that there is no presence of O=C–O groups in the analysis of XPS measurements. The influence of HALS was also studied by comparing the oxygen atomic concentration of the samples. The lower values for the 4% HALS stabilized LDPE samples suggest that the HALS could slow the oxidation of the LDPE, but the difference of oxygen atomic concentrations between unstabilized and 4% HALS stabilized samples suggest that HALS are not the most efficient additives for slowing the hydrolytic degradation.

Acknowledgements

The authors are grateful to Professor Tahar Sadoun of A. Mira de Bejaia University, Algeria, for kindly providing the LDPE samples. This work has been supported by NSERC-Canada.

References

- [1] Corrales T., Catalina F., Peinado C., Allen N. S., Fontan E.: Photooxidative and thermal degradation of polyethylenes: interrelationship by chemiluminescence, thermal gravimetric analysis and FTIR data. *Journal of Photochemistry and Photobiology A: Chemistry*, **147**, 213–224 (2002).
- [2] Stark N. M., Matuana L. M.: Surface chemistry changes of weathered HDPE/wood-flour composites studied by XPS and FTIR spectroscopy. *Polymer Degradation and Stability*, **86**, 1–9 (2004).
- [3] Gugumus F.: Re-examination of the thermal oxidation reactions of polymers – 2. Thermal oxidation of polyethylene. *Polymer Degradation and Stability*, **76**, 329–340 (2002).
- [4] El-Awady M. M.: Natural weathering, artificial photo-oxidation, and thermal aging of low density polyethylene: Grafting of acrylic acid onto aged polyethylene films. *Journal of Applied Polymer Science*, **87**, 2365–2371 (2003).
- [5] Pagès P., Carrasco F., Saurina J., Colom X.: FTIR and DSC study of HDPE structural changes and mechanical properties variation when exposed to weathering aging during canadian winter. *Journal of Applied Polymer Science*, **60**, 153–159 (1996).
- [6] Henry J. L., Ruaya A. L., Garton A.: The kinetics of polyolefin oxidation in aqueous media. *Journal of Polymer Science: Part A Polymer Chemistry*, **30**, 1693–1703 (1992).
- [7] Dörner G., Lang R. W.: Influence of various stabilizer systems on the ageing behavior of PE-MD-I. Hot-water ageing of compression molded plaques. *Polymer Degradation and Stability*, **62**, 421–430 (1998).
- [8] Amato L., Gilbert M., Caswell A.: Degradation studies of crosslinked polyethylene. II Aged in water. *Plastics, Rubbers and Composites*, **34**, 179–187 (2005).
- [9] Bryson III C. E.: Surface potential control in XPS. *Surface Science*, **189/190**, 50–58 (1987).
- [10] Barth G., Linder R., Bryson C.: Advances in charge neutralization for XPS measurements of nonconducting materials. *Surface and Interface Analysis*, **11**, 307–311 (1988).
- [11] Shirley D. A.: High-resolution X-ray photoemission spectrum of the valence bands of gold. *Physical Review: B*, **5**, 4709–4714 (1972).
- [12] Haillant O., Lemaire J.: Natural and artificial photo-aging of non-stabilized and pigmented, hindered-amine stabilized propylene-ethylene copolymers. *Polymer Degradation and Stability*, **91**, 2748–2760 (2006).

- [13] Gerlock J. L., Kucherov A. V., Smith C. A.: Determination of active HALS in automotive paint systems II: HALS distribution in weathered clearcoat/basecoat paint systems. *Polymer Degradation and Stability*, **73**, 201–210 (2001).
- [14] Massey S., Adnot A., Roy D.: Hydrolytic aging of polypropylene studied by X-ray photoelectron spectroscopy. *Journal of Applied Polymer Science*, **92**, 3830–3838 (2004).
- [15] Marcondes A. R., Ueda M., Kostov K. G., Beloto A. F., Leite N. F., Gomes G. F., Lepienski C. M.: Improvements of ultra-high molecular weight polyethylene mechanical properties by nitrogen plasma immersion ion implantation. *Brazilian Journal of Physics*, **34**, 1667–1672 (2004).
- [16] Mähl S., Neumann M., Schlett V., Baalman A.: Some aspects of the fitting of XPS core spectra of polymers. *Surface and Interface Analysis*, **26**, 204–212 (1998).
- [17] Wang M.-J., Chang Y.-I., Poncin-Epaillard F.: Acid and basic functionalities of nitrogen and carbon dioxide plasma-treated polystyrene. *Surface and Interface Analysis*, **37**, 348–355 (2005).
- [18] Rjeb A., Letarte S., Tajounte L., El Idrissi M. C., Adnot A., Roy D., Claire Y., Kaloustian J.: Polypropylene natural aging studied by X-ray photoelectron spectroscopy. *Journal of Electron Spectroscopy and Related Phenomena*, **107**, 221–230 (2000).
- [19] Clark D. T., Cromarty B. J., Dilks A.: Theoretical investigation of molecular core binding and relaxation energies in a series of oxygen-containing organic-molecules of interest in the study of surface oxidation of polymers. *Journal of Polymer Science: Part A Polymer Chemistry*, **16**, 3173–3184 (1978).
- [20] Chien J. C. W.: On the possible initiation of photooxidation by charge-transfer excitation. *Journal of Physical Chemistry*, **69**, 4317–4325 (1965).
- [21] Verdu J.: *Vieillissement des plastiques*. AFNOR Techniques, Paris (1984).
- [22] March J.: *Advanced Organic Chemistry* 4th edition. Wiley and Sons, New York (1992).
- [23] Guillet J. E., Dhanraj J., Golemba F. J., Hartley G. H.: Fundamental processes in the photodegradation of polymers. *Advances in Chemistry Series*, **85**, 272–286 (1968).
- [24] Carlsson D. J., Wiles D. M.: Photooxidative degradation of polypropylene. 1. Photooxidation and photoinitiation processes. *Journal of Macromolecular Science C – Reviews in Macromolecular Chemistry and Physics*, **14**, 65–106 (1976).
- [25] Solomons T. W. G., Fryhle C. B.: *Organic chemistry* 7th edition. Wiley and Sons, New York (2000).
- [26] Basfar A. A., Ali K. M. I.: Effect of various additives on tensile properties of polyethylene films irradiated in air, water, N₂, and vacuum. *Polymer-Plastics Technology and Engineering*, **43**, 389–405 (2004).

Synthesis and characterization of a novel bisphthalonitrile containing benzoxazine

G. P. Cao, W. J. Chen, J. J. Wei, W. T. Li, X. B. Liu*

Institute of Microelectronic & Solid State Electronic, State Key Laboratory of Electronic Thin Films & Integrated Devices, University of Electronic Science and Technology of China, Chengdu 610054, China

Received 4 April 2007; accepted in revised form 3 July 2007

Abstract. The novel bisphthalonitrile containing benzoxazine (BPNBZ) has been synthesized using bisphenol-A, 4-aminophenoxylphthalonitrile and paraformaldehyde. The structure of the monomer was supported by FTIR spectroscopy, $^1\text{H-NMR}$, and $^{13}\text{C-NMR}$ spectra, which have exhibited that the reactive benzoxazine ring and cyano groups exist in molecular structure of BPNBZ. The cure reaction of BPNBZ was monitored by the disappearance of the nitrile peak and the tri-substituted benzene ring that is attached with oxazine ring peak at 2231, 951 cm^{-1} . The thermal polymerization of the BPNBZ was studied by differential scanning calorimetry (DSC) and dynamic rheometer. It was shown that the bisphthalonitrile containing benzoxazine had completely cured with two-stage polymerization mechanisms according to oxazine ring-opening and phthalonitrile ring-forming. The thermal decomposition behaviors of the polymer were examined by thermogravimetry analysis (TGA) in nitrogen and in air. The materials achieve char yields above 73% under nitrogen at 800°C and above 78% under air at 600°C, which exhibited the cured resin has good thermal stability and thermo-oxidative stability.

Keywords: thermosetting resins, thermal properties, thermal polymerization, bisphthalonitrile containing benzoxazine

1. Introduction

The aerospace industry and space programs have created new demands for even higher temperature polymers. There has been increasing interest in phthalonitrile polymers [1–7], owing to their excellent thermal and thermo-oxidative stability, high char yield, good chemical inertness, abrasion resistance, and flame resistance. But, there are several challenges to overcome with regard the processing of these materials with higher melting temperature and high processing temperature.

In recent years, the development of the benzoxazine-based family of phenolic resins has attracted significant attention. The attractive characteristics of benzoxazine polymers include low melt viscosity, no release of volatiles during cure and no need

for harsh catalysts, high thermal stability, good mechanical properties, excellent electrical properties and molecular design flexibility [14–16]. So in order to achieve low melt temperature of phthalonitrile, the presence of aromatic oxazine in the phthalonitrile molecular structure is necessary [11]. In this paper, we report on the synthesis of a bisphthalonitrile monomer containing benzoxazine and the properties of its polymer. Thermal polymerization of this monomer is relatively easy, because of the active benzoxazine ring in the backbone [8–11]. The focus of this research develops a novel bisphthalonitrile containing benzoxazine which expected that this bisphthalonitrile will contribute to the cross-link network formation by its own ring-forming polymerization.

*Corresponding author, e-mail: Liuxb@uestc.edu.cn
© BME-PT and GTE

2. Experimental

2.1. Materials

All chemicals were used as received. Paraformaldehyde (CP), toluene (99.5%), N-N-dimethylformamide (DMF, 99.5%), potassium carbonate (99%), and 1,4-dioxane (99%) were obtained from Tianjin BODI Chemicals. 4-nitrophthalonitrile (99%) was obtained from Alpha Chemical (Dezhou) Co. Ltd. 4-Aminophenol (CP) was obtained from Sinopharm Chemical Reagent Co., Ltd. Bisphenol-A was obtained from Tianjin Guangfu Fine Chemical Research Institute. All solvents used were certified A.C.S grade and used as received.

2.2. Synthesis

2.2.1. Synthesis of

4-aminophenoxyphthalonitrile

To a 250 ml three neck round-bottom flask equipped with a mechanical stirrer, refluxing condenser, and 4-nitrophthalonitrile (34.6 g, 0.2 mol), 4-Aminophenol (21.8 g, 0.2 mol), potassium carbonate (30 g.), and DMF (120 ml) were added. The reaction mixture refluxed at 85°C for 6 h. After 6 h, the mixture was precipitated into dilute NaOH (1 mol/l) using an additional funnel with slow addition rate. The brown precipitate was filtered and dried in vacuum oven at 70°C shown in Figure 1. Melting point (T_m):134°C; typical IR data: 3457 cm^{-1} ($-\text{NH}_2$), 2231 cm^{-1} ($-\text{CN}$), 1247 cm^{-1} (stretch, C–O–C), 1493 cm^{-1} (1, 2 and 4 substitution of benzene ring), 830 cm^{-1} (1, 4 substitution of benzene ring).

2.2.2. Synthesis of the novel bisphthalonitrile containing benzoxazine (BPNBZ)

To a 250 ml three neck round-bottom flask equipped with a mechanical stirrer, refluxing condenser, the 4-aminophenoxyphthalonitrile (23.4 g, 0.1 mol), bisphenol-A (11.4 g, 0.05 mol), and Paraformaldehyde (6 g, 0.2 mol) were dissolved in 40 ml of 1,4-dioxane and 20 ml of toluene and the reaction mixture refluxed at 110°C for 5 h. Then, the solvent was evaporated using a vacuum pump, and the crude product was obtained. Then, the crude product was dissolved in DMF and precipitated into the dilute NaOH (1 mol/l). The brown precipitate was filtered through a glass filter under vacuum and dried in vacuum oven at 70°C, and the purified bisphthalonitrile containing benzoxazine (BPNBZ) was obtained, shown in Figure 1 [11]. The typical IR characteristics data: 2231 cm^{-1} ($-\text{CN}$), 1503, 951 cm^{-1} [12, 13] (tri-substituted benzene ring that is attached with oxazine ring), 1247, 1032 cm^{-1} (stretch, C–O–C) [12, 13], 1086, 830 cm^{-1} (stretch C–N–C) [12], 1420 cm^{-1} (CH_2 antisymmetric stretch); $^1\text{H-NMR}$ (400 MHz, CDCl_3) δ (ppm): 1.621–1.627 (CH_3), 4.615–4.629 (CH_2); 5.350 ($\text{N-CH}_2\text{-O}$), 6.740–6.745 (N-Ar-H), 6.762–6.907 (ortho to N-Ar-). $^{13}\text{C-NMR}$ (400 MHz, CDCl_3) δ (ppm): 31.05 (CH_3), 41.83 ($\text{C}(\text{CH}_3)_2$), 51.03 ($\text{Ar-CH}_2\text{-N}$), 79.10 ($\text{N-CH}_2\text{-O}$), 115.46 ($\text{Ar-C}\equiv\text{N}$), 121.01 ($\text{C-CH}_2\text{-N}$), 143.44 (C_{11}), 146.94 (C_8), 162.35 (C_7).

2.2.3. Thermal polymerization of the monomer

The BPNBZ monomer could be polymerized by heating. The conditions of the BPNBZ polymeriza-

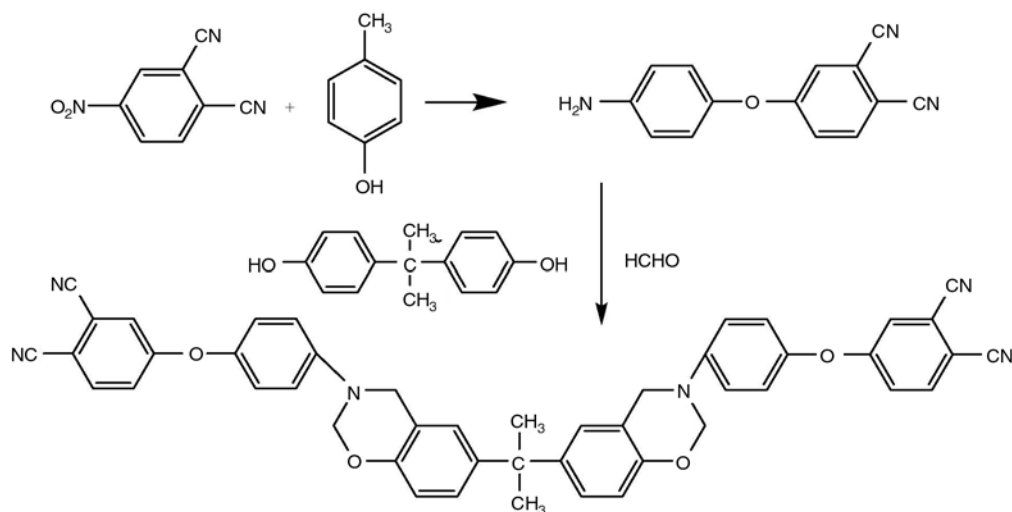


Figure 1. The synthesis of the bisphthalonitrile containing benzoxazine

Table 1. The cured schedule of the prepolymer and polymer

Sample	Time and temperature
b	160°C-12h
c	160°C-12h 180°C-12h
d	160°C-12h 180°C-12h 200°C-8h
e	160°C-12h 180°C-12h 200°C-8h 220°C-6h
f	160°C-12h 180°C-12h 200°C-8h 220°C-6h 250°C-6h

tion were listed in Table 1. The cured samples were heated at 160°C for 12 h, 180°C for 12 h, 200°C for 8 h, 220°C for 6 h and 250°C for 6 h consecutively. A hard shiny blue-black solid was obtained.

2.2.4. Characterizations

The structure of monomer and resins were characterized in KBr pellets at Shimadzu FTIR8400S. The resins with different cured extent were prepared in DSC by heating from 50 to 180 (b), 200 (c), 220 (d), 250 (e) and 275°C (f) at a heating rate 10°C/min respectively.

¹H-NMR and ¹³C-NMR spectra were obtained using a Bruker AV400 nuclear magnetic resonance spectrometer (NMR) at a proton frequency of 400 MHz and the corresponding carbon frequency. The solvent is CDCl₃.

The thermal behaviors of monomer and resins were investigated by the differential scanning calorimetry (DSC) and thermogravimetry analysis (TGA). The differential scanning calorimetry (DSC) was performed on TA Instruments Modulated DSC-Q100 with a heating rate of 10°C/min and a nitrogen flow rate of 50 ml/min. All samples were crimped in hermetic aluminum pans with lids. The thermogravimetry analysis (TGA) was performed on the TA instruments Q50 thermogravimetric analyzer with a heating rate of 20°C/min and a nitrogen flow rate of 50 ml/min or an air flow rate of 50 ml/min.

The dynamic rheological measurements were carried out using TA Instruments AR-G2 Oscillatory Rheometer with a heating rate of 10°C/min and the frequency of 10 Hz under air atmosphere.

3. Results and discussion

3.1. Characterization of structure of BPNBZ and resin

The structure of BPNBZ as shown in Figure 1 was verified by ¹H-NMR and ¹³C-NMR spectroscopy

and the corresponding spectrum was shown in Figure 2 and 3. In ¹H-NMR, resonances appearing at 4.63 and 5.35 ppm are assigned to the methylene protons in the oxazine ring of BPNBZ [13]. The prominent resonance at 1.621 and 1.627 ppm in the aromatic frequency corresponds to methyl of the monomer. Furthermore, the structure of the monomer is confirmed by using ¹³C-NMR and the corresponding chemical shifts are shown in Figure 3, according to chemical shift values, the peak at 79.5 ppm indicates the characteristic resonance of –CH₂– in oxazine ring, and the peak at 115 ppm is the characteristic resonance of –CN. Along with the excellent agreement between the calculated and observed data of the elemental analysis for the purified sample, it shows that the targeted compounds were obtained in high purity [13].

The FTIR spectrum of BENBZ is shown in Figure 4a. The appearance of –CN at 2231 cm⁻¹ and tri-substituted benzene ring that is attached with oxazine ring at 1503, and 951 cm⁻¹ can be observed. The band at 1247 cm⁻¹ is assigned to the C–O–C antisymmetric, while the band at 1032 cm⁻¹ is assigned to the C–O–C symmetric stretch [12, 13]. The antisymmetric and symmetric stretch of the C–N–C is observed at 1086, 830 cm⁻¹. These results show a novel bisphthalonitrile containing benzoxazine could be synthesized by this technique.

The FTIR spectra of resins are shown in Figure 4. The peaks at 951, 1503, 2231, 1360, 1521, 1640 and 3280 cm⁻¹ show changes in intensity as a function of cure temperature. To observe the thermal polymerization and curing reaction mechanisms of BPNBZ, we use the non-isothermal polymerization techniques by DSC instrument scanning to schedule program, so as to explain the way of thermal polymerization and the structures of crosslinked networks. From these results, the changes of all characteristic peaks are no apparent when scanning from 50 to 180°C using non-isothermal polymerization reactions by DSC instrument (Figure 4b), the intensity of the peak at 951 and 1503 cm⁻¹ decreased faintly after scanning to 200°C shown in Figure 4c. At the same time, the peak attributed phenolic hydroxyl group at 3300–3400 cm⁻¹ was enhanced, suggesting the polymerization reaction of oxazine ring-opening appears (Figure 4d). After scanning to 250°C, the band of tri-substituted benzene ring that is attached with oxazine ring disap-

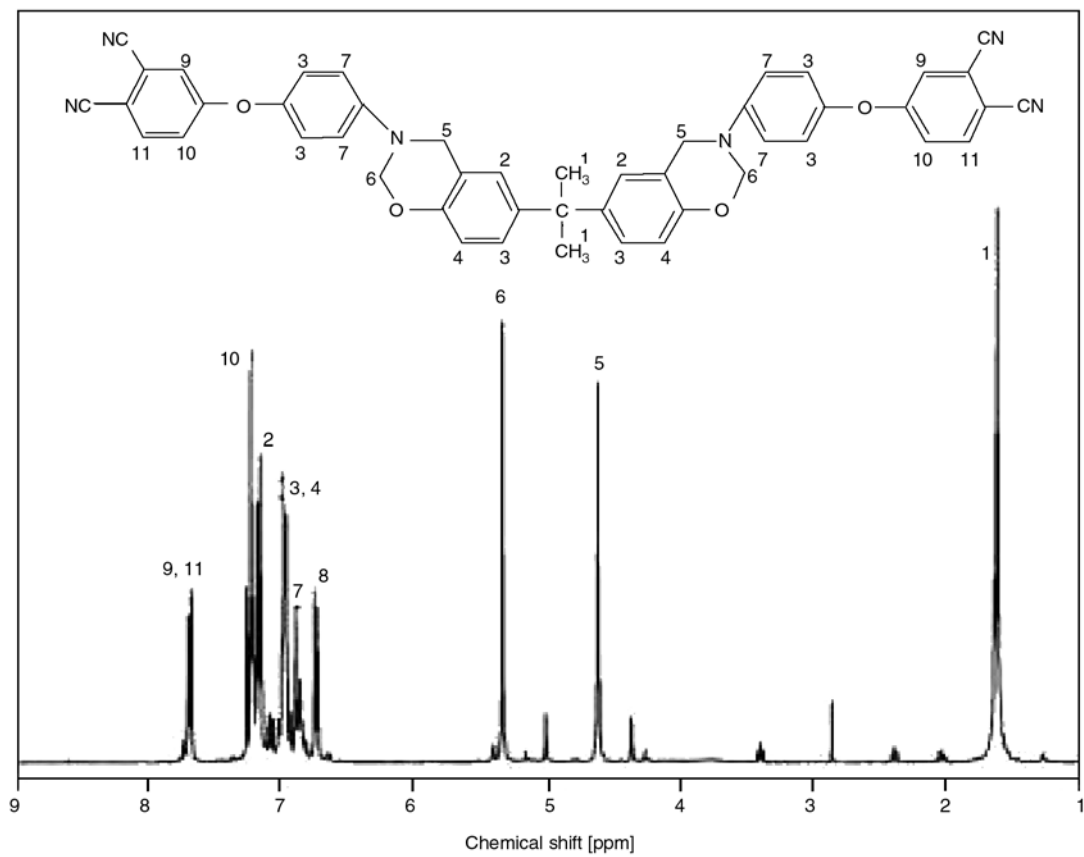


Figure 2. $^1\text{H-NMR}$ spectrum of BPNBZ in CDCl_3

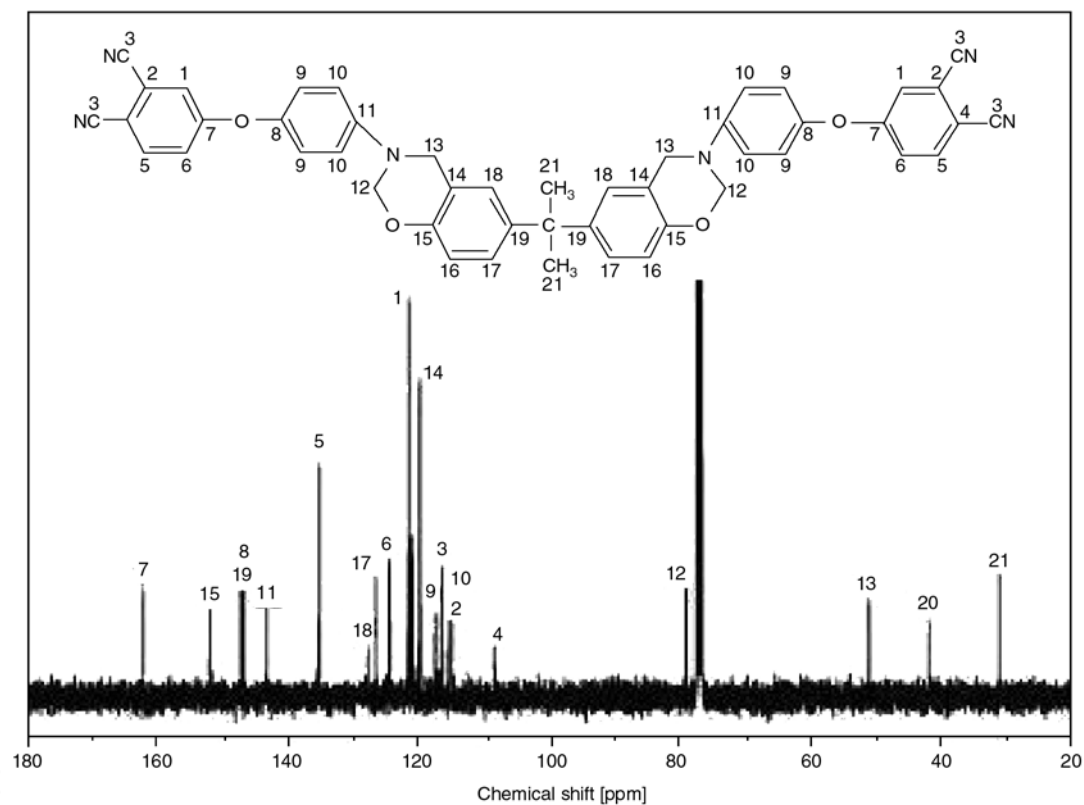


Figure 3. $^{13}\text{C-NMR}$ spectrum of BPNBZ in CDCl_3

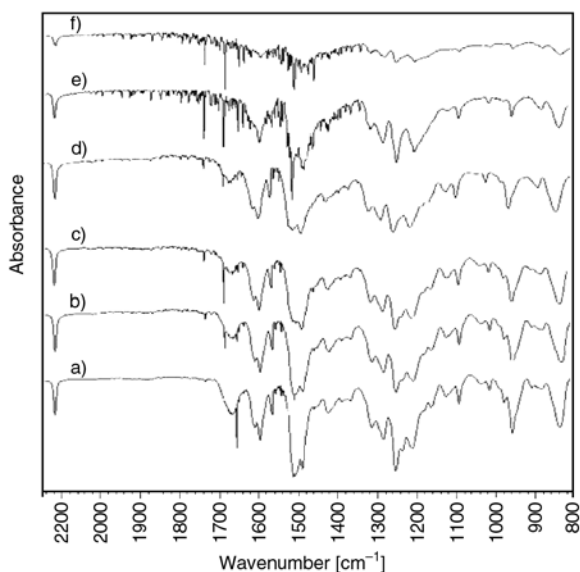


Figure 4. FTIR spectra of the monomer (a), partially cured resin (b), (c), (d), (e) and (f)

pears at 1503 cm^{-1} and the prominent band of tetra-substituted appears at 1500 cm^{-1} , suggesting benzoxazine polymerization via ring-opening is complete. According to the decrease of intensity of the peak at 2231 cm^{-1} and the appearance of new peaks at 1521 , 1360 , 1637 ($-\text{C}=\text{N}-$) and 3275 cm^{-1} ($\text{N}-\text{H}$), which are contributed to the characteristic absorptions of triazine and phthalocyanine, suggest the polymerization reaction of $-\text{CN}$ groups has happened, as shown in Figure 4e. The Figure 5 indicates the typical FTIR spectra of the ring-forming proceedings of $-\text{CN}$ groups, the reactions are enhanced with the elevating of temperature. After scanning to 275°C , the peak of $-\text{CN}$ at 2231 cm^{-1} decreases clearly, shown in Figure 4f. These spectral observations suggest that multiple reaction

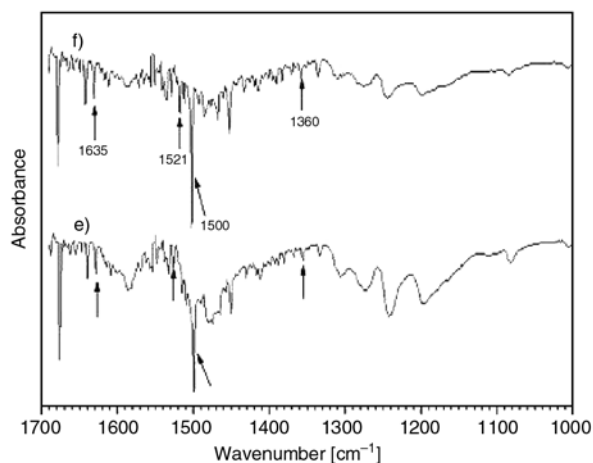


Figure 5. FTIR spectra of the pre-cured resins

mechanisms may be operational in the cure reactions of bisphthalonitrile containing benzoxazine.

3.2. DSC and TGA analysis

The thermal polymerization reactions of the monomer were studied by DSC as shown in Figure 6a. The DSC trace has two well resolved polymerization peaks. The first polymerization peak at the temperature range from 170 to 265°C is mainly attributed to the oxazine ring-opening polymerization, and the second peak at the temperature range from 265 to 300°C owes to the bisphthalonitrile ring-forming polymerization. This result was supported by the FTIR spectra results. From Figure 6, the cured extent of resin increased as a function of cure temperature and time, the peaks decreased with the increase of time and temperature. The resins with different cured extent are shown in Table 1, we found that the first peak had eliminated after curing at 200°C for 8 h (Figure 6d), and from Figure 6e and f, the second peak had eliminated basically after curing at 220°C for 6 h and 250°C for 5 h. There is a peak at the temperature range from 325 to 360°C , the temperature 325°C is post-cure temperature and the 360°C is the initial decomposition temperature, which can be support by the TGA results. As these results, it means that the bisphthalonitrile containing benzoxazine had completely cured with two-stage polymerization mechanisms according to oxazine ring-opening and phthalonitrile ring-forming.

The TGA curves of the polymers as shown in Figure 7. The initial decomposition temperatures (T_{id}) of the polymer under nitrogen and air are about

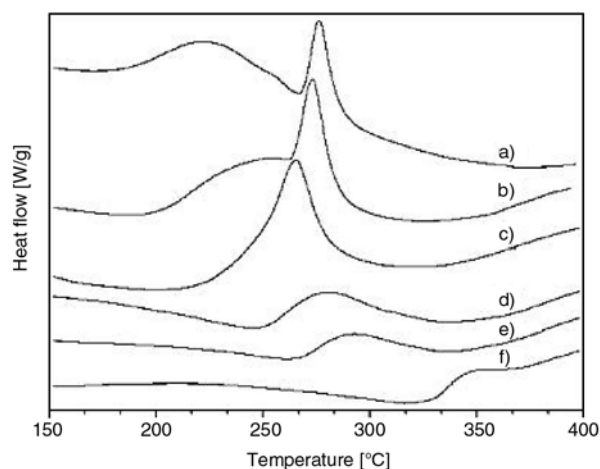


Figure 6. The DSC curves of the monomer (a) and the pre-cured resin (b), (c), (d), (e) and (f)

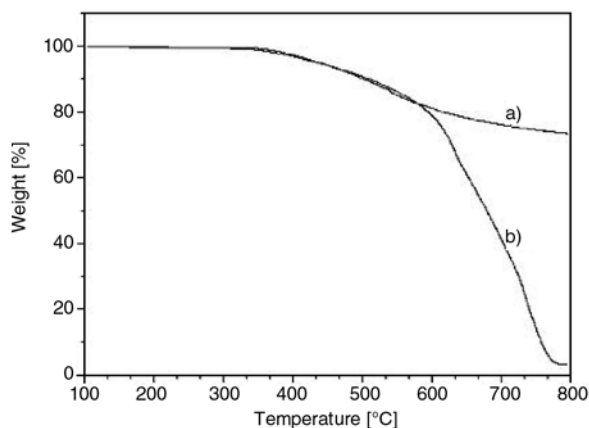


Figure 7. The TGA curves of the polymer a) in N_2 , b) in air

343.38 and 354.06°C, respectively. The temperatures at weight loss 5 and 10% in nitrogen atmosphere are 437.50 and 504.59°C and in air atmosphere are 434.63 and 504.29°C, respectively. The char yield at 800°C under nitrogen is 73.65% and at 600°C under air is 78.66%. In Table 2, the thermal properties of BPNBZ are summarized and compared to other phthalonitrile. The thermal properties of BPNBZ under nitrogen are as well as or decrease slightly than the other two monomers, but there is a significant improvement of the BPNBZ thermal properties under air than the other two. Therefore, the BPNBZ can be used for making heat-resistance high performance composites.

3.3. The rheological behavior

Figure 8 is relationship between rheological behaviors and temperature under curing process of bisphthalonitrile containing benzoxazine. Two transitions of G' appear from 200 to 300°C and two cross

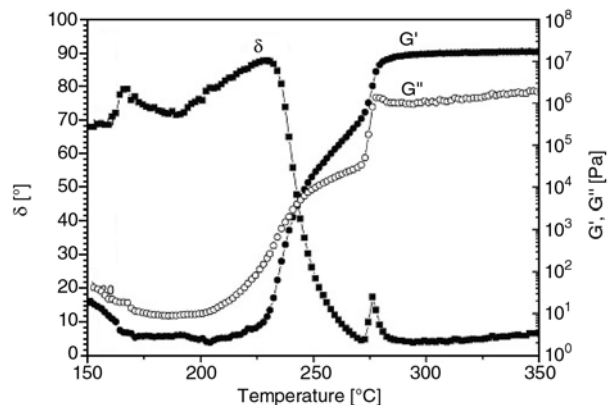


Figure 8. The rheological behaviors of the BPNBZ under non-isothermal curing

points of G' and G'' were observed at 242.7 and 276.1°C, respectively. The G'' has two apparent peaks. The first peak ranges from 200.9 to 242.7°C, and the second peak ranges from 242.7 to 276.1°C. The Delta curve appears two sharp peaks; the temperature of peak top is 230.7 and 276.1°C respectively. As these results, the former suggests primary polymerization of oxazine ring-opening, and the later suggests the bisphthalonitrile polymerizations of nitrile groups. So, it means that the bisphthalonitrile containing benzoxazine had completely cured with two-stage polymerization mechanisms which are consistent with the DSC results.

4. Conclusions

The novel bisphthalonitrile containing benzoxazine (BPNBZ) has been synthesized using bisphenol-A, 4-aminophenoxylphthalonitrile and paraformaldehyde. The structure of the monomer was supported by FTIR spectroscopy, 1H -NMR, and ^{13}C -NMR

Table 2. summary of TGA results

Monomer	Nitrogen			Air		
	T _{5%}	T _{10%}	Char yield [wt%] 800°C	T _{5%}	T _{10%}	Char yield [wt%] 600°C
	437	505	73	434	504	78
	414	505	73	378	420	0
	544	596	80	390	450	75

spectra, which have exhibited that the reactive benzoxazine ring and cyano groups exist in molecular structure of BPNBZ. The cure reaction mechanism of BPNBZ was monitored by the disappearance of the nitrile peak and the tri-substituted benzene ring that is attached with oxazine ring peak at 2231, 951 cm^{-1} . The bisphthalonitrile containing benzoxazine polymer possesses excellent thermal stability, thermal-oxidation stability and high char yield in nitrogen and air. The materials char yields achieved 73% at 800°C under nitrogen and 78% at 600°C under air. The temperatures at weight loss 5% and 10% under air are 434.63 and 509.29°C, respectively. According to the observations of thermal polymerization by DSC and dynamical rheology, the curing process of bisphthalonitrile containing benzoxazine has two stages polymerization mechanisms according to oxazine ring-opening and phthalonitrile ring-forming. The cured extent is a function of temperature and time. It can be used as a matrix of advanced composites.

Acknowledgements

This project was sponsored by 'Excellent Talents Program' of University of Electronic Science and Technology of China.

References

- [1] Keller T. M., Dominguez D. D.: High temperature resorcinol-based phthalonitrile polymer. *Polymer*, **46**, 4614–4618 (2005).
- [2] Warzel M. L., Keller T. M.: Tensile and fracture properties of a phthalonitrile polymer. *Polymer*, **34**, 663–666 (1993).
- [3] Dominguez D. D., Jones H. N., Keller T. M.: The effect of curing additive on the mechanical properties of phthalonitrile-carbon fiber composites. *Polymer Composites*, **25**, 554–561 (2004).
- [4] Sastri S. B., Armistead J. P., Keller T. M.: Phthalonitrile-carbon fiber composites. *Polymer Composites*, **17**, 816–822 (1996).
- [5] Zhang J., Liu X., Wen H., Xie M., Cai X.: Investigation of the properties of phthalocyanine resin containing bismaleimide groups. *Polymer International*, **42**, 363–366 (1997).
- [6] Dominguez D. D., Keller T. M.: Properties of phthalonitrile monomer blends and thermosetting phthalonitrile copolymers. *Polymer*, **48**, 91–97 (2007).
- [7] Laskoski M., Dominguez D. D., Keller T. M.: Synthesis and properties of a bisphenol A based phthalonitrile resin. *Journal of Polymer Science Part A: Polymer Chemistry*, **43**, 4136–4143 (2005).
- [8] Kim H. J., Brunoyska Z. B., Ishida H.: Molecular characterization of the polymerization of acetylene-functional benzoxazine resins. *Polymer*, **40**, 1815–1822 (1999).
- [9] Rimdusit S., Ishida H.: Development of new class of electronic packaging materials based on ternary systems of benzoxazine, epoxy, and phenolic resins. *Polymer*, **41**, 7941–1949 (2000).
- [10] Takeichi T., Guo Y., Agag T.: Synthesis and characterization of poly (urethane-benzoxazine) films as novel type of polyurethane/phenolic resin composites. *Journal of Polymer Science Part A: Polymer Chemistry*, **38**, 4165–4176 (2000).
- [11] Brunovska Z., Lyon R., Ishida H., Riga A., Collins R.: Thermal properties of phthalonitrile functional polybenzoxazines. *Thermochimica Acta*, **357–358**, 195–203 (2000).
- [12] Dunkers J., Ishida H.: Vibrational assignments of 3-alkyl-2, 4-dihydro-1, 3-benzoxazines. *Spectrochimica Acta, Part A: Molecular Spectroscopy*, **51**, 1061–1074 (1995).
- [13] Ishida H., Ohba S.: Synthesis and characterization of maleimide and norbornene functionalized benzoxazines. *Polymer*, **46**, 5588–5595 (2005).
- [14] Salamone J. C.: *Polymeric materials encyclopedia*. New York, CRC Press (1996).
- [15] Ishida H. J., Allen D. J.: Physical and mechanical characterization of near-zero shrinkage polybenzoxazine. *Polymer Science, Part B: Polymer Physics*, **34**, 1019–1030 (1996).
- [16] Ishida H., Low H. Y.: A study on the volumetric expansion of benzoxazine-based phenolic resin. *Macromolecules*, **30**, 1099–1106 (1997).

All-PP composites (PURE[®]) with unidirectional and cross-ply lay-ups: dynamic mechanical thermal analysis

T. Abraham, K. Banik, J. Karger-Kocsis*

Institute for Composite Materials (Institut für Verbundwerkstoffe GmbH), Technical University Kaiserslautern, D-67663 Kaiserslautern, Germany

Received 19 May 2007; accepted in revised form 3 July 2007

Abstract. All polypropylene (all-PP) composite laminates with unidirectional (UD) and cross-ply (CP) lay-ups were produced by hot consolidation from oriented coextruded PP tapes (PURE[®]). The consolidation of the tapes, wound on a steel plate, occurred in autoclave vacuum bag molding. The set processing conditions resulted in all-PP laminates of high rigidity as the PP copolymer surface layers of the tapes were molten and thus forming the matrix, while their PP homopolymer core remained unaffected and thus fulfilled its role as reinforcement. Specimens cut off from the laminates were subjected to dynamic mechanical thermal analysis (DMTA) in a broad temperature range ($T = -50 \dots 120^\circ\text{C}$) at various frequencies ($f = 10^{-2} \dots 10^1$). For the DMTA results the time-temperature superposition principle was adopted and master curves in the form of storage modulus vs. frequency ($f = 10^{-9} \dots 10^{20}$) and loss factor vs. frequency were created.

Keywords: polymer composites, thermal properties, polypropylene, all-polypropylene composite, PURE[®]

1. Introduction

The original concept of self-reinforced composite, a composite with matrix and reinforcement from the same polymer, was presented by Capiati and Porter [1] three decades ago for high density polyethylene. Later this concept was adopted to polypropylene (PP) [2–5], polyethylene [6–10], polyethylene terephthalate [11–13], polyethylene naphthalate [14], poly(methyl methacrylate) [15–18], polyamide [19] and liquid crystal polymers [20, 21]. Particularly, in a series of recent papers, Alcock and coworkers [22–24] described composite materials in which both the reinforcement and the matrix were based on PP. The related composites under the trade name of PURE[®] are produced from highly oriented co-extruded tapes having a skin-core-skin (A:B:A) morphology. The skin layer (A) contains a PP random copolymer, whereas the core layer (B) is composed of PP homopolymer.

Since the copolymer skin layer has a melting temperature below that of the homopolymer core, self-reinforced (also termed as homocomposites or all-PP composites) PP systems can be produced using a suitable processing window. Note that during consolidation the PP copolymer forms the matrix, while the highly oriented PP homopolymer fraction acts as continuous reinforcement. This approach (i. e. copolymer for the matrix and homopolymer for the reinforcement) can be used to produce all-PP composites using the film stacking technique, as well [25]. The most recent development with all-PP composites is to exploit the polymorphism-related difference in the melting range between the beta- (giving the matrix) and alpha-phases (serving as reinforcement) PPs [26, 27]. All-PP composites are characterized by their outstanding mechanical properties at very low density. Their main advantage over conventional glass fiber reinforced ver-

*Corresponding author, e-mail: karger@ivw.uni-kl.de
© BME-PT and GTE

sions is the easy recycling, because they comprise a single material (PP).

It is well known that the physical properties of a polymeric material are strongly dependent on its morphology, structure and relaxation processes corresponding to internal changes and molecular motions. Dynamic mechanical measurements over a wide temperature or frequency ranges are useful to understand the viscoelastic behavior and provide valuable insights into the relationship between structure, morphology and properties of polymers and related composites. Structure-property relationships in fiber reinforced PP composites were disclosed based on dynamic mechanical thermal analysis (DMTA) data (e.g. [28]). However, DMTA was less considered for all-PP composites [29].

The main aim of this study is to investigate the DMTA response of highly oriented PP tapes and all-PP composite laminates of various lay-up manufactured using these PP tapes. DMTA tests were run at different frequencies over a wide range of temperatures. By using the DMTA data, master curves can be created to predict the performance of all-PP composites at much higher frequencies than achievable in the laboratory.

2. Experimental

2.1. Manufacture of laminates

The tape used for the preparation of the composite laminates was a highly oriented, co-extruded PP tape (PURE®) manufactured at Lankhorst-Indutech (Sneek, The Netherlands). Characteristics of PP tapes used for the preparation of the laminates are summarized in Table 1. The manufacture of the PP laminates involved a two-stage process – winding of the PP tapes, both unidirectional (0°)(UD) and cross-ply (0/90°)(CP), and consolidation of the related tape assemblies at a suitable temperature and pressure in an autoclave. The schematic of the

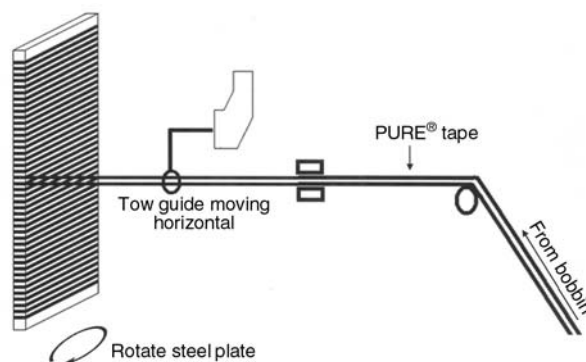


Figure 1. Scheme of the tape winding process for the fabrication of all-PP composites (in this case with UD structure)

tape winding process is shown in Figure 1. Using a typical winding machine, supplied by Bolenz & Schaefer Maschinenfabrik (Biedenkopf, Germany), PP tapes were wound from a bobbin onto a thin steel plate rotating at a constant speed of 40 rpm. In each case, the total number of layers was kept the same (30 layers). For producing CP laminates, the winding direction on the steel plate was sequentially changed. After laying two UD layers, another two layers of tapes were positioned perpendicular to them. A similar process for manufacturing UD all-PP composites from coextruded tapes has already been reported in the literature by Alcock *et al.* [22]. To consolidate the all-PP composites, the steel plate with the wrapped plies was placed in between two other steel plates inside a vacuum bag. This bag was connected to a vacuum pump applying negative pressure inside the bag. The entire bag was then placed inside an autoclave obtained from the Scholz Maschinenbau GmbH, (Coesfeld, Germany) and slowly heated to the consolidation temperature (T_C) of 145°C. A thermocouple was used to monitor the temperature rise in the specimen during heating. Simultaneously, the vacuum pump was started when the pressure began to grow in the autoclave until reaching the consolidation pressure ($P = 24$ bar). The time needed by the specimen to reach the consolidation temperature was considerably longer ($t_3 - t_1 \sim 90$ min) than the air temperature inside the autoclave ($t_2 - t_1$). Once the specimen reached T_C , a constant consolidation time ($t_4 - t_3$) of 30 min was given. After consolidation, the laminates were cooled to the release temperature (T_R) of 30°C. The pressure was released when the air temperature inside the autoclave reached 30°C. Cooling of the laminate ($t_5 - t_4$) took approx-

Table 1. Properties of the PURE® PP tape used based on the information of the manufacturer

Width	~2.3 mm
Thickness	~50 μ m
Density, ρ	0.829 g/cm ³
Composition	copolymer:homopolymer: copolymer
Tensile modulus (ISO 527)	15 \pm 2 GPa
Tensile strength (ISO 527)	~500 MPa
Elongation at break (ISO 527)	~6%
Shrinkage at 145°C for 30 min	5.5 \pm 0.5%

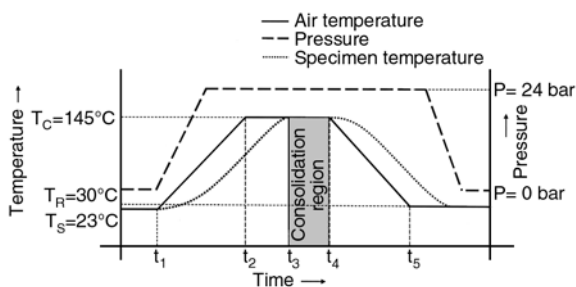


Figure 2. Time-temperature and time-pressure profiles during the autoclave vacuum bag consolidation of the all-PP composites

imately 60 min. Identical consolidation parameters were used for the production of both UD and CP lay-ups. The time-temperature and time-pressure profiles during consolidation are shown schematically in Figure 2.

2.2. Testing

2.2.1. DMTA of single tapes

DMTA was performed on single coextruded PP tapes. Specimens were tested in a TA Instruments DMA Q800 DMTA (New Castle, DE, USA) machine operating in a tensile testing mode. The test specimen was cooled to -50°C , allowed to stabilize and then heated at a rate of $3^{\circ}\text{C}\cdot\text{min}^{-1}$ until 150°C . The frequency of oscillation was fixed at 1 Hz and the strain amplitude was $20\ \mu\text{m}$. Storage modulus (E'), loss modulus (E'') and mechanical loss factor ($\tan\delta$) were determined during the test and plotted against temperature.

2.2.2. DMTA of all-PP composites

DMTA of all-PP composite laminates was performed in dual cantilever flexural mode. Specimens were cut from the UD and CP composite plates with dimensions of approximately $60\ \text{mm} \times 15\ \text{mm} \times 2\ \text{mm}$ (length \times width \times thickness) in the same DMTA machine equipped with a data acquisition software. The specimens were cooled to -50°C . The temperature was allowed to stabilize and then the chamber was heated at a rate of $3^{\circ}\text{C}\cdot\text{min}^{-1}$ until 120°C . The specimen was subjected to a sinusoidal flexural displacement applying a maximum tensile strain of 0.1% (which was well within the viscoelastic region) at frequencies 0.01 Hz, 0.1 Hz, 1 Hz, 5 Hz and 10 Hz. For each frequency, the complex dynamic modulus and loss factor were recorded.

2.2.3. Differential scanning calorimetry (DSC)

The crystallinity content of the coextruded tapes and the all-PP composites were characterized from the enthalpy associated during melting using a Mettler-Toledo DSC821 instrument (Greifensee, Switzerland). Heating scans were performed from 25 to 200°C at a heating rate of $10^{\circ}\text{C}/\text{min}$ with nitrogen blanketing inside the sample chamber. An average of three specimens was taken for each measurement. A higher enthalpy of fusion corresponds to the presence of more crystalline domains inside the specimen.

2.2.4. Time-temperature superposition principle

Theoretically and experimentally, dynamic mechanical properties of a polymer (for instance, storage modulus) is influenced by both temperature and frequency (or the response time) of the dynamic loading. This time-dependent behavior implies that the only way to accurately evaluate material performance for a specific application is to test the material under those temperature and time conditions the material will see during application. But there are difficulties in attaining the adequate range of temperatures or frequencies in the laboratory conditions for a specific application. In order to predict the behavior of materials over very high frequencies, the time-temperature superposition (TTS) helps to obtain information about frequencies outside the range that cannot be achieved experimentally. By assuming equivalence of time and temperature, the viscoelastic behavior of a polymer at a chosen reference temperature, T_{ref} , can be related to the viscoelastic behavior of the polymer at a different temperature by a shift, a_T , in the time-scale. For any reference temperature chosen, a fully overlapped curve could be formed, which is called the master curve. It is also widely accepted that a minor vertical shift factor may also be applied to more accurately model master curves [30]. However in this study, a vertical shift factor was not applied.

An attempt was made to apply the TTS to the DMTA data measured as function of both temperature ($T = -50\dots+120^{\circ}\text{C}$) and frequency ($f = 0.01\dots 10\ \text{Hz}$). Master curves in form of storage modulus (E') vs. frequency were produced by superimposing the storage modulus vs. frequency traces using the TTS principle. A reference temperature ($T_{ref} = 22^{\circ}\text{C}$) was used for this superposition (shift-

ing) process. The related shift factor a_T is given by Equation (1):

$$a_T = \frac{E'(T, f)}{E'(T_{ref}, f)} \quad (1)$$

The shift factors of a master curve have some relationship with temperature. Fitting the experimentally determined shift factors to a mathematical model permits the creation of a master curve in form of stiffness vs. frequency. With a multi-frequency measurement, frequencies beyond the measurable range of the DMTA can be achieved by using the superposition method based on the Williams-Landel-Ferry (WLF) equation [31, 32]. For the temperature range above the glass transition temperature, it is generally accepted that the shift factor-temperature relationship is best described by WLF equation (2):

$$\log a_T = \log \left(\frac{f}{f_0} \right) = \frac{-C_1(T - T_{ref})}{C_2 + (T - T_{ref})} \quad (2)$$

where C_1 and C_2 are constants.

For the temperature range below the glass transition temperature, the Arrhenius equation is generally acknowledged as suitable to describe the relationship between the shift factors of the master curve and the temperature. In the latter case, the activation energy (E_a) for shifting the curves can be obtained by Equation (3):

$$\ln a_T = \frac{E_a}{R} \left(\frac{1}{T} - \frac{1}{T_{ref}} \right) \quad (3)$$

3. Results and discussion

3.1. DMTA of PP tape

Figure 3 represents the typical dynamic mechanical behavior of all-PP tapes at 1 Hz frequency. It shows that at temperatures well below 0°C (supposed to be the glassy region of PP) the stiffness is fairly high. With increasing temperature the storage modulus decreases whereas the loss modulus increases, as expected. Above 50°C the stiffness of the tapes drops significantly. Although the tapes lost much of their elastic response above this temperature, their residual stiffness at 120°C (end of the test) is still higher ($E' = 3.2$ GPa) than that of an isotropic PP. The stiffness of the tape at ambient temperature (E' value) is similar to that reported in the literature

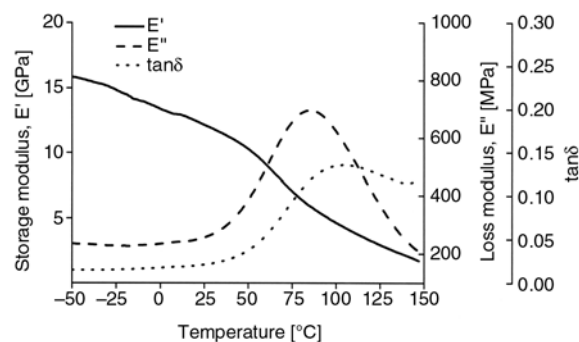


Figure 3. DMA plots of storage modulus, loss modulus and $\tan\delta$ vs. temperature for the PURE® PP tape at frequency 1 Hz

earlier [33, 34]. The high stiffness is attributed to the highly oriented crystals and polymer chains owing to the high draw ratio of the tape. This implies that the tape possesses a residual orientation even at this higher temperature.

Figure 3 also exhibits the correlation of $\tan\delta$ (ratio of E''/E') with temperature, which shows a maximum at $\sim 106^\circ\text{C}$. The maximum $\tan\delta$ value recorded for the all-PP tape was 0.135. Generally, the $\tan\delta$ peaks represent the transition temperatures [32]. However, Figure 3 does not resolve any $\tan\delta$ peak corresponding to the glass-transition of PP ($T_g \sim -10^\circ\text{C} \dots 0^\circ\text{C}$), but a more definite $\tan\delta$ peak is seen corresponding to T_α at approximately 106°C (Figure 2). Since these tapes are produced by high draw ratio (typically > 10), it is reasonable to expect that at such a higher draw ratio, the amorphous phase becomes highly oriented between the crystalline regions and it has less freedom to be involved in segmental motions [35]. Therefore, in highly oriented PP systems, the magnitude of T_g peaks compared to isotropic PP is greatly reduced. The $\tan\delta$ value at around 106°C , corresponding to the α transition (T_α), is believed to be the result of molecular motions which resist the softening effect of the applied heat. While T_g reflects mobility within the amorphous regions, T_α dictates the onset of segmental motion within the crystalline regions [35–37]. A broad peak of α relaxation indicates the delay (retardation) of the relative motion of the lamellae due to the high orientation of the chain segments.

3.2. DMTA of all-PP composites

Figure 4 shows the stiffness of all-PP composites with temperature at a frequency of 1 Hz. At room

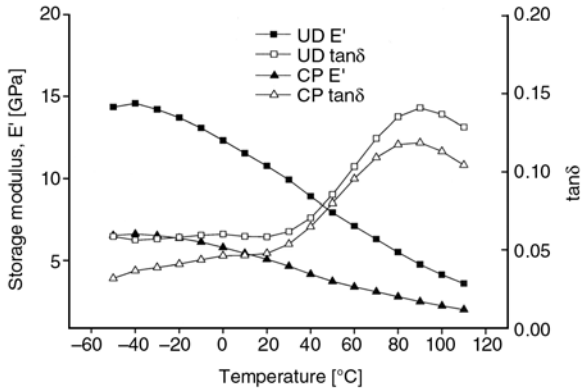


Figure 4. DMA plots of storage modulus and $\tan\delta$ vs. temperature for the all-PP composite laminates with UD and CP lay-ups at frequency 1 Hz

temperature (23°C) the UD and CP all-PP composites possess storage moduli of 10.5 GPa and 5.1 GPa, respectively, which are similar to the previously reported values [29].

The loss factor as a function of temperature for all-PP with UD and CP lay-ups are also shown in Figure 4. Similar to the DMTA data of the single tape, composite specimens also do not show any clear $\tan\delta$ peak corresponding to the β relaxation (T_g). However $\tan\delta$ peak corresponding to the α transition was found to be higher for UD than for CP lay-up.

3.3. Time-temperature superposition (TTS)

Storage modulus for a wider range of frequencies can be obtained by TTS using the data from multi-frequency DMTA tests. Figures 5 and 6 show the variation of storage modulus for a range of temperature between -20°C and 80°C for the all-PP composites having UD and CP lay-ups tested at 0.01 Hz, 0.1 Hz, 1 Hz, 5 Hz and 10 Hz, respec-

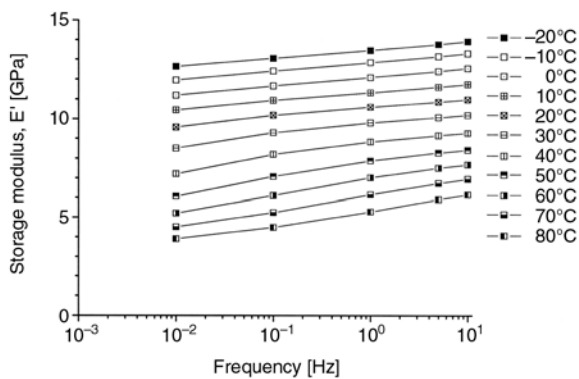


Figure 5. Storage modulus vs. frequency for a range of temperatures for the all-PP composite with UD lay-up

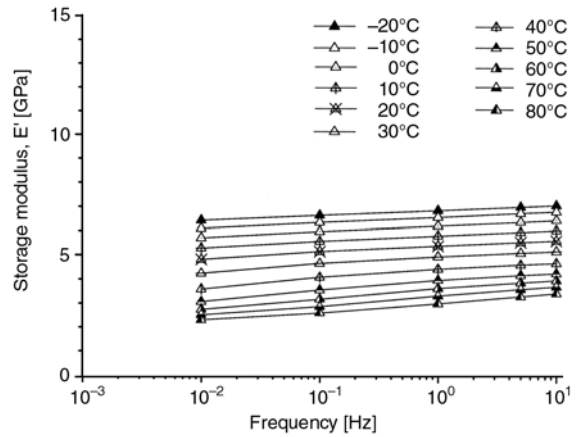


Figure 6. Storage modulus vs. frequency for a range of temperatures for the all-PP composite with CP lay-up

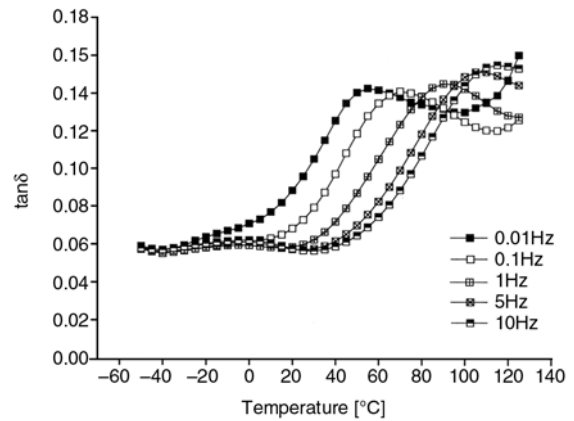


Figure 7. Loss factor ($\tan\delta$) vs. temperature for the all-PP composite with UD lay-up at different frequencies

tively. There is an increase in the storage modulus for both UD and CP with increasing frequency and decreasing temperature, as expected. The variation of $\tan\delta$ with temperature at different frequencies for the UD and CP lay-ups are shown in Figures 7

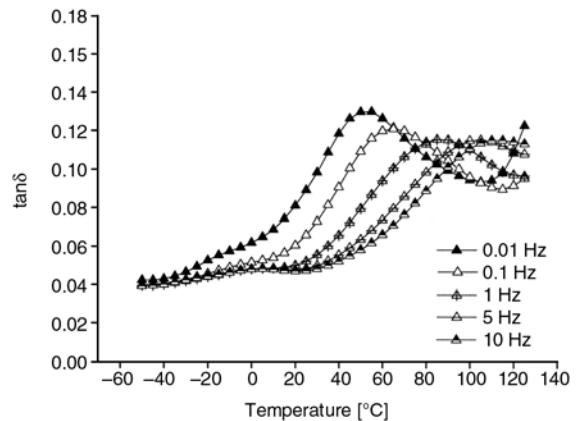


Figure 8. Loss factor ($\tan\delta$) vs. temperature for the all-PP composite with CP lay-up at different frequencies

and 8. A remarkable influence of frequency was observed for the α relaxation of the composites. The frequency increase affected the intensity of $\tan\delta$ and shifted the position of the relaxation region to higher temperatures. The peak became broader and less pronounced due to the additional melting region at higher temperatures. The $\tan\delta$ peak corresponding to the α transition for UD and CP lay-ups were found to be around 89°C and 86°C, respectively, at 1 Hz frequency. The shifting of T_α to higher temperature for UD may arise from higher crystallinity (indicated by higher enthalpy of fusion) of the UD compared to CP composites. The average enthalpies of fusion obtained from the DSC investigations were found to be 105.6 and 102.5 J/g for UD and CP lay-ups, respectively. The shift factors used for the generation of master curves for UD and CP lay-ups are shown in Figure 9. The shift factor plot is slightly curved, reflecting the WLF-type behaviour. The WLF equation was thus selected to relate the shift factors to the temperature. The symbols represent the experimentally determined shift factors, where the lines follow the WLF model. Master curves of the storage modulus and $\tan\delta$ against frequencies created at a reference temperature of 22°C were shown in Figures 10 and 11 respectively, for all-PP composites with UD and CP lay-ups. The storage modulus master curve provides a useful prediction of the modulus over loading frequencies from 10⁻⁹ to 10²⁰ Hz. Similarly the $\tan\delta$ master curves also give an overview to the damping of the material at different frequencies which is useful to measure how well the material can dissipate mechanical energy and very important for the design of material for vibration damping applications. However, it must

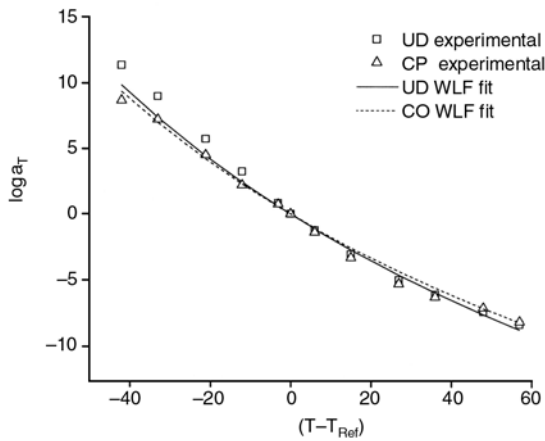


Figure 9. Experimentally determined shift factors and the CP WLF fit

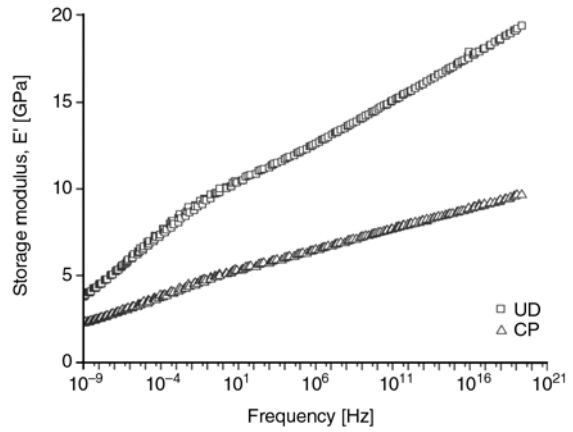


Figure 10. Storage modulus vs. frequency master curves at a reference temperature of 22°C for the all-PP composites with UD and CP lay-ups

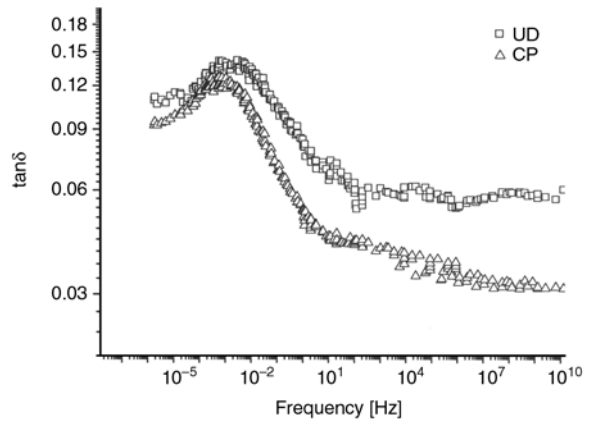


Figure 11. $\tan\delta$ vs. frequency master curves at a reference temperature of 22°C for the all-PP composites with UD and CP lay-ups

be emphasized that these master curves are quite reliable for short term, but significant deviation may occur at large time scales.

The Arrhenius equation was also applied to verify the experimental shift data obtained from the DMTA investigations. In Figure 12, $(\log a_T)$ is thus plotted against the reciprocal of the absolute temperature and the activation energy, E_a , was determined using Equation (4):

$$E_a = m(2.303 \cdot R) \tag{4}$$

where m is the gradient of fit line (in Figure 12) and R is the universal gas constant (8.314 J·K⁻¹·mol⁻¹). The activation energies calculated from the slope of the regression curve were found to be 348 and 307 kJ·mol⁻¹ for UD and CP lay-ups, respectively. Note that they are of the same order as previously reported in the literature [38–41]. The activation energy for shifting the master curve for UD is

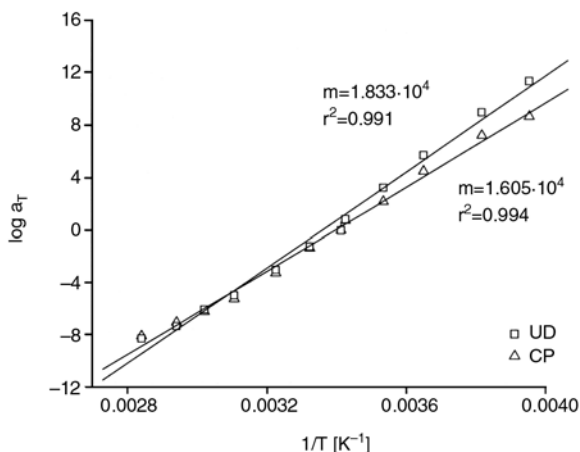


Figure 12. Determination of the activation energy for the all-PP composites with UD and CP lay-ups. Line represents the linear fit

higher than that of CP. Higher activation energy of the all-PP composites with UD lay-up compared to the CP one may be linked with the higher storage modulus of the former.

4. Conclusions

All-PP composites with UD and CP lay-ups were successfully produced from highly oriented coextruded PP tapes (PURE®) by hot consolidation in an autoclave. The dynamic mechanical responses of these tapes and their composites at different frequencies were investigated and analyzed. The storage modulus data obtained from the multi frequency experiments were used to create master curves by assuming time-temperature superposition principle. They can predict the modulus values at frequencies not attainable in the laboratory. The experimental shift factors showed a good agreement with both WLF and Arrhenius models. Using Arrhenius equation, the activation energies required for the UD and CP lay-up composites were calculated. The results showed that higher activation energy was required for shifting the storage modulus curves to obtain the master curve for all-PP composites with UD lay-ups owing to higher stiffness resulting from higher crystallinity (revealed by higher enthalpy of fusion) in the specimens. Additionally, DMTA investigations showed no significant glass transition for the all-PP tapes and their composites due to the high degree of crystallinity and molecular orientation in the all-PP tapes. This is advantageous resulting in a tough failure mode at sub- T_g temperatures and thus broadens the application temperature range of these

recyclable, environment friendly composites toward lower temperatures.

Acknowledgements

The authors thank the German Science Foundation for the financial support of this project (DFG Ka 1202/17)

References

- [1] Capiati N. J., Porter R. S.: The concept of one polymer composites modelled with high density polyethylene. *Journal of Material Science*, **10**, 1671–1677 (1975).
- [2] Loos J., Schimanski T., Hofman J., Peijs T., Lemstra P. J.: Morphological investigations of polypropylene single-fibre reinforced polypropylene model composites. *Polymer*, **42**, 3827–3834 (2001).
- [3] Houshyar S., Shanks R. A.: Morphology, thermal and mechanical properties of poly propylene fibre matrix composites. *Macromolecular Materials and Engineering*, **288**, 599–606 (2003).
- [4] Hine P. J., Ward I. M., Jordan N. D., Olley R. H., Bassett D. C.: The hot compaction behaviour of woven oriented polypropylene fibres and tapes.1. mechanical properties. *Polymer*, **44**, 1117–1131 (2003).
- [5] Ward I. M., Hine P. J.: The science and technology of hot compaction. *Polymer*, **45**, 1413–1427 (2004).
- [6] Hine P. J., Ward I. M., Olley R. H., Bassett D. C.: The hot compaction of high modulus melt-spun polyethylene fibres. *Journal of Material Science*, **28**, 316–324 (1993).
- [7] Yan P. J., Hine P. J., Ward I. M., Olley R. H., Bassett D. C.: The hot compaction of SPECTRA gel-spun polyethylene fibre. *Journal of Material Science*, **32**, 4821–4831 (1997).
- [8] Megremis S. J., Duray S., Gilbert J. L.: Self reinforced composite polyethylene (SRC-PE): a novel material for orthopedic applications. *ASTM Special Technical Publication*, **1346**, 235–255 (1999).
- [9] Hine P. J., Ward I. M., Jordan N. D., Olley R. H., Bassett D. C.: A comparison of the hot-compaction behaviour of oriented, high modulus, polyethylene fibres and tapes. *Journal of Macromolecular Science, Part B: Physics*, **40**, 959–89 (2001).
- [10] Jordan N. D., Olley R. H., Bassett D. C., Hine P. J., Ward I. M.: The development of morphology during hot compaction of tensylon high modulus polyethylene tapes and woven cloths. *Polymer*, **43**, 3397–3404 (2002).
- [11] Rasburn J., Hine P. J., Ward I. M., Olley R. H., Bassett D. C., Kabeel M. A.: The hot compaction of polyethylene terephthalate. *Journal of Material Science*, **30**, 615–622 (1995).
- [12] Hine P. J., Ward I. M.: Hot compaction of woven poly(ethylene terephthalate) multifilaments. *Journal of Applied Polymer Science*, **91**, 2223–2233 (2004).

- [13] Rojanapitayakorn P., Mather P. T., Goldberg A. J., Weiss R. A.: Optically transparent self-reinforced poly(ethylene terephthalate) composites: molecular orientation and mechanical properties. *Polymer*, **46**, 761–773 (2005).
- [14] Hine P. J., Astruc A., Ward I. M.: Hot compaction of polyethylene naphthalate. *Journal of Applied Polymer Science*, **93**, 796–802 (2004).
- [15] Gilbert J. L., Ney D. S., Lautenschlager E. P.: Self-reinforced composite poly(methyl methacrylate)-static and fatigue properties. *Biomaterials*, **16**, 1043–1055 (1995).
- [16] Wright D. D., Lautenschlager E. P., Gilbert J. L.: Bending and fracture toughness of woven self-reinforced composite poly(methyl methacrylate). *Journal of Biomedical Materials Research*, **36**, 441–453 (1997).
- [17] Wright D. D., Gilbert J. L., Lautenschlager E. P.: The effect of processing temperature and time on the structure and fracture characteristics of self-reinforced composite poly(methyl methacrylate). *Journal of Materials Science: Materials in Medicine*, **10**, 503–512 (1999).
- [18] Wright D. D., Lautenschlager E. P., Gilbert J. L.: Hot compaction of poly(methyl methacrylate) composites based on fibre shrinkage results. *Journal of Materials Science: Materials in Medicine*, **16**, 967–975 (2005).
- [19] Hine P. J., Ward I. M.: Hot compaction of woven nylon 6,6 multifilaments. *Journal of Applied Polymer Science*, **101**, 991–997 (2006).
- [20] Pegoretti A., Zanolli A., Migliaresi C.: Flexural and interlaminar mechanical properties of unidirectional liquid crystalline single polymer composites. *Composites Science and Technology*, **66**, 1953–1962 (2006).
- [21] Pegoretti A., Zanolli A., Migliaresi C.: Preparation and tensile mechanical properties of unidirectional liquid crystalline single polymer composites. *Composites Science and Technology* **66**, 1970–1979 (2006).
- [22] Alcock B., Cabrera N. O., Barkoula N. M., Loos J., Peijs T.: The mechanical properties of unidirectional all-polypropylene composites. *Composites, Part A*, **37**, 716–726 (2006).
- [23] Alcock B., Cabrera N. O., Barkoula N. M., Peijs T.: Low velocity impact performance of recyclable all-polypropylene composites. *Composites Science and Technology*, **66**, 1724–1737 (2006).
- [24] Alcock B., Cabrera N. O., Barkoula N. M., Spoelstra A. B., Loos J., Peijs T.: The mechanical properties of woven tape all-polypropylene composites. *Composites, Part A*, **38**, 147–161 (2007).
- [25] Bárány T., Izer A., Czirány T.: On consolidation of self-reinforced polypropylene composites. *Plastics, Rubber and Composites*, **35**, 375–379 (2006).
- [26] Bárány T., Karger-Kocsis J., Czirány T.: Development and characterization of self-reinforced poly(propylene): carded mat reinforcement. *Polymer for Advanced Technologies*, **17**, 818–824 (2006).
- [27] Karger-Kocsis J.: Verbundwerkstoff aus Polypropylenverstärkung und Polypropylenmatrix sowie verschiedene Verfahren zu dessen Herstellung, Patentschrift DE 10237803, Institut für Verbundwerkstoffe GmbH (2007).
- [28] Felix J. M., Gatenholm P.: Formation of entanglements at brushlike interfaces in cellulose-polymer composites. *Journal of Applied Polymer Science*, **50**, 699–708 (1993).
- [29] Alcock B., Cabrera N. O., Barkoula N. M., Reynolds C. T., Govaert L. E., Peijs T.: The effect of temperature and strain rate on the mechanical properties of highly oriented polypropylene tapes and all-polypropylene composites. *Composites Science and Technology*, **67**, 2061–2070 (2007).
- [30] Ward I. M., Sweeney J.: An introduction to the mechanical properties of solid polymers. Wiley, New York (2004).
- [31] Williams M. L., Landel R. F., Ferry J. D.: The temperature dependence of relaxation mechanisms in amorphous polymers and other glass forming liquids. *Journal of American Chemical Society*, **77**, 3701–3707 (1955).
- [32] Ferry J. D.: Viscoelastic properties of polymers, Wiley, New York (1970).
- [33] Yang J., Chaffey C. E., Vancso G. J.: Structure, transitions, and mechanical properties of polypropylene oriented by roll-drawing. *Plastic Rubber and Composites Processing and Applications*, **21**, 201–210 (1994).
- [34] Tariya A. K., Richardson A., Ward I. M.: Production and properties of highly oriented polypropylene by die drawing. *Journal of Applied Polymer Science*, **33**, 2559–2579 (1987).
- [35] Boyd R. H.: Relaxation processes in crystalline polymers: molecular interpretation- a review. *Polymer*, **26**, 1123–1133 (1985).
- [36] Hu W. G., Schmidt-Rohr K.: Polymer ultradrawability: the crucial role of alpha relaxation chain mobility in the crystallites. *Acta Polymerica*, **50**, 271–285 (1999).
- [37] Roy S. K., Kyu T., St. John Manley R.: Mechanical relaxations of oriented gelation-crystallized polyethylene films. *Macromolecules*, **21**, 1741–1756 (1988).
- [38] Ariyama T., Mori Y., Kaneko K.: Tensile properties and stress relaxation of polypropylene at elevated temperatures. *Polymer Engineering and Science*, **37**, 81–90 (1997).
- [39] Faucher J. A.: Viscoelastic behaviour of polyethylene and polypropylene. *Journal of Rheology*, **3**, 81–93 (1959).
- [40] Klompen E. T. J., Govaert L. E.: Nonlinear viscoelastic behaviour of thermorheologically complex materials. *Mechanics of Time-Dependent Materials*, **3**, 46–69 (1999).
- [41] Amash A., Zugenmaier P.: Thermal and dynamic mechanical investigations on fiber-reinforced polypropylene composites. *Journal of Applied Polymer Science* **63**, 1143–1154 (1996).

Development of thermoplastic elastomers based on maleated ethylene propylene rubber (m-EPM) and polypropylene (PP) by dynamic vulcanization

K. Chatterjee, K. Naskar*

Rubber Technology Centre, Indian Institute of Technology, Kharagpur, Kharagpur-721302, West Bengal, India

Received 24 May 2007; accepted in revised form 3 July 2007

Abstract. Dicumyl peroxide (DCP)-cured thermoplastic vulcanizates (TPVs) based on blends of maleated ethylene propylene rubber (m-EPM) and polypropylene (PP) using maleated-PP as a compatibilizer have been developed. Physical properties of these TPVs change significantly with concentrations of DCP and rubber/plastic blend ratios. Important correlations were obtained from rheometer delta torque values with various physical properties of the TPVs like tension set and crosslink density etc. Wide angle X-ray diffraction study confirms that concentration of DCP has a strong influence on the crystallinity of PP, which might affect the final physical properties of TPVs. The recyclability and ageing characteristics of these TPVs are also found excellent.

Keywords: polymer blends and alloys, maleated ethylene propylene rubber, polypropylene, dynamic vulcanization, peroxide

1. Introduction

A thermoplastic elastomer (TPE) is defined as a polymeric material with properties and functional performance similar to those of a conventional vulcanized rubber; still it can be processed in a molten state as a thermoplastic polymer. Because of their unique characteristics, TPEs find very useful and attractive applications in a variety of markets, such as automotives, buildings and constructions, wires and cables etc. TPEs are gradually replacing conventional vulcanized rubbers or elastomers in the above-mentioned fields of application. TPEs based on rubber/thermoplastic blends are generally classified into two main categories: first category consists of simple uncross-linked blends and is commonly designated by thermoplastic elastomeric olefins (TEO), in the second category, the rubber phase is dynamically vulcanized in presence of a suitable cross-linking or curing agent, giving rise to

a thermoplastic vulcanizate (TPV) or dynamic vulcanizate [1–3]. Various TPVs are reported by many authors [4–15]. Very recently Naskar and coworkers [16–21] pursued extensive research on the effects of various peroxides including multifunctional peroxides as cross-linking agents in TPVs. A TPV is typically characterized by finely dispersed (micron-sized) cross-linked rubber particles, distributed in a continuous thermoplastic matrix. Generally the rubber particle size varies in the range of 0.5–2 μm . Commercialized TPVs are commonly based on the blends of ethylene propylene diene rubber (EPDM) and polypropylene (PP), and to a lesser extent of combinations of natural rubber, butyl rubber or nitrile rubber with either PP or polyethylene. The literature survey indicates that at present TPVs comprise of the fastest growing thermoplastic elastomer market with a global annual growth rate of about 15%.

*Corresponding author, e-mail: knaskar@rtc.iitkgp.ernet.in
© BME-PT and GTE

The unique characteristic of EPDM or EPM rubber is its excellent ageing characteristics due to saturated main chain backbone. Maleated ethylene propylene rubber (m-EPM) is basically a chemically modified EPM rubber. Incorporation of polar maleic group gives some additional features to EPM rubber. For instance, m-EPM has moderate tensile strength and elongation at break; it shows very high heat resistance, weather resistance and resistance to different aggressive chemicals like acid, alkali etc. In addition, it exhibits very good electrical properties, excellent fatigue resistance, good abrasion resistance and also good low temperature properties and good adhesion characteristics, especially with polar substrates. Only a limited research has been carried out so far in the field of polar m-EPM rubber based TPVs. There is hardly any openly published literature available in this field because of commercial sensitivity. Potential areas of applications of m-EPM based TPVs could be in automotive industries (under-the-hood applications) and soft-touch appliances.

Cross-linking of elastomers with peroxides has been known for many years already. Mechanism of peroxide cross-linking of EPDM or EPM is very simple. In general, the cross-linking process of high polymers by organic peroxides can be divided into three successive steps. The first step is the homolytic decomposition of peroxide and generation of free radicals. This step is the rate-determining step of the overall reaction. The second step is the abstraction of hydrogen atom from the polymer chain, resulting in stable peroxide decomposition products and polymer radicals. The third and final step consists of the combination of two polymer radicals to form a C–C crosslink. Sometimes, undesired side reactions like disproportionation or chain scission can also occur during the cross-linking process [22–24].

The basic objective of the present paper is to investigate the effects of dicumyl peroxide as cross-linking agent at a fixed and as well as at varied PP/m-EPM blend ratios in dynamically vulcanized blends using maleated-PP as a compatibilizer. The preparation, characterization and various properties of these new TPVs have been extensively studied.

2. Experimental

2.1. Materials used

Polypropylene, Koylene® was obtained from Reliance Industries, India having a density of 0.91 g/cc and melt flow index (MFI) of 12 g/10 min measured at 230°C and 2.16 kg load. Maleated PP (m-PP) was obtained from Vin Industries, New Delhi, India. The MFI of the m-PP, measured at 230°C and 2.16 kg load is 60.20 g/10 min. The extent of maleic anhydride (MAH) is 0.9–1.0%. M-EPM was obtained from DSM Elastomers, The Netherlands, having 2.1 wt% of maleic anhydride, C₂/C₃:50/50, and a density of 0.86 g/cc. The number average molecular weight of m-EPM (M_n) is 45 000 g/mol, weight average molecular weight (M_w) is 90 000 g/mol and Z-average molecular weight (M_z) is 180 000 g/mol as obtained from gel permeation chromatography (GPC). Dicumyl peroxide (DCP) (98%) and triallyl cyanurate (TAC) (50%) were obtained from Akzo Nobel Polymer Chemicals, The Netherlands. DCP was used as the primary cross-linking agent and TAC was used as a co-agent (booster for peroxide).

2.2. Preparation of TPVs

All m-EPM based TPVs were prepared by a batch process in a Brabender Plasti-Corder PLE-330, having a mixing chamber volume of 70 cm³. The batch size was kept 60–65 grams. The mixer temperature was kept at 180–190°C in order to melt PP. A constant rotor (cam type) speed of 80 rpm was used during mixing.

PP and m-PP were first melt mixed. Then m-EPM was added together with paraffinic oil (process aid). Finally the cross-linking agents (DCP and TAC) were added. Mixing was continued for another 4 minutes to achieve the dynamic vulcanization. Immediately after mixing, the composition was removed from the mixer chamber and while still molten, passed once through a cold two-roll mill to achieve a sheet of about 2 mm thickness. The sheet was then cut and pressed for 4 minutes in a compression moulding machine (Moore Press, Birmingham, UK) at 200°C and 5 MPa pressure. Aluminum foil was placed between the sheet and the press plates. The sheet was then cooled down to room temperature under pressure. Test specimens were die-cut from the compression molded sheet

and used for testing after 24 hours of storage at room temperature.

2.3. Testing procedures

2.3.1. Curing characteristics

Curing characteristics of only m-EPM rubber (without any PP) containing cross-linking agents, DCP/TAC were carried out by using Monsanto Rheometer R100S (an oscillating disc rheometer, ODR) at 180°C for 30 minutes.

2.3.2. Mechanical properties

Tensile tests were carried out according to ASTM D412-98 on dumb-bell shaped specimens using a universal tensile testing machine Hounsfield H10KS at a constant cross-head speed of 500 mm/min.

Hardness of the samples was measured by a Durometer (Shore A type) as per ASTM D 2240.

Tension set was measured in universal tensile testing machine Hounsfield H10KS. The test was carried out at room temperature after stretching the TPV samples for 10 minutes at 100% elongation according to ASTM D 412-98.

2.3.3. Cross-link density

The overall cross-link density of the TPV samples was determined on the basis of equilibrium solvent-swelling measurements (in cyclohexane at 23–25°C) by application of the well-known modified Flory-Rehner equation for tetrafunctional networks. A 2 mm thick sample was submerged in cyclohexane. After 24 hours, the cyclohexane was refreshed. After another 24 hours, the swollen sample was weighed, dried and weighed again. From the degree of swelling, the crosslink density (ν) was calculated by modified Flory-Rehner equation (1):

$$\nu = -\frac{1}{V_s} \cdot \frac{\ln(1-V_r) + V_r + \chi V_r^2}{V_r^{1/3} - 0.5 \cdot V_r} \quad [\text{mol/ml}] \quad (1)$$

where V_s – molar volume of cyclohexane, χ – polymer-swelling solvent interaction parameter or Flory-Huggins parameter, which in this cases is 0.3 and V_r is the volume fraction of rubber in the swollen network, V_r is expressed as $V_r = 1/(A_r+1)$ where, A_r is the ratio of the volume of absorbed cyclohexane to that of rubber after swelling.

2.3.4. X-ray diffraction

Wide angle X-ray diffraction (WAXS) was used to evaluate the influence of peroxide on the PP crystal structure in the blend. WAXS was carried out in Philips PW 1710 diffractometer (CuK α target). The samples were scanned from $2\theta = 10$ to 50° with a scanning rate of $30^\circ/\text{min}$.

2.3.5. Recycling study

The compression moulded TPV samples were again melt-mixed in the internal mixer for 4 minutes. Then they were remolded and finally properties after recycling were determined.

2.3.6. Ageing test

Ageing test was carried out keeping the TPV samples in an ageing oven at 100°C for 72 hours.

3. Results and discussion

3.1. Influence of peroxide at a fixed blend ratio

3.1.1. Mechanical properties

Table 1 shows TPV compositions with different DCP concentrations (0–3 phr) at a fixed blend ratio and Table 2 shows their corresponding mechanical properties. In this case, 10 phr (previously optimized concentration) of m-PP was used as a compatibilizer for m-EPM and PP blends; since m-EPM is polar in nature whereas PP is a non-polar polymer.

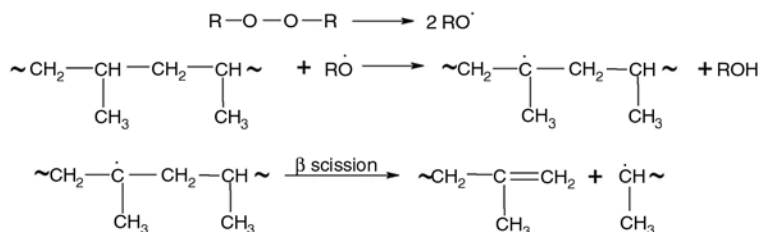
From Table 2, it is seen that tensile strength of m-EPM based TPVs varies from 3.5 to 7.3 MPa and elongation at break varies from 120 to 240%. Tensile strength and elongation reach a maximum at 2 phr of DCP concentration. During vulcanization, two competing processes take place simultaneously in presence of DCP. One is cross-linking in rubber

Table 1. TPV compositions (in parts per hundred rubber or phr) with different DCP concentrations at a fixed m-EPM/ PP blend ratio

Components	N-01	N-02	N-03	N-04	N-05	N-06
m-EPM	100	100	100	100	100	100
PP	60	60	60	60	60	60
m-PP	10	10	10	10	10	10
Paraffinic oil	25	25	25	25	25	25
DCP (98%)	0	1.0	1.5	2.0	2.5	3.0
TAC (50%)	0	4	4	4	4	4

Table 2. Physical properties of different TPVs

Physical properties	N-01	N-02	N-03	N-04	N-05	N-06
Tensile strength [MPa]	3.5	6.3	6.6	7.3	6.2	5.7
Elongation at break [%]	120.0	178.0	219.0	240.0	159.0	177.0
Modulus at 50% [MPa]	3.5	3.9	4.0	4.1	4.2	4.3
Modulus at 100% [MPa]	4.5	5.0	5.1	5.2	5.8	5.9
Modulus at 150% [MPa]	–	5.7	5.8	5.9	6.1	6.3
Hardness [Shore A]	60.0	65.0	68.0	70.0	72.0	73.0
Overall crosslink density $\nu \cdot 10^5$ [mol/ml]	–	14.5	15.3	19.6	20.7	22.1
Tension set [%]	–	16.1	14.2	12.2	10.2	8.2
Tear strength [N/mm]	–	20.1	35.0	42.4	45.8	52.1

**Figure 1.** General scheme of β -chain scission of PP in presence of peroxide

phase and the other is degradation in PP-phase by β -chain scission by abstraction of tertiary hydrogen atoms from the main chain of the olefinic polymer [23, 24]. General scheme of β -chain scission of PP in presence of peroxide is shown in Figure 1.

In this particular case, 2 phr concentration of DCP is found to be optimum. Other mechanical properties like the moduli, hardness, tear strength and overall cross-link density of TPVs have also been found to increase with increasing DCP concentration. Modulus at 50% varies from 3.5 to 4.3 MPa, modulus at 100% varies from 5 to 5.9 MPa and modulus at 150% varies from 5.7 to 6.3 MPa with increasing DCP concentration from 1 to 3 phr. Hardness is lying in between 60 to 73 Shore A. Tear strength increases from 20 to 52 N/mm. On the other hand, the tension set value decreases from 16.1 to 8.2% indicating better elastic recovery behaviour of these TPVs.

3.1.2. Curing characteristics

In order to achieve a better in-sight into the chemistry involved with dynamic vulcanization in m-EPM/PP blends in presence of DCP, it is essential to know the vulcanization characteristics of pure m-EPM gum compounds without any PP at various DCP concentrations. Table 3 shows the recipes of m-EPM gum compounds at different DCP concentrations for ODR study.

Table 3. Recipes of m-EPM gum compounds at different DCP concentrations

Ingredients	N-07	N-08	N-09	N-10	N-11
m-EPM	100	100	100	100	100
Paraffinic oil	25	25	25	25	25
DCP (98%)	1.0	1.5	2.0	2.5	3.0
TAC (50%)	4	4	4	4	4

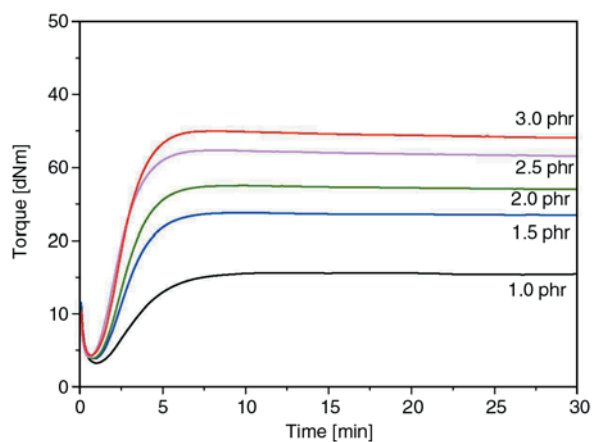
**Figure 2.** Rheograms of pure m-EPM vulcanizates containing various DCP concentrations at 180°C

Figure 2 shows rheograms of pure m-EPM vulcanizates at 180°C and Table 4 demonstrates the corresponding rheometer data.

The delta torque (maximum-minimum torque) values obtained from ODR generally correlates with the cross-linking efficiency of the peroxide, which is defined as the number of moles of chemical cross-links formed per mole of peroxide. It should

Table 4. Rheometer data of m-EPM gum compounds at 180°C for 30 minutes

Formulation	Minimum torque [dNm]	Maximum torque [dNm]	Delta torque [dNm]	T _{C90} [min]	T _{S2} [min]
N-07	3.23	15.62	12.39	6.3	2.1
N-08	3.82	23.76	19.94	5.0	1.6
N-09	3.85	27.50	23.65	4.8	1.5
N-10	4.04	32.34	28.30	4.3	1.2
N-11	4.29	35.00	30.71	4.5	1.3

be noted however, that the latter could be measured by static vulcanization only in absence of PP; which is not exactly a one-to-one comparison to dynamic vulcanization, due to lack of high shear rate and the longer time scales.

From Table 4, it is observed that delta torque values increase with increasing peroxide concentrations. It clearly indicates that with increasing DCP

concentration more cumyloxy or methyl radicals are formed, which basically leads to higher extent of cross-linking in m-EPM phase. Reduction in optimum cure time (T_{c90}) and scorch time (T_{S2}) with increasing DCP concentrations also explain the same. An attempt was made to find whether there is any correlation between ODR delta torque and various physical properties of TPVs. Figures 3 and 4 show relations between ODR delta torque and cross-link density and tension set of TPVs respectively. Linear correlations have been noticed which indicate that ODR delta torque of DCP/TAC-cured mEPM (without any PP though) is directly proportional to the cross-link density and tension set values of TPVs.

In order to understand the deterioration of physical properties of TPVs at higher concentration of DCP, wide angle X-ray diffraction (WAXS) study has been carried out to check if there is any influence of DCP on PP crystallinity. Figure 5 shows WAXS graph of TPVs with 1 phr of DCP. The major peaks correspond to 130, 111, 131 and 041 planes in the crystal respectively. The pattern of PP in the blend samples shows α form (monoclinic) only, because there is no line at $2\theta = 16.10$, which is normally associated with β form (hexagonal). All other XRD graphs of TPV samples containing various DCP concentrations are not shown, because the basic

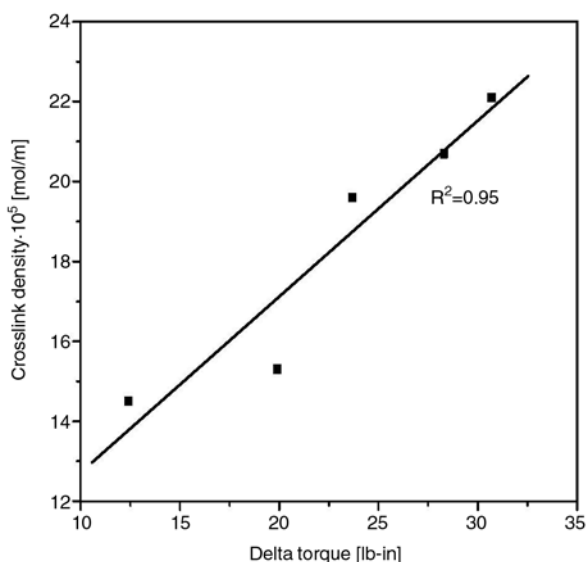
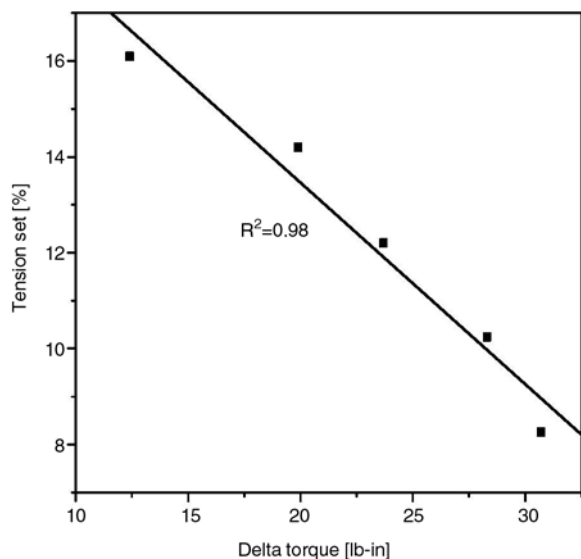
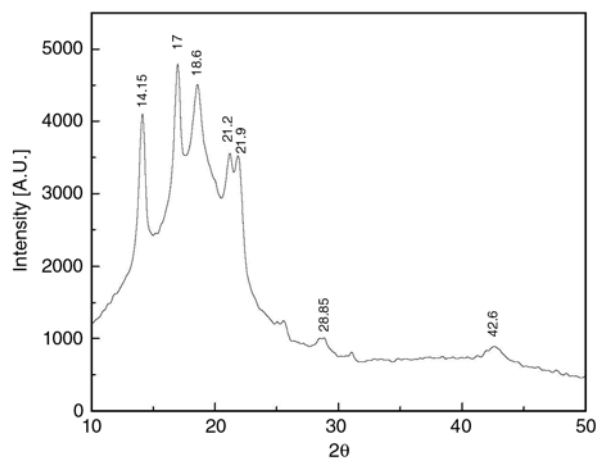
**Figure 3.** Cross-link density as a function of delta torque**Figure 4.** Tension set as a function of delta torque**Figure 5.** XRD graphs of TPV with 1.0 phr of DCP

Table 5. Percent crystallinity of different TPVs with different DCP concentrations

Sample designation and peroxide concentration	% crystallinity
N-01 (0 phr)	56
N-02 (1 phr)	48
N-04 (2 phr)	42
N-06 (3 phr)	40

nature of all other graphs are very similar. From the XRD graphs, percent crystallinity was calculated for different samples, which is shown in Table 5.

Table 5 shows that the % crystallinity decreases with increasing concentration of peroxide. From the table it is also observed that, without DCP the crystallinity is maximum, which is 56%. With the increase in concentration of DCP from 1 to 3 phr, the crystallinity decreases from 48 to 40%. This explains why the mechanical properties of TPVs decrease at higher DCP concentration.

3.1.3. Recycling study

One of the major advantages of the TPEs and TPV is its ability of recycling without significant deterioration of mechanical properties. Recycling study has been performed on the TPVs with varied concentrations of DCP. After the recycling, it is found that there are only minor changes in the properties, which indicates that these TPVs show very good recyclability. Table 6 shows the properties after the recycling.

Table 6. Physical properties of TPVs with different DCP concentrations after recycling

Properties	N-01	N-02	N-03	N-04	N-05	N-06
Tensile strength [MPa]	3.4	5.0	5.2	5.7	5.5	5.4
Elongation at break [%]	110	140	149	190	156	140
Modulus at 50% [MPa]	3.2	3.5	3.9	4.0	4.3	4.9
Modulus at 100% [MPa]	3.4	4.9	5.1	5.2	5.8	6.0
Tear strength [N/mm]	18	25	30.2	35.1	40.1	45.2

Table 7. Physical properties of TPVs before and after ageing

Sample designation	Tensile strength (before ageing)	Tensile strength (after ageing)	Elongation at break (before ageing)	Elongation at break (after ageing)
N-02	6.3	6.2	178	150
N-03	6.6	6.3	219	195
N-04	7.3	7.1	240	210
N-05	6.2	5.9	159	148
N-06	5.7	5.5	177	139

3.1.4. Ageing study

Table 7 shows the physical properties of the aged samples. The results show that there are not significant changes after ageing. So the ageing characteristics are good for these TPVs. Reason for achieving good ageing characteristics is that upon peroxide cross-linking C–C bond is formed, which has high bond energy.

3.2. Influence of peroxide at varied blend ratios

3.2.1. Mechanical properties

Table 8 shows the TPV compositions at varied m-EPM/PP ratios at a fixed DCP concentration of 2 phr and Table 9 shows their corresponding properties.

From Table 9, it is noticed that the tensile strength varies from 4.5 to 8.8 MPa as the amount of PP increases from 20 to 100 phr. However the elongation at break decreases from 210 to 150%. This is because of the fact that PP itself has high strength but low elongation at break. The modulus at 50% increases from 1.9 to 7.4 MPa; the modulus at 100% increases from 2.7 to 8.3 MPa and the modu-

Table 8. TPV compositions (in phr) at varied m-EPM/PP ratios at a fixed DCP concentration

Ingredients	N-12	N-13	N-04	N-14	N-15
m-EPM	100	100	100	100	100
PP	20	40	60	80	100
m-PP	10	10	10	10	10
Paraffinic oil	25	25	25	25	25
DCP (98%)	2	2	2	2	2
TAC (50%)	4	4	4	4	4

Table 9. Physical properties of different blends

Properties	N-12	N-13	N-04	N-14	N-15
Tensile strength [MPa]	4.5	6.5	7.3	8.2	8.8
Elongation at break [%]	210.0	215.0	240.0	191.0	150.0
Modulus at 50% [MPa]	1.9	3.3	4.1	5.8	7.4
Modulus at 100% [MPa]	2.7	4.4	5.2	6.8	8.3
Modulus at 150% [MPa]	3.5	5.4	5.9	7.7	8.8
Tear strength [N/mm]	23.8	40.6	42.4	54.1	66.2
Hardness [Shore A]	60.0	68.0	70.0	76.0	81.0
Tension set [%]	8.3	10.2	12.2	14.2	18.1

lus at 150% increases from 3.5 to 8.8 MPa. Tear strength is also increased from 23.8 to 66.2 N/mm with increasing amount of PP. Hardness varies from 60 to 81 Shore A. Tension set is found to increase indicating poor set property. The reason for increased tensile strength, modulus and hardness with the increasing amount of PP is due to the increased thermoplastic hard component in the blends.

4. Conclusions

Peroxide-cured TPVs based on blends of m-EPM and PP using m-PP as a compatibilizer have been developed. Physical properties of these TPVs change significantly with DCP concentrations and rubber/plastic blend ratios. The concentration of DCP is optimized at 2 phr. Important correlations were obtained from ODR delta torque values with various physical properties of m-EPM based TPVs like tension set and crosslink density. WAXS data indicate that concentration of DCP has a strong influence on the crystallinity of PP that might affect the final physical properties of TPVs. The recyclability and ageing properties of the TPVs are found excellent.

References

- [1] Legge N. R., Holden G., Schroeders H. E.: Thermoplastic elastomer: A Comprehensive review. Hanser, Munich (1987).
- [2] Bhowmick A. K., Stephens H. L.: Handbook of Elastomers: New developments and technology. Marcel Dekker, New York (1988).
- [3] De S. K., Bhowmick A. K.: Thermoplastic elastomers from rubber plastic blends. Horwood, London (1990).
- [4] Fisher W. K.: Thermoplastic blend of partially cured monoolefin copolymer rubber and polyolefin plastic. US Patent 3862106, USA (1973).
- [5] Coran A. Y., Patel R.: Rubber-thermoplastic compositions. Part IV. Thermoplastic vulcanizates from various rubber-plastic combinations. *Rubber Chemistry and Technology*, **54**, 892–903 (1981).
- [6] Coran A. Y., Das B., Patel R. P.: Thermoplastic vulcanizates of olefin rubber and polyolefin resin. US Patent 4130535, USA (1978).
- [7] Abdou-Sabet S., Fath M. A.: Thermoplastic elastomeric blends of olefin rubber and polyolefin resin. US Patent 4311628, USA (1982).
- [8] Coran A. Y., Patel R.: Rubber-thermoplastic compositions. Part I. EPDM-polypropylene thermoplastic vulcanizates. *Rubber Chemistry and Technology*, **53**, 141–150 (1980).
- [9] Coran A. Y., Patel R.: Rubber-thermoplastic compositions. Part II. NBR-nylon thermoplastic elastomeric compositions. *Rubber Chemistry and Technology*, **53**, 781–794 (1980).
- [10] Coran A. Y., Patel R.: Rubber-thermoplastic compositions. Part III. Predicting elastic moduli of melt mixed rubber-plastic blends. *Rubber Chemistry and Technology*, **54**, 91–100 (1981).
- [11] Coran A. Y., Patel R., Williams D.: Rubber-thermoplastic compositions. Part V. Selecting polymers for thermoplastic vulcanizates. *Rubber Chemistry and Technology*, **55**, 116–136 (1982).
- [12] Coran A. Y., Patel R.: Rubber-thermoplastic compositions. Part VI. The swelling of vulcanized rubber-plastic compositions in fluids. *Rubber Chemistry and Technology*, **55**, 1063–1077 (1981).
- [13] Coran A. Y., Patel R.: Rubber-thermoplastic compositions. Part VII. Chlorinated polyethylene rubber nylon compositions. *Rubber Chemistry and Technology*, **56**, 210–225 (1983).
- [14] Coran A. Y., Patel R.: Rubber-thermoplastic compositions. Part VIII. Nitrile rubber polyolefin blends with technological compatibilization. *Rubber Chemistry and Technology*, **56**, 1045–1060 (1983).
- [15] Coran A. Y.: Vulcanization: conventional and dynamic. *Rubber Chemistry and Technology*, **68**, 351–375 (1995).
- [16] Naskar K., Noordermeer J. W. M.: Dynamically vulcanized PP/EPDM blends—Effects of different types of peroxide on the properties. *Rubber Chemistry and Technology*, **76**, 1001–1018 (2003).

- [17] Naskar K., Noordermeer J. W. M.: Multifunctional peroxide as a means to improve properties of dynamically vulcanized PP/EPDM blends. *Kautschuk, Gummi, Kunststoffe*, **57**, 235–239 (2004).
- [18] Naskar K., Kokot D., Noordermeer J. W. M.: Influence on various stabilizers on aging of dicumyl peroxide cured polypropylene/ethylene-propylene-diene thermoplastic vulcanizates. *Polymer Degradation and Stability*, **85**, 831–839 (2004).
- [19] Naskar K., Noordermeer J. W. M.: Dynamically vulcanized PP/EPDM blends - effects of multifunctional peroxides as a crosslinking agents. *Rubber Chemistry and Technology*, **77**, 955–971 (2004).
- [20] Naskar K., Noordermeer J. W. M.: Thermoplastic elastomers by dynamically vulcanization. *Progress in Rubber, Plastics and Recycling Technology*, **21**, 1–26 (2005).
- [21] Datta S., Naskar K., Jelenic J., Noordermeer J. W. M.: Dynamically vulcanized PP/EPDM blends by multifunctional peroxides: Characterization with various analytical techniques. *Journal of Applied Polymer Science*, **98**, 1393–1403 (2005).
- [22] Loan L. D.: Mechanism of peroxide vulcanization of elastomers. *Rubber Chemistry and Technology*, **40**, 149–176 (1967).
- [23] Baldwin F. P., Borzel P., Cohen C. A., Makowski H. S., Van de Castle J. F.: The influence of residual olefin structure on EPDM vulcanization. *Rubber Chemistry and Technology*, **43**, 522–548 (1970).
- [24] Hofmann W., Crosslinking agents in ethylene-propylene rubbers. *Kautschuk, Gummi, Kunststoffe*, **40**, 308–332 (1987).

Conventional and atom transfer radical copolymerization of phenoxycarbonylmethyl methacrylate-styrene and thermal behavior of their copolymers

G. Barim, K. Demirelli*, M. Coşkun

University of Firat, Faculty of Science and Arts, Department of Chemistry, 23119 Elazığ, Turkey

Received 19 February 2007; accepted in revised form 5 July 2007

Abstract. The atom transfer radical polymerization (ATRP) of phenoxycarbonylmethyl methacrylate (PCMMA) with styrene (St) were performed in bulk at 110°C in the presence of ethyl 2-bromoacetate, cuprous(I)bromide (CuBr), and N,N,N',N'',N'''-pentamethyldiethyltriamine. Also, a series conventional free-radical polymerization (CFRP) of PCMMA and styrene were carried out in the presence of 2,2'-azobisisobutyronitrile in 1,4-dioxane solvent at 60°C. The structure of homo and copolymers was characterized by IR, ¹H and ¹³C-NMR techniques. The composition of the copolymers was calculated by ¹H-NMR spectra. The average-molecular weight of the copolymers were investigated by Gel Permeation Chromatography (GPC). For copolymerization system, their monomer reactivity ratios were obtained by using both Kelen-Tüdös and Fineman-Ross equations. Thermal analysis measurements of homo- and copolymers prepared CFRP and ATRP methods were measured by TGA-50 and DSC-50. Blends of poly(PCMMA) and poly(St) obtained via ATRP method have been prepared by casting films from dichlorormethane solution. The blends were characterized by differential scanning calorimetry. The initial decomposition temperatures of the resulting copolymers increased with increasing mole fraction of St.

Keywords: polymer synthesis, molecular engineering, polymer composites, thermal properties

1. Introduction

Controlled/living vinyl addition polymerization giving a wide range of polymer structures is continuing to receive widespread attention [1]. This allows the controlled synthesis of a range of polymeric structures such as block copolymers, graft copolymers, functional polymes, star polymers [2, 3]. In comparison to the other controlled radical polymerization processes, atom transfer radical polymerizations is mechanistically more complex. Thus, the catalyst reactivity depends on the ligand, the transition metal itself, and the initiating organic halide [4]. So far, copper-based systems seem to be the most efficient [5] when compared to other transition metals such as iron [6], nicke [7], ruthenium

[8], rhodium [9]. The counterions are often chloride and bromide, and bromide normally yields higher rates [10].

The majority of studies on living radical polymerization focuses either on hopolymerization or copolymerization [11]. Some works focus on statistical copolymerizations and it is a common practice to evaluate the monomer reactivity ratios of the living radical copolymerization system, and compare the results with the free radical copolymerization analogue [12]. The finding that the reactivity ratios for monomers under living free radical conditions are essentially the same as under normal free radical conditions is also fundamentally important. Thus, random copolymers prepared by living free radical processes are different on a molecular level

*Corresponding author, e-mail: kdemirelli@firat.edu.tr
© BME-PT and GTE

to those prepared by normal free radical methods, even though they may appear the same on the macroscopic level [13]. There have been several reports on monomer reactivity ratios in ATRP and other transition-metal mediated polymerizations [14, 15]. This study was extended to a series of PCMMA in order to investigate the effect of the increasing molecular weight on monomer reactivity. Similar results were seen as for the amino methacrylates, with higher levels of incorporation into the copolymer in transition metal mediated polymerizations than in free radical polymerizations for all molecular weights [16].

In this work, our investigation concentrates on both the living radical copolymerization and conventional free radical copolymerization of phenoxycarbonylmethyl methacrylate (PCMMA) and styrene (St), the characterization of the resulting copolymers and their the monomer reactivity ratios were determined by both the Kelen-Tüdös and Fineman-Ross procedures. The glass transition and the degradation temperature, and average-molecular weights of copolymers were determined by differential scanning calorimetry (DSC), thermogravimetric analysis (TGA) and Gel Permeation Chromatography (GPC) measurements, respectively. Thermal analysis results are given for comparison purpose with each other for all polymers. Blends of poly(PCMMA) and poly(St) obtained via ATRP method are characterized by differential scanning calorimetry.

2. Experimental

2.1. Materials

Styrene (St) (Aldrich) were distilled under vacuum after washing with 5% NaOH aqueous solution just before copolymerization. Cuprous(I)bromide/ N,N,N',N'',N''' -pentamethyldiethyltriamine and ethyl 2-bromoacetate as initiator were used as received and phenoxycarbonylmethyl methacrylate was synthesized in our laboratory.

2.2. Synthesis of phenoxycarbonylmethyl methacrylate (PCMMA)

Phenoxycarbonylmethyl methacrylate was synthesized by the reaction of phenoxycarbonyl bromomethane with sodium methacrylate by using triethylbenzylammonium chloride (TEBAC)

(Aldrich) as a phase transfer catalyst and distilled under vacuum (bp: 162°C at 5 mmHg), yield: 72%. IR (cm^{-1} , the most characteristic bands): 1784 (C=O stretch adjacent to phenoxy), 1730 (C=O stretch), 1638 (C=C stretch in the vinyl group), 1592 (C=C stretch in aromatic ring).

$^1\text{H-NMR}$ (CDCl_3 , δ): 2.03 (s, 3H), 5.72 (s, 1H), 6.29 (s, 1H), 6.9–7.4 (aromatic ring protons).

2.3. Characterization techniques

Infrared spectra were obtained on a Perkin Elmer Spectrum One FT-IR spectrometer. NMR spectra were recorded on a Jeol FX 90Q NMR spectrometer at room temperature in CDCl_3 . Thermogravimetric analysis (TGA) measurements were carried out under a nitrogen flow with a TGA-50 thermobalance at a heating rate of $10^\circ\text{C}\cdot\text{min}^{-1}$. Gel Permeation Chromatography (GPC) analyses were carried out using a high pressure liquid chromatography pump with Agilent 1100 system equipped with a vacuum degasser, a refractive index detector. The eluting solvent was tetrahydrofuran (THF), the flow rate was $1\text{ ml}\cdot\text{min}^{-1}$. Calibration was achieved with polystyrene.

2.4. Atom transfer radical copolymerization of PCMMA with St

The general procedure for the copolymerization of PCMMA with St of six compositions was as follows: In all cases, predetermined amounts of monomers, ethyl 2-bromoacetate as initiator, N,N,N',N'',N''' -pentamethyldiethyltriamine as ligand and the calculated amount of CuBr as catalyst were added to a flask. The mixture was first degassed three times and sealed in vacuo. The flask was shaken until the mixture was dissolved, immersed in an oil bath, and heated to the required temperature (at 110°C). After a given time, the flasks were opened and dichloromethane was added to the sample to dissolve the copolymer. The heterogeneous solution was filtered. The copolymers were isolated by precipitation in ethylalcohol and dried under vacuum at 40°C for 24 h. The conversion of the copolymerization was under 15%.

2.5. Conventional Free-radical copolymerization of PCMMA with St

Six copolymers of PCMMA with St were prepared in 1,4-dioxane at 60°C in the presence of AIBN. Predetermined amounts of the monomers, AIBN and the solvent were mixed in a polymerization tube. The mixture was degassed about 10 minute with argon and kept in a thermostatted oil bath at 60°C. After desired time, the mixture was cooled to ambient temperature. The copolymers were precipitated into excess ethanol and purified by reprecipitation, and then the copolymers were dried under vacuum at 40 for 24 h.

2.6. Preparation of polymer blends

Blend samples of Poly(PCMMA) ($M_n=50\ 000$) and poly(St) ($M_n=32\ 000$) – prepared under conditions above mentioned via ATRP method – were prepared by solution casting from dichloromethane at room temperature, and the blends were dried at 40°C for 24 h under vacuum.

3. Results and discussion

3.1. Characterization of polymers

The $^1\text{H-NMR}$ spectrum of poly(PCMMA-co-St) showed signals at 4,62 ppm (OCH_2CO , 2H) and 6,7–7,35 ppm (aromatic ring protons, 10H) in PCMMA and St units. While the PCMMA units in the copolymer increase from 13 to 73% for copolymer prepared via ATRP, from 12 to 76% for copolymer prepared via conventional free radical polymerization. The FT-IR spectra of the copolymers prepared by conventional free radical polymerization in various feed ratios of PCMMA and St is illustrated in Figure 1. The FT-IR spectra for

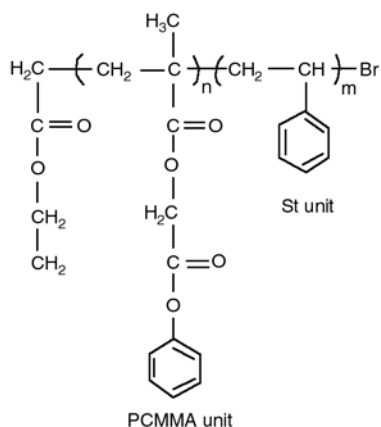


Figure 1. The structure of PCMMA and St copolymer

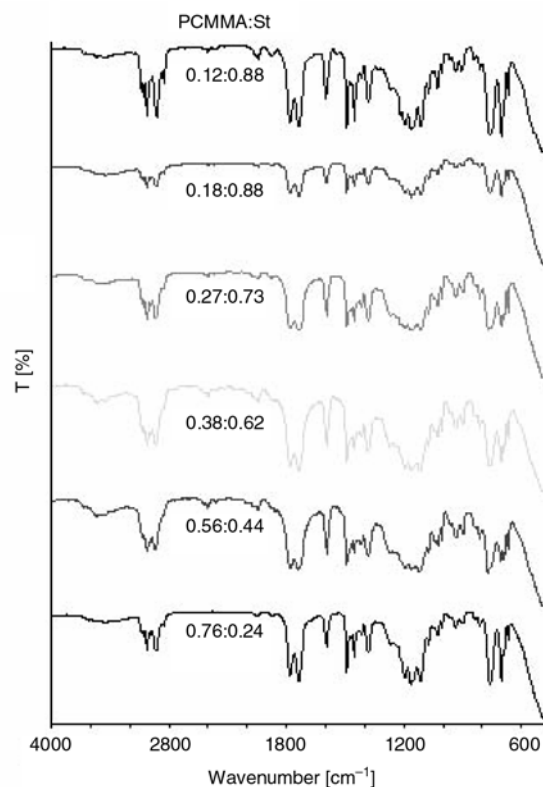


Figure 2. FT-IR spectra of PCMMA-St copolymer system

copolymers both Atom Transfer Radical and conventional free radical polymerizations showed two ester carbonyl bands at 1781 and 1736 cm^{-1} , respectively. Also, $^{13}\text{C-NMR}$ spectrum showed the signals attributed to $-\text{CH}-$ of the St unit at 45.6 ppm and the $-\text{CH}_2-$, which is adjacent to ester oxygene in PCMMA unit at 60.0 ppm. The other signals are in a good agreement with structure of copolymer showed in Figure 2.

3.2. Atom transfer random copolymerization of PCMMA and St

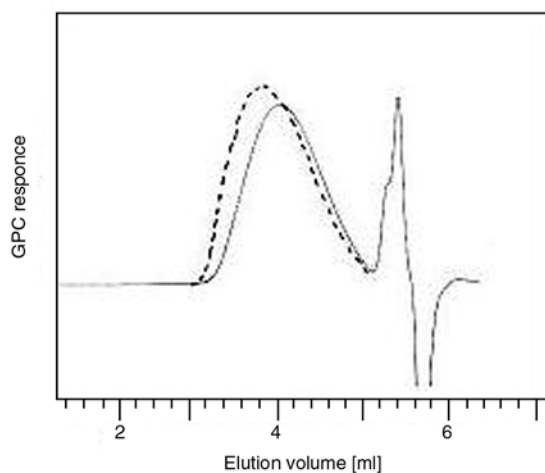
The copolymerization of six compositions with PCMMA and St was carried out in presence of Cuprous(I)bromide/ $\text{N,N,N',N'',N'''}\text{-pentamethyl-diethyltriamine}$ as catalyst system and ethyl 2-bromoacetate as initiator at 110°C. The average-number molecular weights and polydispersities were determined by GPC. The decrease in M_n values with an increasing molar fraction of PCMMA in the copolymer is probably due to manipulating by the controlled polymerization conversion of St units. In addition, as PCMMA unit increased in the resulting copolymers, PD (M_w/M_n) was increased ($1.48 < M_w/M_n < 1.92$). On the other hand, PD (M_w/M_n) for the conventional free radical polymerization

Table 1. GPC results in copolymers prepared via ATRP

Entry	M_n	M_w/M_n
Poly(PCMMA0.12-co-St)	20 300	1.48
Poly(PCMMA0.27-co-St)	39 900	1.92
Poly(PCMMA0.77-co-St)	49 800	1.91

Table 2. GPC results in copolymers prepared via conventional free radical polymerization

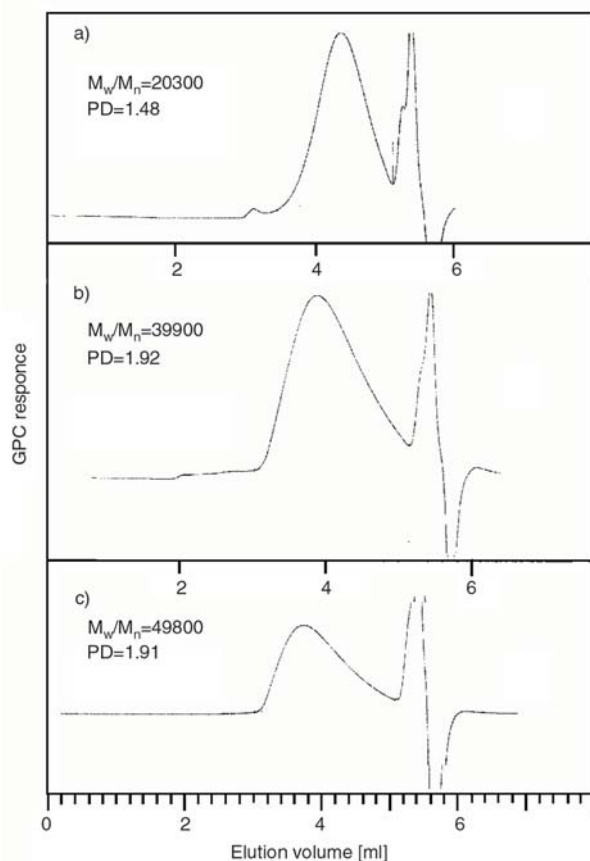
Entry	M_n	M_w/M_n
Poly(PCMMA0.13-co-St)	35 800	1.64
Poly(PCMMA0.18-co-St)	36 300	1.72
Poly(PCMMA0.27-co-St)	40 500	1.76
Poly(PCMMA0.38-co-St)	43 300	1.87

**Figure 3.** GPC curves of poly(PCMMA-co-St) in two various composition prepared by CFRP method [(poly(PCMMA0.12-co-St) Continuous line, $M_w/M_n = 35\ 000$, PD = 1.64), (poly(PCMMA0.38-co-St), the dashed line, $M_w/M_n = 43\ 300$, PD = 1.87)]

was $1.64 < M_w/M_n < 1.87$. This suggests that the contribution of chain breaking and transfer as well as termination reactions during copolymerization can be neglected until a higher polymerization conversion, which is similar to the results reported by Zhou *et al.* [17]. The results are summarized in Table 1 and Table 2, respectively. The single GPC profiles of two resulting copolymers for the conventional free radical polymerization, and atom transfer radical polymerization are presented in Figure 3 and 4, respectively.

3.3. Calculation of monomer reactivity ratios of PCMMA and St

Conventional free radical polymerization and the atom transfer radical random copolymerization of PCMMA and St initiated by ethyl 2-bromoacetate

**Figure 4.** GPC curves of poly(PCMMA-co-St) in three different copolymer composition prepared by ATRP method**Table 3.** Comonomer compositions in feed and copolymer via ATRP^a and free radical polym

Copolymers	in feed (M_1) ^b	in copolymer via ATRP (m_1) ^c	in copolymer via CFRP (m_1) ^c
1	0.10	0.13	0.12
2	0.20	0.18	0.18
3	0.35	0.33	0.27
4	0.50	0.42	0.38
5	0.70	0.48	0.56
6	0.85	0.73	0.76

^a[Monomer]:[CuBr]:[Ligand]:[Initiator] = 100:1:2:1 at 110°C

M_1^b – mole fraction of PCMMA in feed,

m_1^c – mole fraction of PCMMA in copolymer

for various ratios of PCMMA to St has been carried out. Chemoselectivity of PCMMA and St radicals generated in ATRP and conventional free radical polymerization are compared by determining the monomer reactivity ratios. Table 3 shows the influence of the initial molar compositions of the comonomers on those of the comonomers in the copolymers, in both ATR copolymerization and conventional free radical copolymerization. ¹H-NMR spectroscopy has been used extensively to

evaluate the microstructure of styrene-metacrylate copolymers. The monomer sequence distribution of these copolymers was also calculated theoretically from the monomer reactivity ratios and compared with the experimental data obtained by ¹H-NMR [18, 19]. In this study, the copolymer compositions were also analyzed with ¹H-NMR spectra. The peaks at 6.6–7.4 ppm correspond to the aromatic protons in PCMMA and St units, the signal centered at 4.7 ppm is assigned to methylene protons, which is adjacent to oxygene in PCMMA units. The other signals at 1–2.2 ppm are assigned to methylene and methyl in polymer main chain. Thus, the mole fractions of PCMMA and St in the copolymer were determined from the ratio of the integral intensities of aromatic protons of PCMMA in 6.8–7.4 ppm and the methylene protons in PCMMA unit between at 4.7 ppm. The copolymer compositions for ATRP have been calculated from the Equation (1):

$$C = \frac{\text{Integral intensities of aromatic protons (Iar)}}{\text{Integral intensities of aliphatic protons (Ialf)}} = \frac{5}{2m_1} \quad (1)$$

where m_1 is mole fraction of PCMMA, and m_2 is that of St in copolymer.

Similar calculations have been also made for conventional free radical copolymerization. The K-T and F-R parameters were calculated, using data in

Table 3, for both the living radical copolymerization and conventional free radical copolymerization of PCMMA and St, and the results were summarized in Table 4 and Table 5, respectively. Plots of PCMMA mole fraction in feed vs. PCMMA mole fraction in copolymers, synthesized by ATRP and CFRP, are shown in Figure 5. These plots exhibit azeotropic points at 0.22 for both CFRP and ATRP. One of the aims of this work was to determine whether the observed difference in monomer reactivity ratios could be due to monomer coordination to the transition metal used in transition-metal mediated polymerization. It is well known that monomer reactivity ratios can offer the message of

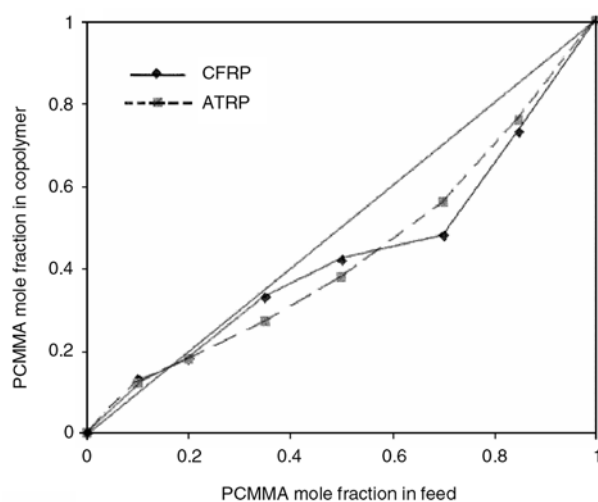


Figure 5. Composition diagrams of ATRP and conventional free radical copolymerization methods

Table 4. Results of the living radical copolymerization of PCMMA and St

Sample No	F = M ₁ /M ₂	f = m ₁ /m ₂	G = F(f - 1)/f	H = F ² /f	η = G/α + H	ξ = H/α + H
1	0.111	0.149	-0.633	0.082	-0.592	0.076
2	0.250	0.219	-0.891	0.285	-0.700	0.224
3	0.538	0.492	-0.555	0.588	-0.352	0.373
4	1.000	0.724	-0.381	1.381	-0.160	0.583
5	2.333	0.923	-0.194	5.896	-0.028	0.856
6	5.666	2.700	3.567	11.890	0.277	0.923

M₁ – mole fraction of PCMMA in feed, M₂ – mole fraction of St in feed, m₁ – mole fraction of PCMMA in copolymer, m₂ – mole fraction of St in copolymer. (H_{min}·H_{max})^{1/2} = 0.987; H_{min} – lowest value of H, H_{max} – highest value of H

Table 5. Results of the conventional free radical copolymerization of PCMMA and St

Sample No	F = M ₁ /M ₂	f = m ₁ /m ₂	G = F(f - 1)/f	H = F ² /f	η = G/α + H	ξ = H/α + H
1	0.111	0.136	-0.705	0.090	-0.674	0.086
2	0.250	0.219	-0.891	0.285	-0.718	0.229
3	0.538	0.369	-0.919	0.784	-0.528	0.450
4	1.000	0.612	-0.633	1.633	-0.244	0.630
5	2.333	1.272	0.506	4.279	0.096	0.817
6	5.666	3.166	3.876	10.140	0.349	0.913

M₁ – mole fraction of PCMMA in feed, M₂ – mole fraction of St in feed, m₁ – mole fraction of PCMMA in copolymer, m₂ – mole fraction of St in copolymer. (H_{min}·H_{max})^{1/2} = 0.955; H_{min} – lowest value of H, H_{max} – highest value of H

Table 6. Monomer reactivity ratios of PCMMA-St monomer pair in ATRP and CFRP methods

System	Methods	r_1^a	r_2	$r_1 \cdot r_2$
Atom transfer radical polymerization	K-T	0.24	0.76	0.18
	F-R	0.33	0.96	0.31
Conventional Free radical polymerization	K-T	0.32	0.90	0.28
	F-R	0.47	1.16	0.54

^a r_1 – monomer reactivity ratio of PCMMA

relative reactivity of comonomers [20–22]. To estimate the relative reactivity of PCMMA and St in the atom transfer radical polymerization and conventional free radical polymerization, the Kelen-Tüdös [23] and Fineman-Ross [24] equations were used, which are $\eta = (r_1 + r_2/\alpha)\xi - r_2/\alpha$ and $G = r_1H - r_2$, respectively (Notations in the equations have been described in Table 4 or 5). The plots of G versus H and η versus ξ for both systems were obtained, respectively. From the slope and intercept of the straight line, the monomer reactivity ratios of PCMMA and St were determined and given in Table 6. Monomer reactivity ratios of PCMMA and St is significantly lower than those for ATR and CFR polymerizations by both methods. The results show that the copolymers possess a predominantly random structure in a wide range of monomer feeds.

Apparently, the values of monomer reactivity ratios indicate that the growing radicals with PCMMA end were not added at a nearly same rate to PCMMA or St monomers. The r_2 according to K-T and F-R methods shows that the styrene monomer is more reactive than PCMMA toward the poly(PCMMA) radical. Initially, the copolymer sequence will be made richer by the St units and the arrangement will be statistical. The r_1 and r_2 values obtained via both polymerization methods are the similar to that of n-octyl acrylate-styrene copolymer system [25]. For the ATR copolymerization were evaluated through plots of the copolymer compositions (m_1) measured from ¹H-NMR as the molar fraction of PCMMA versus the feed compositions measured as the molar fraction of PCMMA (M_1). The copolymerization experiments were carried out at different temperatures. It is seen that compositions of copolymers obtained by the two copolymerization techniques are somewhat different from each other. But it can be suggested that random copolymers prepared by living free radical processes are different on a molecular level from

those prepared by normal free radical methods. This can be ascribed not to the different nature of the propagating species but to the difference in the time scale of monomer addition or other factors. Thus, in the studies done on copper catalyzed copolymerization of n-alkylmethacrylate and styrene [26, 27], no significant differences were observed in monomer reactivity ratio as well as in monomer sequence between the copper-catalyzed and conventional radical polymerization techniques. The two monomers have a strong tendency to form random copolymer because the value of $r_1 \cdot r_2$ is between 0 and 1. For living radical systems all chains are initiated at the same time and grow at approximately the same rate, in the case of conventional free radical polymerization, continuous initiation leads to chains initiating and terminating at different stages of the polymerization [28].

3.4. Differential scanning calorimetry (DSC) measurements

The glass transition temperatures of the copolymers of PCMMA and St prepared by ATRP and conventional free radical polymerization were measured by DSC. Representative DSC curves of the copolymers heated at 20°C/min to 200°C were showed in Figure 6 and 7, respectively. The T_g values of poly(PCMMA) and poly(St) were measured as 80 and 103°C, respectively. The unique transition observed for PCMMA-St copolymer system prepared by CFRP and ATRP methods corresponds to

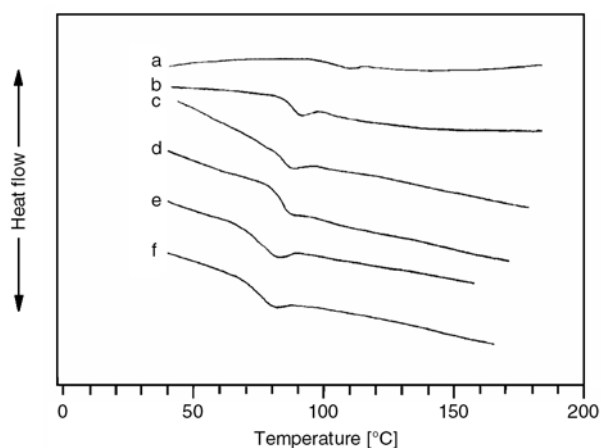


Figure 6. Differential scanning calorimeter (DSC) curves of phenoxycarbonyl methyl methacrylate and styrene copolymer system prepared by conventional radical polymerization method. PCMMA unit in copolymer prepared by CFRP; a: 0.13, b: 0.18, c: 0.33, d: 0.42, e: 0.48, f: 0.73.

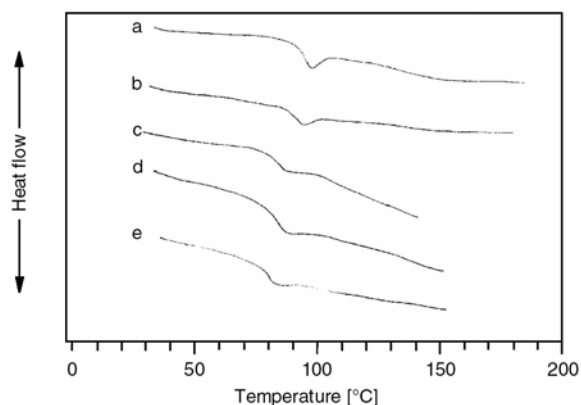


Figure 7. Differential scanning calorimetry (DSC) curves of phenoxycarbonyl methyl methacrylate and styrene copolymer system prepared by atom transfer radical polymerization method. PCMMA unit in copolymer prepared by ATRP; a: 0.12, b: 0.18, c: 0.38, d: 0.56, e: 0.76.

Table 7. Characterization of PCMMA and St copolymers

Entry	(m_1) ^a	(m_1) ^b	T_g [°C] (by ATRP)	T_g [°C] (by CFRP)
1	0.13	0.12	101	96
2	0.18	0.18	88	92
3	0.33	0.27	84	88
4	0.42	0.38	82	85
5	0.48	0.56	77	–
6	0.73	0.76	75	79

m_1^a – PCMMA unit in copolymer prepared by ATRP;

m_1^b – PCMMA unit in copolymer by CFRP

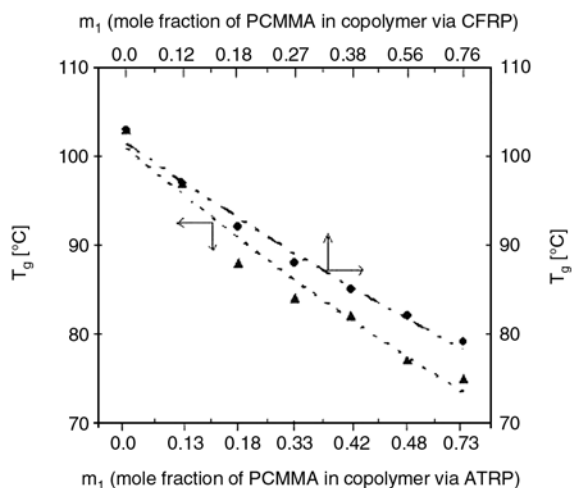


Figure 8. Plots of the T_g of a series of PCMMA-St copolymers as a function of PCMMA mole fraction in the copolymer prepared by ATRP and conventional radical polymerization methods

the glass transition of the soft PCMMA segments and appears at higher temperatures. The feature may be attributed to miscibility of both types of

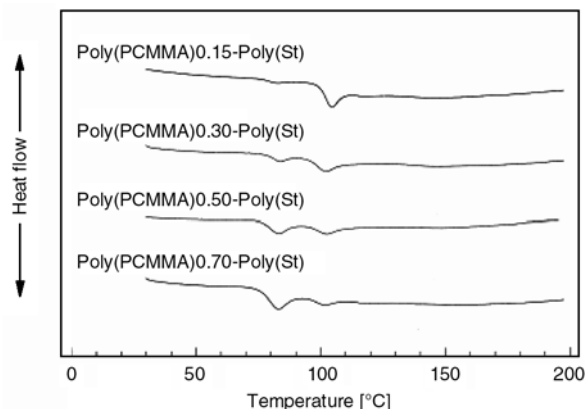


Figure 9. DSC traces of blend polymers heated at 20°C/min to 200°C

segments. The T_g 's of all the copolymers synthesized by CFRP and ATRP methods are also collected in Table 7. The glass transition temperatures of copolymers measured by depending on an increase of the PCMMA unit are between 75–101°C and 79–96°C, respectively. The plots of the T_g values versus mole fraction of PCMMA in the copolymers is shown in Figure 8. The observed T_g 's of the copolymers indicate a slightly negative deviation with respect to linearity that can be associated with a slightly lower free volume.

The glass transition temperatures were measured to analyze the phase behavior of poly(PCMMA) and poly(St) homopolymers. The existence of one or more glass transition temperatures is important for discussing whether or not a miscible or immiscible presents one or more phase. It is known that an immiscible blend shows glass transition temperature of each individual polymer, but a miscible blend has only one glass transition temperature. DSC curves of polymer blends prepared in various ratios for comparison purpose were showed in Figure 9. Each polymer blend prepared in this study showed two separate T_g 's, which can be attributed to poly(PCMMA) and poly(St) to give the incompatible blends. While poly(PCMMA), which is one of polymers contains polar ester and apolar alkyl groups, poly(St) contains apolar group. This means that it does not indicate similar kinds of interactions between both polymers. But, most of polymers having these kinds of properties are generally incompatible [29].

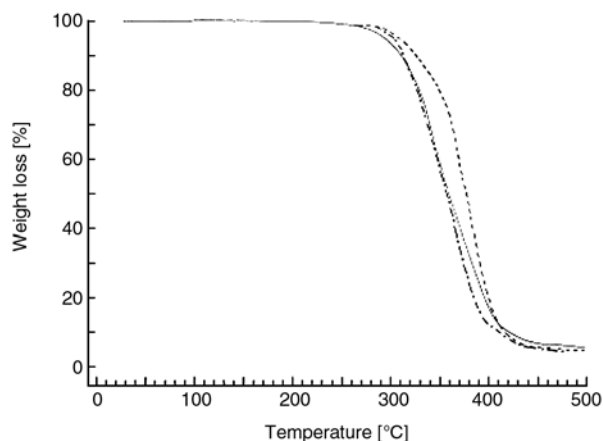


Figure 10. TGA curves of the polymers (heating rate under N₂ flow at 10°C/min)

3.5. Thermogravimetric study

The some of thermogravimetric curves obtained from room temperature to 500°C at a heating rate of 10°C/min under nitrogen flow for poly(PCMMA-co-St), and poly(PCMMA)s prepared by ATRP and conventional free radical polymerization were given in Figure 10 for comparison. The decomposition of poly(PCMMA) proceeds in two steps, the first of which is at 270°C. The second stage, that is, more rapid weight loss is attributed to the degradation reaction by either the side chain decomposition or the random chain scission in the backbone. That of polystyrene synthesized by conventional free radical polymerization occurs in only one step. Also, poly(PCMMA), is more stable thermally than poly(PCMMA) prepared by free radical initiator. The temperatures at which weight loss begins for the PCMMA-St copolymers are somewhat lower than that of poly(St). The thermal stability of copolymer increases with the increasing styrene unit content in the copolymer system. TGA results of the polymers are summarized in Table 8.

When poly(PCMMA) was heated to 270°C, and then to 320°C, the residual polymer was completely dissolved in most of solvents such as tetrahydrofuran, methylenechloride, chloroform, acetonitrile, 1,4-dioxane and dimethylsulphoxide. This means that poly(PCMMA) heated at least to 320°C is not crosslinked. Thus, during degradation of poly(PCMMA) rupture of an allylic carbon-carbon bond forms two radicals, one tertiary and the other a resonance stabilized allylic radical. Then decomposition of poly(PCMMA) continues by elimination of monomer, the driving force being formation of tertiary radical. The average molecular weight decreased from 50 000 to 39 000. This means that decreases 50 PCMMA units from poly(PCMMA) chain. The residue of poly(PCMMA) heated to 380°C was not dissolved in any solvent. Average molecular weights of residue for polymer heated to 270°C and 320°C were characterized by GPC. They were illustrated in Figure 11. Although average molecular weight of residues decrease when heated from room temperature to 320°C, polydispersities were expanded considerably from 1.91 to 3.01. This may be a result of elimination of monomer, the side group elimination or the random chain scission in the backbone during the degradation.

4. Conclusions

Phenoxycarbonylmethyl methacrylate (PCMMA) and styrene (St) were copolymerized by conventional polymerization at 60°C and atom transfer radical polymerization at 110°C in different ratios using AIBN and in the presence of ethyl 2-bromoacetate, cuprous(I)bromide (CuBr), and N,N,N',N'',N'''-pentamethyldiethyltriamine, respectively. The monomer reactivity ratios were calculated from the feed composition and copolymer

Table 8. TGA data for the polymers prepared by ATRP and CFRP methods

Polymers	T _i ^a [°C]	T ₅₀ [°C]	Weight loss at 300°C [%]	Weight loss at 350°C [%]	Weight loss at 400°C [%]
Poly(PCMMA) by ATRP	270	312	3	34	83
Poly(PCMMA) by CFRP	243	341	25	55	82
Poly(St) by CFRP	310	392	0	9	67
Poly(PCMMA0.76-co-St) by CFRP	280	356	4	43	88
Poly(PCMMA0.38-co-St) by CFRP	272	371	3	27	81
Poly(PCMMA0.18-co-St) by CFRP	275	375	4	20	80
Poly(PCMMA0.12-co-St) by CFRP	270	379	4	25	82
Poly(PCMMA0.73-co-St) by ATRP	275	360	6	43	82
Poly(PCMMA0.42-co-St) by ATRP	291	365	2	28	86

^aInitial decomposition temperature

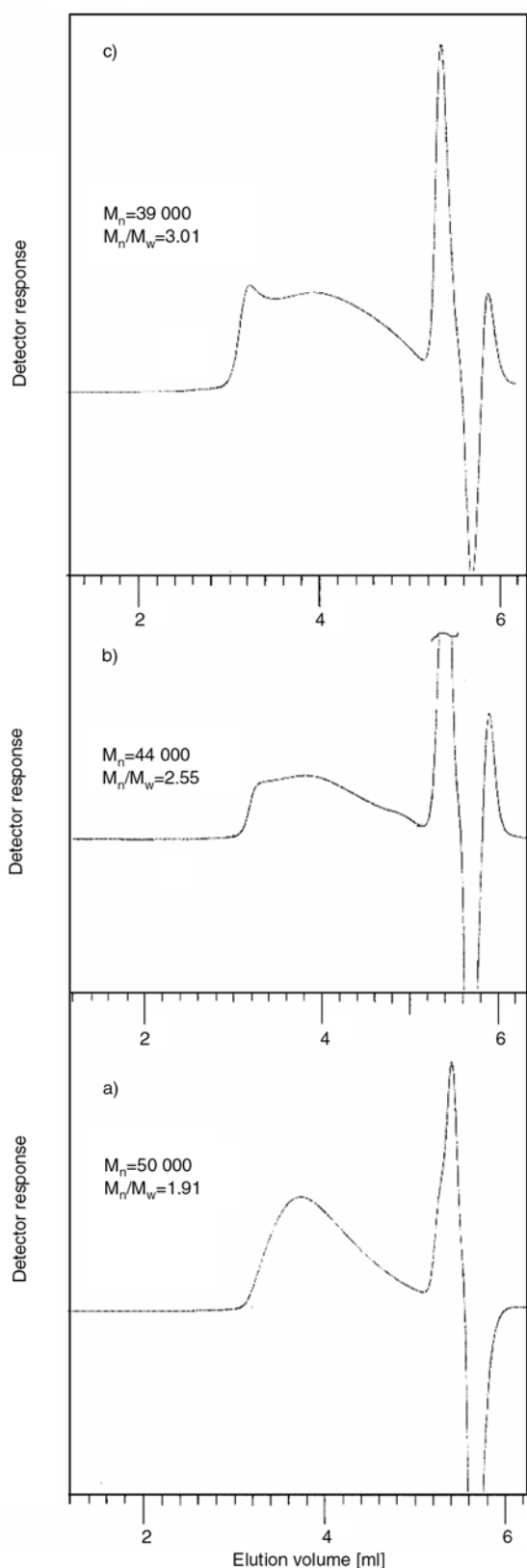


Figure 11. GPC curves of residue a) original poly(PCMMA), b) residue copolymer heated to 270°C, and c) to 320°C

composition determined by $^1\text{H-NMR}$ spectroscopy. Their monomer reactivity ratios were determined

by the K-T and F-R methods. In this copolymerization system, two monomers have a tendency to form alternatif copolymer. The monomer reactivity ratios of PCMMA-St monomers pair do not vary much ($r_{\text{PCMMA}} = 0.33$; $r_{\text{St}} = 0.96$) by changing polymerization temperature and polymerization method i. e., ATRP and CFRP. The DSC curves of all the copolymers synthesized by CFRP and ATRP methods showed single transition. The glass transition temperatures of copolymers measured by depending on an increase of the PCMMA unit are between 75–101°C and 79–96°C, respectively. In case of poly(PCMMA-co-St) prepared by CFRP and ATRP methods, initial decomposition temperature of copolymers increased with an increasing in St content. While poly(PCMMA) heated to 320°C was dissolved in various solvents, average molecular weight of residue polymer was decreased from 50 000 to 39 000 and polydispersity changed from 1.91 to 3.01. Each polymer blend prepared in this study showed two glass transitions, which can be attributed to the immiscibility of poly(PCMMA) and poly(St) resulting in microphase separation.

Acknowledgements

The authors wish to thank the State Planning Organization, in Turkey, (DPT-2003).

References

- [1] Webster O. W.: Living polymerization methods. *Science*, **251**, 887–893 (1991).
- [2] Abraham S., Ha C-S., Kim I.: Synthesis of poly(styrene-block-tert-butyl acrylate) star polymers by atom transfer radical polymerization and micellization of their hydrolyzed polymers. *Journal of Polymer Science, Part A: Polymer Chemistry*, **43**, 6367–6378 (2005).
- [3] Hawker C. J.: ‘Living’ free radical polymerization: A unique technique for the preparation of controlled macromolecular architectures. *Accounts of Chemical Research*, **30**, 373–382 (1997).
- [4] KICKELBICK G., Reinöhl U., Ertel T. S., Betagnolli H., Matyjaszewski K.: The copper catalyst in atom-transfer radical polymerizations: Structural observations. *Abstracts of Papers of the American Chemical Society*, **768**, 211–222 (1999).
- [5] Queffelec J., Gaynor S. G., Matyjaszewski K.: Optimization of atom transfer radical polymerization using Cu(I)/tris(2-(dimethylamino)ethyl)amine as a catalyst. *Macromolecules*, **33**, 8629–8639 (2000).

- [6] Ando T., Kamigaito M., Sawamoto M.: Iron(II)chloride complex for living radical polymerization of methyl methacrylate. *Macromolecules*, **30**, 4507–4510 (1997).
- [7] Dubois P., Ropson N., Jerome R., Teyssie P.: Macromolecular engineering of polylactones and polylactides .19. Kinetics of ring-opening polymerization of ϵ -caprolactone initiated with functional aluminum alkoxides. *Macromolecules*, **29**, 1965–1975 (1996).
- [8] Kato M., Kamigaito M., Sawamoto M., Higashimura T.: Polymerization of methyl-methacrylate with the carbon-tetrachloride dichlorotris (triphenylphosphine) ruthenium(II) methylaluminum bis(2,6-di-tert-butylphenoxide) initiating system- possibility of living radical polymerization. *Macromolecules*, **28**, 1721–1723 (1995).
- [9] Moineau G., Dubois P., Granel C., Jérôme R., Senninger T., Teyssie P.: Alternative atom transfer radical polymerization for MMA using FeCl_3 and AIBN in the presence of triphenylphosphine: An easy way to well-controlled PMMA. *Macromolecules*, **31**, 545–547 (1998).
- [10] Fischer H.: The persistent radical effect: A principle for selective radical reactions and living radical polymerizations. *Chemical Reviews*, **101**, 3581–3610 (2001)
- [11] Matyjaszewski K., Ziegler M. J., Arehart S. V., Greszta D., Pakula T.: Gradient copolymers by atom transfer radical copolymerization. *Journal of Physical Organic Chemistry*, **13**, 775–786 (2000).
- [12] Ziegler M. J., Matyjaszewski K.: Atom transfer radical copolymerization of methyl methacrylate and n-butyl acrylate. *Macromolecules*, **34**, 415–424 (2001).
- [13] Hawker C. J., Bosman A. W., Harth E.: New polymer synthesis by nitroxide mediated living radical polymerizations. *Chemical Reviews*, **101**, 3661–3688 (2001).
- [14] Moineau G., Minet M., Dubois P., Teyssie P., Senninger T., Jérôme R.: Controlled radical polymerization of (meth)acrylates by ATRP with $\text{NiBr}_2(\text{PPh}_3)_2$ as catalyst. *Macromolecules*, **32**, 27–35 (1999).
- [15] Haddleton D. M., Crossman M. C., Hunt K. H., Topping C., Waterson C., Suddaby K. G.: Identifying the nature of the active species in the polymerization of methacrylates: Inhibition of methyl methacrylate homopolymerizations and reactivity ratios for copolymerization of methyl methacrylate n-butyl methacrylate in classical anionic, alkyllithium/trialkylaluminum-initiated, group transfer polymerization, atom transfer radical polymerization, catalytic chain transfer, and classical free radical polymerization. *Macromolecules*, **30**, 3992–3998 (1997).
- [16] Lad J., Harrison S., Haddleton D. M.: Mechanistic aspects of copper-mediated living radical polymerization. *ACS Symposium Series*, **854**, 148–160 (2003).
- [17] Zhou P., Chen G. Q., Hong H., Du F. S., Li Z. C., Li F. M.: Synthesis of C-60-end-bonded polymers with designed molecular weights and narrow molecular weight distributions via atom transfer radical polymerization. *Macromolecules*, **33**, 1948–1954 (2000).
- [18] Simionescu C. I., Barboiu V., Simionescu B. C., Talmaciu V., Sava C.: On the copolymerization model and microstructure of methyl acrylate- styrene radical copolymer- influence of ZnCl_2 . *Journal of Polymer Science, Part A: Polymer Chemistry*, **24**, 851–860 (1986).
- [19] Uebel J. J., Dinan F. J.: A reassessment of the H-1-Nmr spectra of styrene methyl-methacrylate copolymers. *Journal of Polymer Science, Part A: Polymer Chemistry*, **21**, 2427–2438 (1983).
- [20] Percec V., Barboiu B., Kim H-J.: Arenesulfonyl halides: An universal class of functional initiators for metal-catalyzed ‘living’ radical polymerization of styrene(s), methacrylates, and acrylates. *Journal of the American Chemical Society*, **120**, 305–316 (1998).
- [21] Shinoda H., Miller P. J., Matyjaszewski K.: Macromolecules, improving the structural control of graft copolymers by combining ATRP with the macromonomer method. *Macromolecules*, **34**, 3186–3194 (2001).
- [22] Yee L. H., Heuts J. P. A., Davis T. P.: Copolymerization propagation kinetics of dimethyl itaconate and styrene: Strong entropic contributions to the penultimate unit effect. *Macromolecules*, **34**, 3581–3586 (2001).
- [23] Tüdös F., Kelen T.: Analysis of linear methods for determining copolymerization reactivity ratios. 1. New improved linear graphic method. *Journal of Macromolecular Science, Part A: Chemistry*, **9**, 1–27 (1975).
- [24] Fineman M., Ross S. D.: Linear method for determining monomer reactivity ratios in copolymerization. *Journal of Polymer Science*, **5**, 259–262 (1950).
- [25] Bisht H. S., Ray S. S., Chatterjee A. K.: Conventional and atom transfer radical copolymerization of n-octyl acrylate-styrene: Chemoselectivity and monomer sequence distribution by $^1\text{H-NMR}$. *European Polymer Journal*, **39**, 1413–1420 (2003).
- [26] Arehart S. V., Matyjaszewski K.: Atom transfer radical copolymerization of styrene and n-butyl acrylate. *Macromolecules*, **32**, 2221–2231 (1999).
- [27] Kamigaito M., Ando T., Sawamoto M.: Metal-catalyzed living radical polymerization. *Chemical Reviews*, **101**, 3689–3746 (2001).
- [28] Wang J-S., Matyjaszewski K.: Controlled living radical polymerization: Atom-transfer radical polymerization in the presence of transition-metal complexes. *Journal of The American Chemical Society*, **117**, 5614–5615 (1995).
- [29] Nolley E., Barlow J. W., Paul D. R.: Mechanical properties of polypropylene-low density polyethylene blends. *Polymer Engineering and Science*, **20**, 364–369 (1980).